Master thesis

Spin 1 Haldane phase in one-dimensional systems of Rydberg atoms

Johannes Mögerle

February 01, 2022

Supervisor: Prof. Dr. Hans Peter Büchler
Secondary Corrector: Prof. Dr. Jörg Main

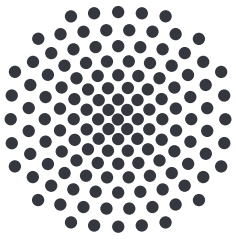

Institute for Theoretical Physics III
University of Stuttgart
Pfaffenwaldring 57, 70550 Stuttgart

Statutory declaration

Hereby, I declare that I have composed the presented paper independently on my own and without any other resources than the ones indicated. All thoughts taken directly or indirectly from external sources are properly denoted as such.
The thesis was not examined before, nor has it been published. The submitted electronic version of the thesis matches the printed version.

Stuttgart, February 01, 2022 Johannes Mögerle

Abstract

Quantum many body physics features a wide range of interesting phenomena that often exceeds our imagination based on daily contact with classical physics. One of the main aspects that distinguishes quantum from classical many body physics is entanglement. Entanglement describes whether and how the state of a subsystem depends on the state of the rest of the system and thus cannot be fully described on its own. This entanglement allows for new, so called topological, quantum phases with remarkably properties. The integer quantum Hall effect [1] in 1980 was the first discovered topological phase. In 1983 Haldane [2] proposed another interesting quantum state in one-dimensional spin systems, that later was found to be in a symmetry protected topological phase. One of the interesting properties appearing in this Haldane phase are edge states of fractionalized spins.

In the last years major progress was made in realizing topological phases in different platforms of artificial matter. One promising platform are Rydberg atoms, which due to their strong and tunable interactions can be used as quantum simulators. Recent experiments include two-dimensional spin liquids [3] as well as the realization of the one-dimensional SSH chain [4], that is closely connected to the Haldane state. Also in ultracold optical lattices the Haldane phase was realized using spin 1/2 fermions on a ladder [5].

In these implementations [4, 5] characteristic properties of the Haldane phase like a hidden antiferromagnetic order (the string order) as well as edge states were measured. However, both realizations used particles with a two-level system to build the Haldane phase. Thus, the spin 1/2 degrees of freedom at the emerging edge states in these models, while still very interesting and a huge step in understanding topological edge states, do not show the fractionalization of spins.

In this work we are going to focus on how one can realize the Haldane phase using Rydberg atoms via a three level system, that can be mapped to a spin 1 particle. By verifying that the resulting edge states still have a spin 1/2 degree of freedom one would be able to demonstrate the fractionalization of the spin in the edge states of the Haldane phase.

This thesis is structured as following. In chapter 1 we are going to give a theoretical introduction to the basic topics and concepts that were used in this work. A strong emphasis will be on the matrix product state formalism. This allows us also to treat the AKLT state, a prime example for the Haldane phase, analytically and discuss its characteristic properties.
In chapter 2 we will then introduce the Rydberg three level system used to realize an effective spin 1 model. We will choose states near to a Förster resonance and discuss possible parameters and interactions that can be tuned in this system.
After that in chapter 3 it follows a detailed discussion of the Haldane phase. In particular, we are going to study the stability of the Haldane phase in the context of the possible interactions of the Rydberg three level system. This is done by employing the (infinite) density matrix renormalization group to calculate the ground states of the corresponding quantum many body systems. We end the phase diagram discussion by proposing a parameter set, which has strong signatures of the Haldane phase and also is in the range of experimentally realizable interactions.
Finally, in chapter 4 we discuss how to tune the interactions of the Rydberg states to match the proposed parameters. We end up with a proposal for an experimental setup, which resulting Hamiltonian features the Haldane phase. Last but not least, we discuss the properties of the ground state, including a finite string order, a fourfold ground state degeneracy as well as fractional edge states.

Zusammenfassung

Quanten-Vielteilchenphysik weist verschiedenste interessante Phänomene auf, die oft unsere alltäglichen Erfahrungen mit klassischer Physik übersteigen. Eines der wichtigsten Aspekte, die Vielteilchen Quantenphysik von klassischer Physik unterscheidet ist Verschränkung (engl. *entanglement*). Entanglement beschreibt, ob und wie stark der Zustand eines Teilsystems vom Zustand des restlichen Systems abhängt, bzw. wie das Teilsystem mit dem restlichen System verschränkt ist und alleine keinen wohldefinierten Zustand hat. Diese Verschränkungen erlauben für neue, sogenannte topologische, Quantenphasen, die oftmals bemerkenswerte Eigenschaften aufweisen. Der integrale Quanten-Hall-Effekt [1] war in 1980 die erste solche entdeckte topologische Phase. In 1983 stellte Haldane [2] einen weiteren interessanten Zustand einer eindimensionalen Spinkette vor, der sich später als Symmetrie geschützter topologischer Zustand herausstellte. Einer der interessanten Eigenschaften der Haldane Phase ist das Auftreten von Randzuständen mit fraktionalisiertem Spin.

In den letzten Jahren gab es große Fortschritte in der Realisierung topologischer Phasen auf verschiedenen Plattformen künstlicher Materie. Eine vielversprechende Plattform sind Rydbergatome, die aufgrund ihrer großen und verstellbaren Wechselwirkungen als Quantensimulatoren genutzt werden können. Aktuelle Experimente mit Rydbergatomen umfassen zweidimensionale Quantenspinflüssigkeit [3] also auch die Realisierung der eindimensionalen SSH-Kette [4], die eng mit dem Haldane Zustand verknüpft ist. Auch in ultrakalten optischen Gittern konnte die Halden Phase realisiert werden durch Spin 1/2 Fermionen auf einer Leiter [5].

In diesen beiden Experimenten [4, 5] konnten charakteristische Merkmale der Haldane Phase gemessen werden, wie zum Beispiel die versteckte antiferromagnetische Ordnung und auch Randzustände. Allerdings wurden in beiden experimentellen Umsetzungen Teilchen mit einem Zwei-Niveau-System verwendet, um den Zustand in der Haldane Phase zu erzeugen. Deshalb ist das Auftauchen der Spin 1/2 Freiheitsgrade der Randzustände in diesen Modellen zwar immer noch sehr interessant und ein großer Fortschritt für das Verständnis von topologischen Randzuständen, aber keine Demonstration einer Spinfraktionaliserung.

In dieser Arbeit werden wir uns darauf fokussieren wie man die Haldane Phase mithilfe von Rydbergatomen realisieren kann, indem man mit einem Drei-Niveau-System aus Rydbergzuständen ein Spin 1 Teilchen darstellen kann. Wenn man nun zeigen kann, dass die Randzustände für dieses System wiederum Spin 1/2 Freiheitsgrade sind, könnte man demonstrieren, dass der Spin der Randzustände fraktionalisiert ist.

Die vorliegende Arbeit ist wie folgt strukturiert. In Kapitel 1 geben wir eine theoretische Einführung zu den grundlegenden Themen und Konzepten, die in dieser Arbeit behandelt werden. Ein Fokus wird der Formalismus von Matrix-Produkt-Zuständen sein. Damit können wir auch den AKLT Zustand, der ein Paradebeispiel für die Haldane Phase ist, analytisch lösen und dessen charakteristischen Eigenschaften diskutieren.
In Kapitel 2 werden wir dann das Drei-Niveau-System in Rydbergatomen vorstellen, welches wir nutzen werden, um ein effektives Spin 1 Modell zu beschreiben. Dafür werden wir Rydbergzustände nahe einer Förster Resonanz nutzen. Zudem diskutieren wir die möglichen Wechselwirkungen dieses Systems.
Danach folgt in Kapitel 3 eine ausführliche Diskussion der Haldane Phase. Besonders werden wir die Stabilität der Haldane Phase in Bezug auf die möglichen Wechselwirkungen der Rydbergatome untersuchen. Dafür werden wir mithilfe der (i)DMRG (engl. *(infinite) density matrix renormalization group*) Methode die Grundzustände der Quanten-Vielteilchensysteme bestimmen. Wir schließen die Diskussion der Phasendiagramme ab, indem wir Parameter auswählen, die deutlich die Eigenschaften der Haldane Phase aufzeigen und zugleich im Bereich experimentell realisierbarer Wechselwirkungen liegen.
Zum Schluss diskutieren wir in Kapitel 4 wie man die Wechselwirkungen der Rydbergzustände so einstellen kann, dass diese mit den ausgewählten Parametern übereinstimmen. Damit können wir einen experimentellen Aufbau vorschlagen, mit dem man die Haldane Phase realisieren kann. Schließlich untersuchen wir die Eigenschaften des Grundzustands dieses Modells, die unter anderem einen nicht verschwindenden Stringordnungsparameter, einen vierfach entarteten Grundzustand sowie fraktionalisierte Randzustände beinhalten.

Contents

1 Theoretical basics

This chapter is supposed to give a theoretical background on the topics related to this work. It will by no means provide a universal introduction to the different topics, but might help as reminder as well as introduction to the notations used throughout this work.

The sections in this chapter are structured as following.
We will start by roughly sketching the bigger picture of topological phases of matter to end up with some general discussion of the Haldane phase, leaving a more detailed discussion to the second to last section of this chapter, where we will look at famous AKLT state, a prime example of the Haldane phase.
The second section of this chapter will serve as introduction to the matrix product state formalism. We will also get more familiar with these concepts when looking at the AKLT example. Furthermore, we will introduce the density matrix renormalization group in this second section, which will be the main tool used to obtain the results in chapter 3.
After that we are going to recap the spin 1 algebra as well as introduce all relevant symmetries and order parameters, that will become useful for the later phase diagram discussions. This third section therefore also serves as summary of the notation conventions for operators and order parameters in this work.
As mentioned before we will then have a more detailed discussion about the AKLT model. This will put together all the aforementioned concepts and therefore serves as instructive, analytical solvable example.
We finish this chapter with a final section about Rydberg atoms and their interactions. This introduction on Rydberg atoms will then link seamlessly to the next chapter, where we will continue the discussion of Rydberg states and Rydberg interactions and link them to an effective spin 1 model.

1.1 Topological phases of matter

Let us start with a short introduction to topological phases of matter (TPMs) to then embed the Haldane phase, which will be the focus of this thesis, in this bigger picture. The interested reader may find more details on TPMs in [6–9].

In this section we will first introduce the Landau paradigm and will then expand it by the concept of topological phases. Furthermore, we will discuss the idea of symmetry protected topological phases (SPTs) and with that we can introduce the Haldane phase, which is a prime example for these SPTs. However, we will end this section with only a very short discussion of the Haldane phase and will continue a more detailed discussion about the Haldane phase by looking at the AKLT model in a later section, after introducing some important basic tools like the MPS formalism.

Landau paradigm

Two quantum phases of matter are considered distinct from each other if there is a qualitative difference of the ground state properties for the two phases. For example, this might be a change of the ground state degeneracy or some qualitative change of an order parameter (e.g. the order parameter being zero in one phase and finite in the other phase). Moreover, two distinct gapped phases (i.e. phases where the excitation gap from the ground state manifold to the first excited state is finite even in the thermodynamic limit of an infinite system) can only be connected in the parameter space via paths that have a critical point at which the gap closes.

The prime example for such quantum phases and phase transitions is the transverse field Ising model (TIM) in 1D. The Hamiltonian for this model in a one-dimensional periodic chain of N spin 1/2 particles reads

$$H^{\mathrm{TIM}} = -J \sum_{i=1}^{N} \sigma_i^z \sigma_{i+1}^z - h \sum_{i=1}^{N} \sigma_i^x \,, \tag{1.1}$$

where σ are the Pauli spin 1/2 matrices (see (1.48)) and periodic boundary conditions are applied (i.e. we identify the first and the $(N+1)$th site).

The ground state of this model has a simple solution for the two cases i) $J \to 0$ and ii) $h \to 0$.

- First, for $J \to 0$ the ground state is unique and a product state of all spins being in the $|+_x\rangle = (|\uparrow\rangle + |\downarrow\rangle)/\sqrt{2}$ eigenstate of the σ^x matrix: $|\psi_{\mathrm{para}}\rangle = |+_x +_x ... +_x\rangle$. We will refer to this phase as *paramagnetic* phase.

- Second, for $h \to 0$ the ground state is twofold degenerate and a product state of all spins pointing in the same direction: $|\psi_{\text{ferro}\uparrow}\rangle = |\uparrow\uparrow \ldots \uparrow\rangle$ and $|\psi_{\text{ferro}\downarrow}\rangle = |\downarrow\downarrow \ldots \downarrow\rangle$. We will refer to this phase as *ferromagnetic* phase.

Since the ground state degeneracy of these two cases is different we find that these two parameter regimes belong to two different quantum phases. Furthermore, we could distinguish these two phases by a *local* order parameter $\mathcal{O} = \lim_{|i-j|\to\infty} \langle \sigma_i^z \sigma_j^z \rangle$, which vanishes in the paramagnetic phase but is finite in the ferromagnetic phase.

These two phases can in parameter space only be connected to each other by going over some critical point, at which the gap closes, and the energy spectrum goes from a unique ground state to a double degenerate ground state manifold. For the TIM this phase transition happens at the point $J/h = 1$. However, the Landau paradigm [10] suggest that such phase transitions only occur together with a spontaneous symmetry breaking (SSB). For that let us look again at the different ground states. Our Hamiltonian (1.1) is symmetric under a π rotation around the x axis, which can be written as applying local σ^x operators at each site $X = \prod_i \sigma_i^x$ ($X H^{\text{TIM}} X = H^{\text{TIM}}$). While the paramagnetic ground state is symmetric under this rotation ($X |\psi_{\text{para}}\rangle = |\psi_{\text{para}}\rangle$), the ferromagnetic ground states are not ($X |\psi_{\text{ferro}\uparrow}\rangle = |\psi_{\text{ferro}\downarrow}\rangle$ and $X |\psi_{\text{ferro}\downarrow}\rangle = |\psi_{\text{ferro}\uparrow}\rangle$). Thus, the Landau paradigm holds true for the TIM as well as for many other quantum systems.

Some short aside note. While $\left|\psi_{\text{ferro}\uparrow(\downarrow)}\right\rangle$ are indeed not symmetric under X, one can construct a symmetric basis for the twofold ground state manifold $|\psi_{\text{ferro}\pm}\rangle \propto |\psi_{\text{ferro}\uparrow}\rangle \pm |\psi_{\text{ferro}\downarrow}\rangle$, with $X |\psi_{\text{ferro}\pm}\rangle = \pm |\psi_{\text{ferro}\pm}\rangle$. However, these states are so-called *cat states*, which means they are a superposition of macroscopic different quantum states. Such states are first of all non-physical ground states for large systems, since the tiniest perturbation or measurement would collapse the wave function to one of the superposition states. Furthermore, it is mathematical not that simple to treat such states in the thermodynamic limit of an infinite system size, to be precise the *superselection rules* forbid such states to be pure quantum states. The (oversimplified) message being that treating the SSB as we did before is correct.

Topological phases

However, there is no a priori rule that two distinct phases have to have a SSB. Therefore, it might be possible that there are two distinct phases, where the ground states of both phases do not break any symmetry (or the exact same symmetries). For such phases the Landau paradigm would break and the phase transition would not be accompanied by a SSB. Nevertheless, for distinct phases there must be a phase transition at which the excitation gap closes. In fact, such phases do exist and we refer to them as topological

phases (TPs). These TPs are often described by their entanglement patterns instead of some SSB. Some prime examples for these TPs are the fractional quantum Hall effect [11] and the toric code [12]. TPs defined in this way all have a long range entanglement pattern [13]. One also refers to these TPs as intrinsic topological ordered phases. Having introduced that it also has been proven, that such TPs cannot exist in one-dimensional systems [14].

Symmetry protected topological phases

Fortunate this is not the end of the story. We can apply additional symmetry constraints to our system. Due to these constraints topological phases as well as the trivial phase can split up in more fine-grained phases, since now we might not be able to connect points in the phase space without either closing the gap or breaking the symmetry anymore. The new phases emerging from splitting a topological phase with long range entanglement into new phases will be called symmetry enriched topological phases (SETs), while the splitting of the trivial phase with short ranged entanglement into new phases will be called symmetry protected topological phases (SPTs). These SPTs can also occur in one-dimensional systems. The most prominent example for a SPT is probably the Haldane phase, which we will also focus on in this work.

Haldane phase

The existence of the Haldane phase was first discussed by Haldane in two papers from 1983 [2, 15] within the Heisenberg model. Later in 1987 Affleck, Kennedy, Lieb and Tasaki proposed another model, which nowadays is known as the AKLT model [16], to construct a prime example for the Haldane phase which was, by construction, analytically solvable and gave a lot of insight into the properties of the Haldane phase. In contrast, to the paramagnetic and ferromagnetic phases of the TIM, the Haldane phase cannot be characterized by a local order parameter. However, we will later introduce the so-called string order parameters, which are non-local, but nevertheless will allow us to distinguish the Haldane phase. Furthermore, for finite open boundary conditions the Haldane phase has a fourfold degenerate ground state and features fractionalized edge excitations. We will discuss this in more detail at the example of the AKLT model later.

1.2 Matrix product state formalism

This section serves as an introduction to the matrix product state (MPS) formalism. It is based on the literature [17–19], where the interested reader can also find a more in-depth discussion. The MPS formalism can help in many ways to understand different important aspects of TPs and SPTs better, such as entanglement, string order and symmetries to mention just a few. For this reason some reader might find this a helpful and instructive reading.

1.2.1 Entanglement entropy

Before introducing the MPS formalism let us start with some important properties of a general quantum state, which will be important for understanding why the MPS formalism is such a powerful tool. For the rest of this section we will consider a one-dimensional lattice of N sites with a local onsite Hilbert space $\mathcal{H}_{\text{local}}$ of dimension d and basis states $|s_i\rangle$ with $i \in \{1, 2, ..., d\}$. One might think of the basis states as spin states, however the presented concepts are also valid for more general states. The total Hilbert space $\mathcal{H} = \mathcal{H}_{\text{local}}^{\otimes N}$ has a dimension of d^N and a pure state in this Hilbert space can be written as

$$|\psi\rangle = \sum_{\boldsymbol{s}} c_{\boldsymbol{s}} |\boldsymbol{s}\rangle = \sum_{s_1} \sum_{s_2} ... \sum_{s_N} c_{s_1,s_2,...,s_N} |s_1, s_2, ..., s_N\rangle \ . \tag{1.2}$$

Note that one has to store d^N coefficients c to describe this quantum state. In the following we will only be interested in pure quantum states and do not consider any mixed quantum states.

Now we can have a look at the entanglement entropy of this state. Therefore, one can split the Hilbert space into two subspaces $\mathcal{H} = \mathcal{H}_{\text{L}} \otimes \mathcal{H}_{\text{R}}$, where $\mathcal{H}_{\text{L}}$ denotes the Hilbert space of the m leftmost sites and $\mathcal{H}_{\text{R}}$ the Hilbert space of the $(N - m)$ rightmost sites. A state then can always be written in the Schmidt decomposition

$$|\psi\rangle = \sum_{\alpha=1}^{\min\left(d^m, d^{N-m}\right)} \Lambda_\alpha |\alpha\rangle_{\text{L}} \otimes |\alpha\rangle_{\text{R}} \ , \tag{1.3}$$

where $\{|\alpha\rangle_{\text{L}}\}_{\alpha\in\{1,2,...,d^m\}}$ forms an orthonormal basis of $\mathcal{H}_{\text{L}}$ and $\{|\alpha\rangle_{\text{R}}\}_{\alpha\in\{1,2,...,d^{N-m}\}}$ forms an orthonormal basis of $\mathcal{H}_{\text{R}}$ respectively. All Schmidt values $\Lambda_\alpha \geq 0$ are non-negative. Furthermore, $\sum_\alpha \Lambda_\alpha^2 = 1$, where we define $\Lambda_\alpha = 0$ for all $\alpha > \min\left(d^m, d^{N-m}\right)$. One can then easily show that Λ_α^2 are the eigenvalues of the reduced density matrix

$$\rho^{\text{L}} = \text{Tr}_{\text{R}}(\rho) = \sum_{\alpha=1}^{d^{N-m}} \langle\alpha|_{\text{R}} |\psi\rangle \langle\psi| \ |\alpha\rangle_{\text{R}} = \sum_{\alpha=1}^{d^m} \Lambda_\alpha^2 |\alpha\rangle_{\text{L}} \langle\alpha|_{\text{L}} \ . \tag{1.4}$$

From the reduced density matrix one can now calculate the von Neumann entanglement entropy

$$S = -\operatorname{Tr}\left(\rho^{\mathrm{L}} \log\left(\rho^{\mathrm{L}}\right)\right) = -\sum_{\alpha=1}^{d^m} \Lambda_\alpha^2 \log \Lambda_\alpha^2 \,, \tag{1.5}$$

where log refers to the natural logarithm. Furthermore, one defines the entanglement spectrum as

$$\epsilon_\alpha = -\log \Lambda_\alpha^2 \,. \tag{1.6}$$

In the following we will consider a chain of even length N and a bipartition into two equally sized parts $m = N/2$. Then for a maximally entangled state the Schmidt values are all equal $\Lambda_\alpha = 1/\sqrt{d^{N/2}}$. From this one can calculate the entanglement entropy $S = (N/2) \cdot \log d$. Since the entropy grows linear with the partition size $m = N/2$ such a state obeys a volume law. In fact, most quantum states show a volume law behavior. However, it has been shown [20, 21], that in one-dimensional lattices the ground state of a gapped Hamiltonian always shows an area law behavior instead of a volume law. This means the entropy increases proportional to the partition surface instead of the partition size. In one dimension this implies, that the entropy converges to a constant value for a growing system size.

Area law quantum states are only slightly entangled and do not have equal Schmidt values. The most weight of the Schmidt values is contained in only a few values, while all other Schmidt values have strongly decreasing weight. This means that by using only the χ largest Schmidt values and corresponding Schmidt states (instead of all d^m) the error to the original state is very small. A sufficiently large χ will be for large systems still be much smaller than d^m.
This means for one-dimensional area law states one can always find a finite χ for every ε such that the following inequality holds for all (arbitrary big) system sizes N

$$\left\| |\psi\rangle - \sum_{\alpha=1}^{\chi} \Lambda_\alpha \, |\alpha\rangle_{\mathrm{L}} \, |\alpha\rangle_{\mathrm{R}} \right\| = \sum_{\alpha=\chi+1}^{\min\left(d^m, d^{N-m}\right)} \Lambda_\alpha^2 < \varepsilon \,. \tag{1.7}$$

As it will turn out this property is the fundamental reason why the MPS formalism is such a powerful tool for treating ground states of one-dimensional gapped Hamiltonians. Because we can now efficiently approximate these ground states with a finite number of Schmidt values (and states) independent of the system size and do not have to store d^N coefficients, which would exponentially grow with the system size. However, in situations where the area law behavior breaks down, also this approximation will have a non-negligible error. For example, in gapless phases and at gap closing points where the ground state in general does not show an area law but rather a volume law behavior. Moreover, in two-dimensional systems the entropy of area law states will again increase

with system size. Thus, it is hard to treat two-dimensional systems in the MPS formalism. However, for small system sizes, or cylinder geometries with finite circumference, it is still possible to apply the MPS formalism and find ground states with the DMRG algorithm.

1.2.2 Matrix product state

A MPS is an alternative form of writing and storing a quantum state. Instead of writing all the coefficients just as one big tensor $c_{\boldsymbol{s}}$, like in equation (1.2) one can decompose this single big tensor into multiple smaller tensors, where now each tensor corresponds to one site

$$|\psi\rangle = \sum_{\boldsymbol{s}} M^{[1]s_1} M^{[2]s_2} \ \ldots \ M^{[N]s_N} \, |\boldsymbol{s}\rangle = \sum_{\boldsymbol{s}} \sum_{\alpha_0,\alpha_1,\ldots,\alpha_N} M^{[1]s_1}_{\alpha_0\alpha_1} M^{[2]s_2}_{\alpha_1\alpha_2} \ \ldots \ M^{[N]s_N}_{\alpha_{N-1}\alpha_N} \, |\boldsymbol{s}\rangle \ , \tag{1.8}$$

here $M^{[i]}$ is a tensor of rank 3 with dimensions $d \times \chi_{i-1} \times \chi_i$, where χ_{i-1} and χ_i do not have to be the same. The index α_i runs over $1, 2, \ldots, \chi_i$. While d is still the physical dimension of the local Hilbert space $\mathcal{H}_{\text{local}}$, χ_i are called (virtual) bond dimensions, that connect two sites. Note that for a finite MPS the first and last bond dimensions are one $\chi_0 = \chi_N = 1$, and the indices $\alpha_0 = \alpha_N = 1$ are dummy indices.

One important note about the MPS is that the matrices M are not unique. In fact, there is a simple transformation which allows us to change the matrices without changing the state. Consider the product of the two matrices $M^{[i]s_i}$ and $M^{[i+1]s_{i+1}}$ with bond dimensions $\chi_{i-1} \times \chi_i$ and $\chi_i \times \chi_{i+1}$ respectively, then we can transform the two matrices without changing the product by introducing an invertible matrix X with dimension $\chi_i \times \chi_i$

$$M^{[i]s_i} M^{[i+1]s_{i+1}} = \left(M^{[i]s_i} X\right) \left(X^{-1} M^{[i+1]s_{i+1}}\right) = \tilde{M}^{[i]s_i} \tilde{M}^{[i+1]s_{i+1}} \ . \tag{1.9}$$

This transformation can be seen as some kind of generic basis transformation of the matrices M. However, rather than discussing this general transformation we will first proof, that every quantum state (1.2) can be written as MPS and by doing this proof we will also see some of the most important forms of how to choose the basis of the M matrices.

To proof that indeed every quantum state can be written as MPS we introduce the singular value decomposition (SVD), which can be used to decompose a complex matrix A with dimension $(n \times m)$ into the product of three matrices

$$A = U \Lambda V^\dagger \ . \tag{1.10}$$

Here Λ is a diagonal matrix with non-negative entries, called singular values, and dimension $\chi \times \chi$, with $\chi = \min(n, m)$. And the matrices U and V are semi-unitary,

meaning

$$U^\dagger U = \mathbb{1}_\chi \quad \text{and} \quad V^\dagger V = \mathbb{1}_\chi \,. \tag{1.11}$$

This can also be interpreted as writing

$$U = (\boldsymbol{u}_1 \boldsymbol{u}_2, ..., \boldsymbol{u}_\chi) \quad \text{and} \quad V^\dagger = \begin{pmatrix} \boldsymbol{v}_1^\dagger \\ \boldsymbol{v}_2^\dagger \\ ... \\ \boldsymbol{v}_\chi^\dagger \end{pmatrix} , \tag{1.12}$$

where $\boldsymbol{u}_i$ are orthonormal vectors of dimension n, called *left singular vectors*, and respectively $\boldsymbol{v}_j$ are orthonormal vectors of dimension m, called *right singular vectors*

$$(\boldsymbol{u}_i, \boldsymbol{u}_j) = \boldsymbol{u}_i^\dagger \boldsymbol{u}_j = \delta_{i,j} \quad \text{and} \quad (\boldsymbol{v}_i, \boldsymbol{v}_j) = \boldsymbol{v}_i^\dagger \boldsymbol{v}_j = \delta_{i,j} \,. \tag{1.13}$$

The SVD can then also be written as

$$A = \sum_\alpha \lambda_\alpha \boldsymbol{u}_\alpha \boldsymbol{v}_\alpha^\dagger \,. \tag{1.14}$$

Now let us apply the SVD to our coefficient tensor $c_{\boldsymbol{s}}$ with d^N entries by first reshaping it to a $(d \times d^{N-1})$ matrix $c_{s_1,(s_2,...,s_N)}$

$$c_{\boldsymbol{s}} = c_{s_1,(s_2,...,s_N)} = \sum_{\alpha_1} U^{[1]}_{s_1,\alpha_1} \Lambda^{[1]}_{\alpha_1,\alpha_1} \left(V^{[1]\dagger}\right)_{\alpha_1,(s_2,...,s_N)} \,. \tag{1.15}$$

Note that the singular values $\Lambda^{[1]}_{\alpha_1,\alpha_1}$ are actually the Schmidt values of a bipartition at bond 1 (between site 1 and site 2). Let us multiply the $\chi_1 \times \chi_1$ dimensional matrix $\Lambda^{[1]}$ onto $V^{[1]\dagger}$ and again reshape the result to a $(\chi_1 \cdot d \times d^{N-2})$ matrix

$$\Lambda^{[1]}_{\alpha_1,\alpha_1} \left(V^{[1]\dagger}\right)_{\alpha_1,(s_2,...,s_N)} = \left(\Lambda^{[1]} V^{[1]\dagger}\right)_{(\alpha_1,s_2),(s_3,...,s_N)} \,. \tag{1.16}$$

Applying the SVD to this results in

$$\left(\Lambda^{[1]} V^{[1]\dagger}\right)_{(\alpha_1,s_2),(s_3,...,s_N)} = \sum_{\alpha_2} U^{[2]}_{(\alpha_1,s_2),\alpha_2} \Lambda^{[2]}_{\alpha_2,\alpha_2} \left(V^{[2]\dagger}\right)_{\alpha_2,(s_3,...,s_N)} \,, \tag{1.17}$$

where the singular values $\Lambda^{[2]}_{\alpha_2,\alpha_2}$ again correspond to the Schmidt values of a bipartition at bond 2. We will use these $\Lambda^{[i]}$ matrices again later. For now, we repeat this procedure to end up with

$$c_{\boldsymbol{s}} = \sum_{\alpha_1 ..., \alpha_N} U^{[1]}_{s_1,\alpha_1} U^{[2]}_{(\alpha_1,s_2),\alpha_2} ... U^{[N-1]}_{(\alpha_{N-2},s_{N-1}),\alpha_{N-1}} U^{[N]}_{(\alpha_{N-1},s_N)} \,, \tag{1.18}$$

where we dropped the last Λ and $V^\dagger$ matrix, because they have to be trivial 1×1 matrices with entry 1.

We now can introduce the A tensors by reshaping the matrices U to rank 3 tensors

$$A^{[i],s_i}_{\alpha_{i-1},\alpha_i} = U^{[i]}_{(\alpha_{i-1},s_i),\alpha_i} \,, \tag{1.19}$$

where we again used dummy indices α_0 and α_N, which only run over one value. Note that the semi-unitary properties (1.11) and (1.13) of the U matrices for each site i translate to the A tensors as following

$$\sum_{s_i} \left(A^{[i],s_i}\right)^\dagger A^{[i],s_i} = \mathbb{1} \quad \text{or} \quad \sum_{s_i,\alpha_{i-1}} \left(A^{[i],s_i}_{\alpha_{i-1},\alpha_i'}\right)^* A^{[i],s_i}_{\alpha_{i-1},\alpha_i} = \delta_{\alpha_i',\alpha_i} \,. \tag{1.20}$$

Therefore, the A tensors are called *left normalized* (since we are summing over the left bond index α_{i-1}). The resulting MPS build from only A tensors

$$|\psi\rangle = \sum_{\boldsymbol{s}} A^{[1]s_1} A^{[2]s_2} \ldots A^{[N]s_N} |\boldsymbol{s}\rangle = \sum_{\boldsymbol{s}} \sum_{\alpha_0,\alpha_1,\ldots,\alpha_N} A^{[1]s_1}_{\alpha_0\alpha_1} A^{[2]s_2}_{\alpha_1\alpha_2} \ldots A^{[N]s_N}_{\alpha_{N-1}\alpha_N} |\boldsymbol{s}\rangle \,, \tag{1.21}$$

is then called to be in *left canonical* form, and we finished our proof, that every quantum state (1.2) can be written as MPS. Note that this left canonical form is a choice, which fixes the basis of the M matrices (thus applying a transformation X and X^{-1} would destroy the left canonical form).

Naturally instead of starting with the first site, we could start the SVD from the last site, multiplying the Λ matrices to the U matrices and ending up in a form like

$$c_{\boldsymbol{s}} = \sum_{\alpha_1\ldots,\alpha_N} \left(V^{[1]}\right)^\dagger_{s_1,\alpha_1} \left(V^{[2]}\right)^\dagger_{(\alpha_1,s_2),\alpha_2} \ldots \left(V^{[N-1]}\right)^\dagger_{(\alpha_{N-2},s_{N-1}),\alpha_{N-1}} \left(V^{[N]}\right)^\dagger_{(\alpha_{N-1},s_N)} \,. \tag{1.22}$$

We can introduce now B tensors $B^{[i],s_i}_{\alpha_{i-1},\alpha_i} = \left(V^{[i]}\right)^\dagger_{(\alpha_{i-1},s_i),\alpha_i}$, for which the semi-unitary condition translates to

$$\sum_{s_i} B^{[i],s_i} \left(B^{[i],s_i}\right)^\dagger = \mathbb{1} \quad \text{or} \quad \sum_{s_i,\alpha_i} B^{[i],s_i}_{\alpha_{i-1},\alpha_i} \left(B^{[i],s_i}_{\alpha_{i-1}',\alpha_i}\right)^* = \delta_{\alpha_{i-1}',\alpha_{i-1}} \,. \tag{1.23}$$

And we call the B tensors *right normalized* (since we are summing over the right bond index α_i). The MPS only consisting of B tensors

$$|\psi\rangle = \sum_{\boldsymbol{s}} B^{[1]s_1} B^{[2]s_2} \ldots B^{[N]s_N} |\boldsymbol{s}\rangle = \sum_{\boldsymbol{s}} \sum_{\alpha_0,\alpha_1,\ldots,\alpha_N} B^{[1]s_1}_{\alpha_0\alpha_1} B^{[2]s_2}_{\alpha_1\alpha_2} \ldots B^{[N]s_N}_{\alpha_{N-1}\alpha_N} |\boldsymbol{s}\rangle \,, \tag{1.24}$$

is then called to be in *right canonical* form.

It is quite straightforward to see, that we also can come up with a *mixed canonical* form

$$|\psi\rangle = \sum_{\boldsymbol{s}} A^{[1]s_1} \ldots A^{[m]s_m} \Lambda^{[m]} B^{[m+1]s_{m+1}} \ldots B^{[N]s_N} |\boldsymbol{s}\rangle \,, \tag{1.25}$$

by starting the SVD process from right and left, and ending at site m. $\Lambda^{[m]}_{\alpha_m,\alpha_m}$ are the singular values of the SVD at site m and coincide with the Schmidt values for a bipartition at bond m.

Before simplifying the notation with all the different indices by introducing a graphical representation of a MPS, which will be much more suitable for handling MPS, let us introduce another matrix Γ. For that we remember the $\Lambda^{[i]}$ matrices, either from the mixed canonical representation above, or from the SVD sweeps (see equation (1.17)). With that we can define

$$\Gamma^{[i],s_i} = \left(\Lambda^{[i-1]}\right)^{-1} A^{[i],s_i}\,, \quad \text{or rather} \quad A^{[i],s_i} = \Lambda^{[i-1]}\Gamma^{[i],s_i}\,. \tag{1.26}$$

If $\Lambda^{[i-1]}$ has zeroes on the diagonal, we can discard these rows and columns as well as the corresponding rows and columns in $U^{[i-1]}$ and $V^{[i-1]\dagger}$ to make $\Lambda^{[i-1]}$ invertible without changing the MPS. Since the SVD is unique up to degeneracies in Λ (if we order the singular values in Λ) one can verify that the Γ matrices also connect to the B matrices as following

$$B^{[i],s_i} = \Gamma^{[i],s_i}\Lambda^{[i]}\,. \tag{1.27}$$

Inserting this into equation (1.25) yields

$$|\psi\rangle = \sum_{\boldsymbol{s}} \Lambda^{[0]}\Gamma^{[1],s_1}\Lambda^{[1]}\Gamma^{[2],s_2}\ \ldots\ \Lambda^{[N-1]}\Gamma^{[N],s_N}\Lambda^{[N]}\,|\boldsymbol{s}\rangle\,, \tag{1.28}$$

where $\Lambda^{[0]} = \Lambda^{[N]} = [1]_{1\times 1}$ are dummy matrices. In this form one can read off the Schmidt values of a bipartition at bond m (between site m and $m+1$) by just looking at the $\Lambda^{[m]}$ matrix, and we can translate this form trivially to the left, right or mixed canonical form, which is why we will refer to this form just as *canonical* form.

In the case of an area law quantum state, we argued in equation (1.7) that for every (arbitrary large) system size N we can truncate the Schmidt values at some finite χ without causing an error bigger than some $\varepsilon \ll 1$. We can now apply this truncation to the χ largest Schmidt values at every bond by truncating all Λ's to matrices of maximal size $\chi \times \chi$ and also discarding the corresponding rows and columns of the Γ matrices.

Again notice, that this is the reason why the MPS formalism works so good and why algorithms like DMRG (see later) are so successful for one-dimensional gapped systems, where all ground states obey the area law.

To conclude what we gained by using the MPS formalism compared to the coefficient tensor $c_{\boldsymbol{s}}$ remember that in equation (1.2) we need to keep track of d^N coefficients (which scales exponential in system size). The MPS (1.8) in comparison only needs N tensors of maximal dimension $d \times \chi \times \chi$ to approximate area law quantum states efficiently. These

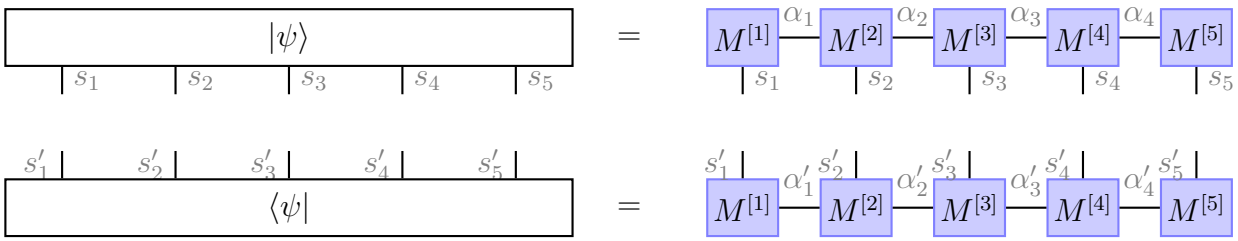

Figure 1.1: General quantum state $|\psi\rangle$ and $\langle\psi|$ represented as MPS.

are in total $Nd\chi^2$ entries, which only scales linear in system size. Moreover, we will see additional advantages of using the MPS formalism, such as that applying an onsite operation on a site i is as simple as multiplying the onsite operator to the local tensor $M^{[i]}$.

MPS as tensor network

As promised we will now introduce a more convenient way of representing a MPS by drawing them as tensor networks. In figure 1.1 one can see a quantum state $|\psi\rangle$ written in MPS form.

A general tensor is denoted as a rectangle, where the number of legs connecting a rectangle corresponds to the rank of the tensor. Vertical legs will always correspond to physical indices, which we denoted so far with s_i, where i corresponded to the lattice site. Horizontal legs will always correspond to bond indices, which so far were denoted by Greek letters, e.g. α_i, where in this case i labeled the bond number (the bond connecting site i with site $i+1$ is denoted as bond i). Indices of legs connecting two tensors are summed over. Furthermore, since the sum of the indices is clear by the leg itself and which tensors it connects, we will often omit to write the leg indices.

A *ket* vector $|\psi\rangle$ will always be drawn with physical legs going to the bottom, while the hermitian conjugate *bra* vector $\langle\psi|$ will be drawn with physical legs going to the top. Additional an asterisk (*) will note the complex conjugation of all tensor elements, while the transposition of tensors is always taken care of by appropriately connecting the legs. Furthermore, in the most cases we will try to stick to the convention of labelling the bond and physical indices of a *bra* vector with an additional prime ($'$) and not using any primes for indices of a *ket* vector. Trivial/Dummy indices, which only run over one value, like α_0 of $M^{[1]}$ for the finite MPS are usually not depicted.

With this graphical representation in mind the whole SVD process, starting from the single tensor $c_{\boldsymbol{s}}$ and ending up with a MPS in left canonical form, is depicted in figure 1.2.

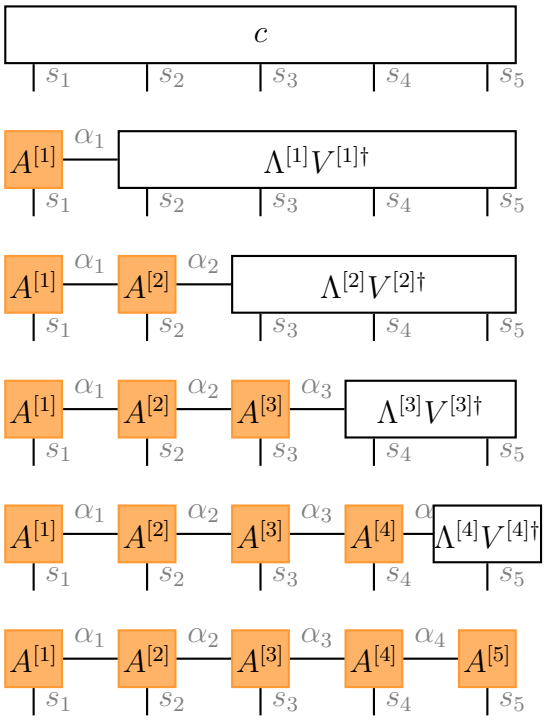

Figure 1.2: Graphical representation of the SVD steps to rewrite the single coefficient tensor $c_{\boldsymbol{s}}$ of a quantum state $|\psi\rangle$ to a MPS representation in left canonical form.

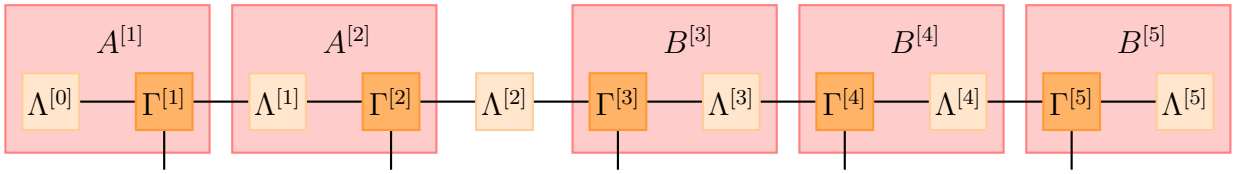

Figure 1.3: Graphical representation of a MPS in (mixed) canonical form. One can also see how the A and B tensors are build from the Γ and Λ tensors.

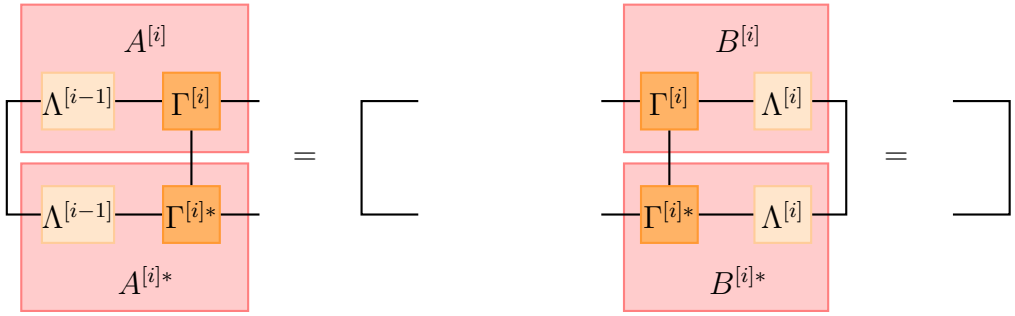

(a) Left normalized condition.

(b) Right normalized condition.

Figure 1.4: Graphical representation of the left and right normalized conditions for the A and B tensors, which can also be interpreted as eigenvalue equations with eigenvalue 1.

A MPS in (mixed) canonical form as in equations (1.25) and (1.28) will be depicted like in figure 1.3.

Also the semi-unitary conditions for the A and B tensors are represented graphically in figure 1.4. By looking at this representation we can interpret the semi-unitary condition for the A and B tensors as eigenvalue equations.
The tensor $A^{[i]s_i}A^{[i]s_i\dagger}$ (i.e. $\sum_{s_i} A^{[i]s_i}_{\alpha_i,\alpha_{i+1}} A^{[i]s_i*}_{\alpha'_i,\alpha'_{i+1}}$) has a left eigenvector $\mathbb{1}$ (i.e. $\delta_{\alpha_i,\alpha'_i}$) with eigenvalue 1. And $B^{[i]s_i}B^{[i]s_i\dagger}$ (i.e. $\sum_{s_i} B^{[i]s_i}_{\alpha_i,\alpha_{i+1}} B^{[i]s_i*}_{\alpha'_i,\alpha'_{i+1}}$) has a right eigenvector $\mathbb{1}$ (i.e. $\delta_{\alpha_{i+1},\alpha'_{i+1}}$) with eigenvalue 1.

Note that we are speaking of eigenvalue equations for rank 4 tensors and eigenvectors of rank 2. One can however always think of combining pairs (or even multiple) indices to one new index such that one ends up with a more usual eigenvalue equation with matrices of rank 2 and vectors of rank 1.

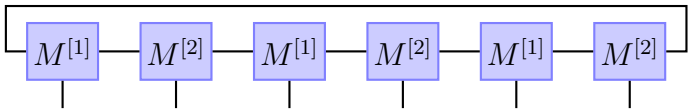

Figure 1.5: Graphical representation of a periodic MPS for a system with $N = 6$ sites and a unit cell of $t = 2$.

MPS boundary conditions

So far we considered a finite system without any translation invariance, therefore at every site i the tensor $M^{[i]}$ might differ from all others, and we draw a generic MPS (1.8) like in figure 1.1.

If we consider a periodic system and a quantum state with a unit cell of t sites (i.e. the quantum state is translation invariant for a shift of t) we can also write the MPS in a periodic way by also using a unit cell structure. Let us assume the system size is $N = n \cdot t$, then we can write the MPS out of n equal blocks, where each block is the MPS for one unit cell $M^{[1]} \dots M^{[t]}$. In total, we can then write the MPS as following

$$|\psi\rangle = \sum_{\boldsymbol{s}} \mathrm{tr}\left[\left(M^{[1]s_1} \dots M^{[t]s_t}\right)\left(M^{[1]s_{t+1}} \dots M^{[t]s_{t+t}}\right) \dots\dots \left(M^{[1]s_{(n-1)t+1}} \dots M^{[t]s_N}\right)\right] |\boldsymbol{s}\rangle \ . \tag{1.29}$$

Here the first and last bond dimension are not dummy indices anymore but can have a dimension $\chi_0 = \chi_{N+1}$, and therefore we need to take the trace of the matrix product to get a coefficient. Graphically we will denote taking the trace by an additional bond between site 1 and site N as shown in figure 1.5.

This notation will furthermore help us to treat translation invariant infinite systems. We can simply expand the periodic MPS with an infinite number of unit cells at the left and right, which then gives us as an infinite MPS (iMPS), which we can write as following

$$|\psi\rangle = \sum_{\boldsymbol{s}} \mathrm{tr}\left[\dots \left(M^{[1]s_{k+1}} \dots M^{[t]s_{k+t}}\right) \dots\right] |\boldsymbol{s}\rangle \ . \tag{1.30}$$

Graphically we will represent an iMPS like in figure 1.6. This iMPS representation allows us to treat infinite systems by just storing t tensors. How to exactly treat the left and right infinite products of these tensors we will see in more detail later when we introduce the transfer matrix.

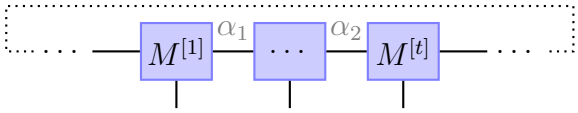

Figure 1.6: Graphical representation of an iMPS for an infinite periodic system.

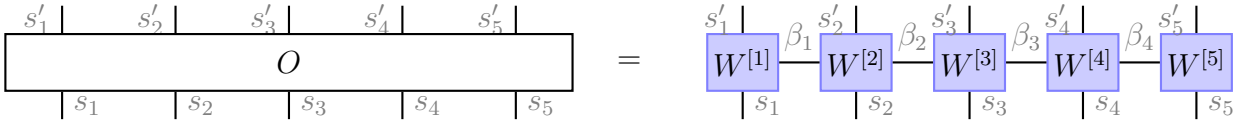

Figure 1.7: Graphical representation of a MPO.

Matrix product operator

Analog to the MPS we can also define a matrix product operator (MPO)

$$O = \sum_{\boldsymbol{s},\boldsymbol{s}'} W^{[1]s_1 s'_1} W^{[2]s_2 s'_2} \ldots W^{[N]s_N s'_N} \left|\boldsymbol{s}\right\rangle \left\langle \boldsymbol{s}'\right| , \tag{1.31}$$

which can also be drawn as a tensor network as in figure 1.7. Note that the operators $W^{[i]}$ are rank 4 tensors and thus have a physical leg to the top and bottom.

As for the MPS it also can be shown that every operator can be written in the form of a MPO. Furthermore, the modifications for special boundary conditions of a MPS can straightforwardly be applied to a MPO as well.

Simple single site operators as well as products of single site operators are trivially already in the MPO form. However, it is not straightforward how to construct the MPO for the sum of such terms (which we will typically need to do to construct the MPO of a Hamiltonian). Without going into detail how to construct the MPO for a specific Hamiltonian, the interested reader is advised to have a look at [18], let us mention that increasing the interaction range of a Hamiltonian (e.g. instead of looking at only nearest neighbor interactions also taking next nearest neighbor interactions (and so on) into account) will in many cases linearly increase the bond dimension of the MPO. However, for exponential decaying interactions there often is a representation with low bond dimensions. This can be used to approximate long range interactions (with a polynomial decaying coupling strength) by fitting it to a sum of exponential decaying interactions.

Applying a MPO to a MPS now is as simple as connecting the corresponding legs and summing over the corresponding indices (which effectively is multiplying the tensors together). This can be seen in figure 1.8. The resulting MPS would have now bond

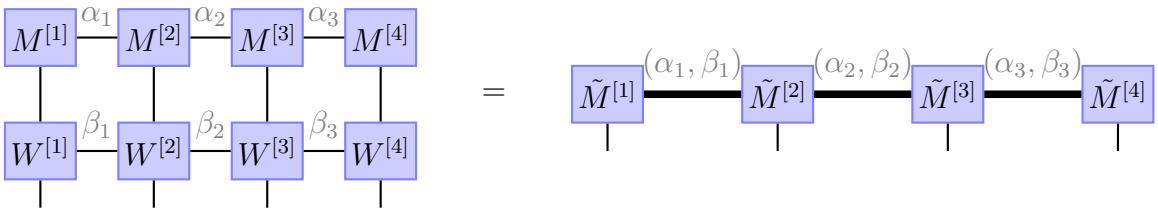

Figure 1.8: Graphical representation of a MPO applied to a MPS. The bond indices of the resulting MPS are given by a combination of the bond indices of the original MPS and MPO.

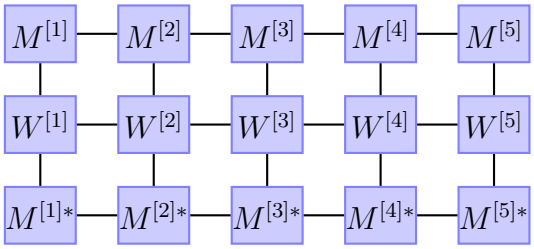

Figure 1.9: Graphical representation of an expectation value for a general MPS and MPO.

dimensions that are simply given by the product of the bond dimensions of the MPS and MPO, since now every bond index is described by two bond indices of the previous MPS and MPO before. However, in practice we are mostly not interested in the resulting MPS but in some expectation value, which can then be evaluated by also multiplying a *bra* vector from the bottom onto the operator, as can be seen in figure 1.9.

The evaluation of such an expectation value becomes especially easy if the MPS is given in a mixed canonical form (with the canonical center being at site m) and we are only interested at the expectation value of locally acting operators at site m. Then we can apply the eigenvalue equations of the A and B tensors (see figure 1.4) at the left and right to simplify the tensor network. This can be seen for a finite MPS and a simple onsite expectation value of the operator O acting on site m in figure 1.10. To evaluate expectation values for an iMPS we first need to introduce the transfer matrix.

Transfer matrix

As introduced earlier in the translation invariant infinite case the iMPS is written in a repeating structure of unit cells consisting of t different tensors $M^{[i]}$ with $i \in \{1 \dots t\}$

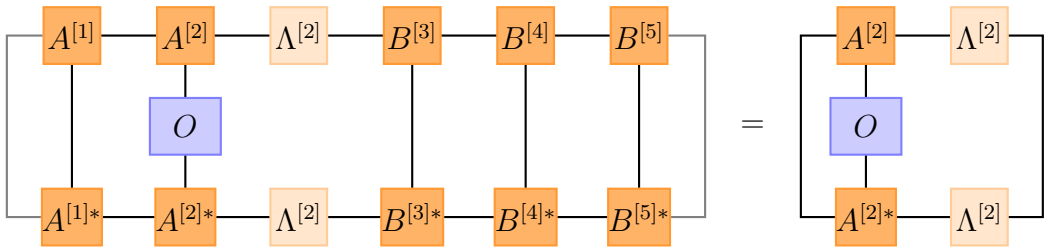

Figure 1.10: Graphical representation of the onsite expectation value, of an operator O acting on site m, for a finite MPS given in mixed canonical representation. The tensor network can be significantly simplified by using the eigenvector equations of figure 1.4.

like in equation (1.30). We can also write the iMPS in a canonical form

$$\begin{aligned} |\psi\rangle &= \sum_{\boldsymbol{s}} \mathrm{tr}\left[\dots \left(A^{[1]s_1}\dots A^{[t]s_t}\right)\dots\right]|\boldsymbol{s}\rangle \\ &= \sum_{\boldsymbol{s}} \mathrm{tr}\left[\dots \Lambda^{[0]}\Gamma^{[1]s_1}\dots\Lambda^{[t-1]}\Gamma^{[t]s_t}\dots\right]|\boldsymbol{s}\rangle\ . \end{aligned} \tag{1.32}$$

For simplicity, we will consider here only the left canonical form with A tensors, but keep in mind that we can always write $A^{[i]s_i} = \Lambda^{[i-1]}\Gamma^{[i]s_i}$, and from this we can also get to a right canonical form with B tensors.

Furthermore, we define the transfer matrix (TM) as

$$\begin{aligned} T_{(\alpha_0,\alpha_0'),(\alpha_t,\alpha_t')} &= \sum_{s_1,\dots,s_t} \left(A^{[1]s_1}\dots A^{[t]s_t}\right)^*_{\alpha_0',\alpha_t'} \left(A^{[1]s_1}\dots A^{[t]s_t}\right)_{\alpha_0,\alpha_t} \\ &= \sum_{s_1,\dots,s_t} \left(\Lambda^{[0]}\Gamma^{[1]s_1}\dots\Lambda^{[t-1]}\Gamma^{[t]s_t}\right)^*_{\alpha_0',\alpha_t'} \left(\Lambda^{[0]}\Gamma^{[1]s_1}\dots\Lambda^{[t-1]}\Gamma^{[t]s_t}\right)_{\alpha_0,\alpha_t}\ , \end{aligned} \tag{1.33}$$

which for $t = 2$ is also shown in figure 1.11 (already as part of an eigenvalue equation).

Note that with the iMPS formalism we are only interested in pure states, which are not *cat states* (*cat states* are a superposition of macroscopic different states). For this pure states the largest eigenvalue of the TM is unique and can be normalized to 1, such that also the quantum state is properly normalized $\langle\psi|\psi\rangle = 1$.

We can now again look at the eigenvectors of the TM for the largest eigenvalue 1. After comparing to the left eigenvector of the A tensors (see equation (1.20) and figure 1.4) we find that for the eigenvalue 1 the left eigenvector of the TM is $\mathbb{1}$ (i.e. $\delta_{\alpha_0,\alpha_0'}$, see figure 1.11). Looking at the right eigenvector of the B tensors (see equation (1.23) and figure 1.4) we find that for the TM the right eigenvector is $\left(\Lambda^{[0]}\right)^2$ (i.e. $\left(\Lambda^{[0]}\right)^2_{\alpha_t,\alpha_t'}$ see figure 1.11). Note that for the right eigenvector we used $\Lambda^{[t]} = \Lambda^{[0]}$.

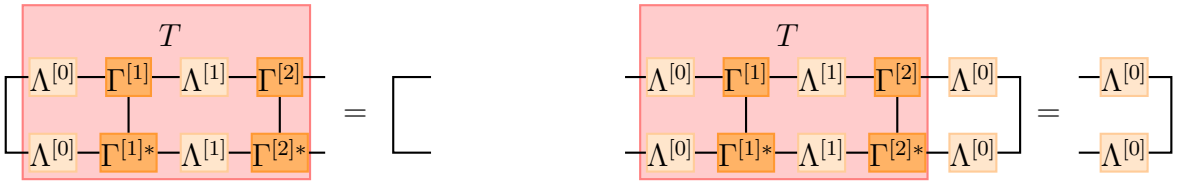

(a) Left eigenvector. **(b)** Right eigenvector.

Figure 1.11: Graphical representation of the left and right eigenvectors of the TM for a unit cell of size $t = 2$.

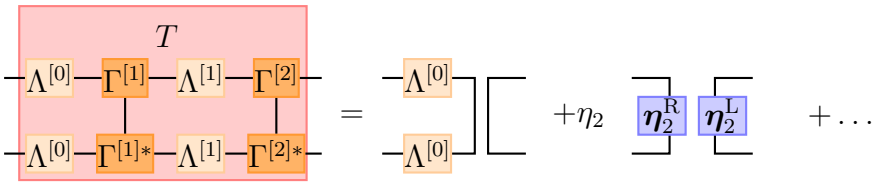

Figure 1.12: Graphical representation of the TM decomposition (for $t = 2$), where only the two largest terms (eigenvalue 1 and the second-largest eigenvalue η_2) are drawn.

We can then expand the TM in terms of the eigenvalues and eigenvectors

$$T_{(\alpha_0,\alpha_0'),(\alpha_t,\alpha_t')} = \left(\Lambda^{[0]}\right)^2_{\alpha_0,\alpha_0'} \delta_{\alpha_t,\alpha_t'} + \eta_2 \left(\boldsymbol{\eta}_2^{\mathrm{R}}\right)_{\alpha_0,\alpha_0'} \left(\boldsymbol{\eta}_2^{\mathrm{L}}\right)_{\alpha_t,\alpha_t'} + \ldots, \tag{1.34}$$

where 1 is the largest eigenvalue and all other eigenvalues η_i (ordered by magnitude) have a smaller magnitude $|\eta_i| < 1$ for all $i \geq 2$. The corresponding left (right) eigenvectors are $\boldsymbol{\eta}_i^{\mathrm{L\ (R)}}$. This expansion is also depicted in figure 1.12.

If we now want to calculate the expectation value of operators acting only at a finite number of sites of the iMPS we note that at the left and right of these operators there will still be an infinite number of TMs. With the above decomposition, and since 1 is the largest eigenvalue, this infinite number of TMs simplifies to the dominant left and right eigenvectors (to the eigenvalue 1) as shown in figure 1.13. We skipped the step of calculating the trace, which evaluates to 1, since $\sum_{\alpha_i} \left(\Lambda^{[0]}_{\alpha_i,\alpha_i}\right)^2 = 1$ is normalized. We end up with the same form as for the expectation value in the finite case.

Let us now look at the expectation value for a correlation function. Therefore, we consider two operators O_i^A and O_j^B acting locally on a single site but at two apart sites i and j, with $d = \lfloor |i-j| / t \rfloor$ unit cells (and thus TMs) between the two sites. We can now not only simplify the infinite TMs at the left and right, but can also expand the TMs between the two sites i and j. This is shown in figure 1.14.

First, note that for $d \to \infty$ the correlation functions converges to

$$\lim_{|i-j|\to\infty} \langle\psi| O_i^A O_j^B |\psi\rangle = \langle\psi| O_i^A |\psi\rangle \langle\psi| O_j^B |\psi\rangle \ . \tag{1.35}$$

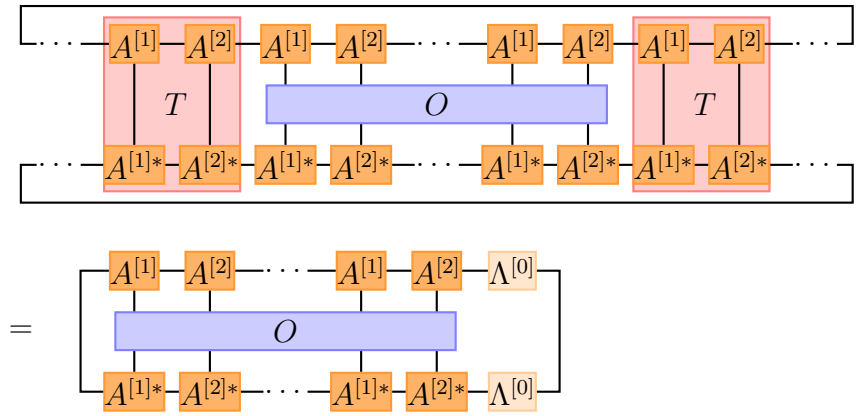

Figure 1.13: Graphical representation of an expectation value for an infinite system. The infinite TMs at the left and right simplify to the dominant eigenvector given by the expansion in figure 1.12.

If we choose O^A and O^B properly we can use this to distinguish symmetry broken and symmetric phases. However, we cannot use these correlation functions with local operators O^A and O^B to identify different symmetric (trivial or topological) phases.

Secondly, note that for large distances d the decay of the correlation function is determined by the second-largest eigenvalue of the TM and is independent on the measured operators themselves. Thus, we define the correlation length

$$\xi = -\frac{tR}{\log|\eta_2|}\,, \tag{1.36}$$

where t is the unit cell size and R the distance between two sites.

Pollmann and Turner introduced in [22] also a generalized transfer matrix (gTM) to study the symmetry of one-dimensional SPT states and the projective phase factors of the corresponding symmetries. We can define the gTM as

$$\begin{aligned} T^{\Sigma}_{(\alpha_0,\alpha_0'),(\alpha_t,\alpha_t')} &= \sum_{s_1,\ldots,s_t} \left(A^{[1]s_1}\ldots A^{[t]s_t}\right)^*_{\alpha_0',\alpha_t'} \Sigma_{\boldsymbol{s},\boldsymbol{s}'} \left(A^{[1]s_1}\ldots A^{[t]s_t}\right)_{\alpha_0,\alpha_t} \\ &= \sum_{s_1,\ldots,s_t} \left(\Lambda^{[0]}\Gamma^{[1]s_1}\ldots\Lambda^{[t-1]}\Gamma^{[t]s_t}\right)^*_{\alpha_0',\alpha_t'} \Sigma_{\boldsymbol{s},\boldsymbol{s}'} \left(\Lambda^{[0]}\Gamma^{[1]s_1}\ldots\Lambda^{[t-1]}\Gamma^{[t]s_t}\right)_{\alpha_0,\alpha_t}\,, \end{aligned} \tag{1.37}$$

where $\Sigma_{\boldsymbol{s},\boldsymbol{s}'}$ a symmetry acting on a unit cell. For simplicity, let us assume a unit cell of $t = 1$ (in fact by regrouping all the sites of a unit cell to one new site living in a bigger Hilbert space, we are always able to make this simplification). This gTM does in general has the largest eigenvalue η_1 with the corresponding right (and left) eigenvectors

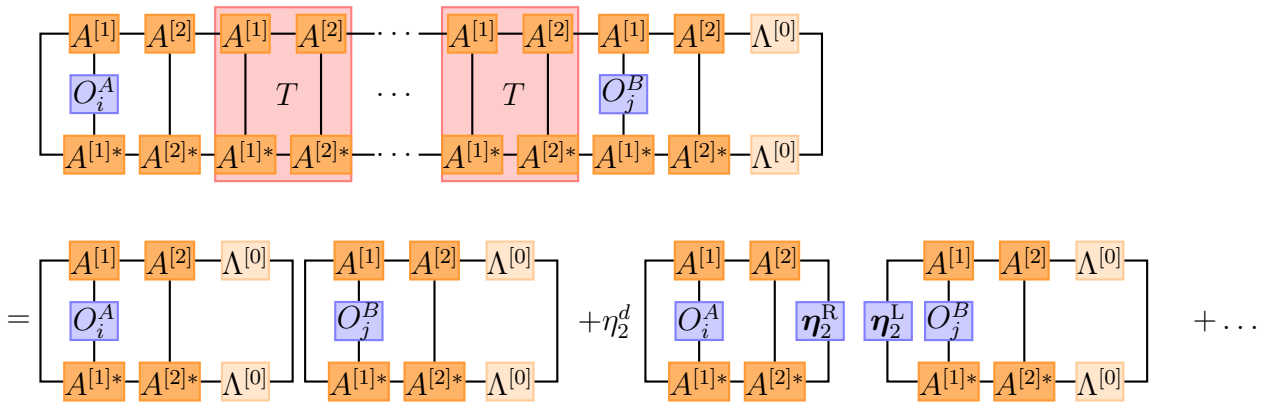

Figure 1.14: Graphical representation of a correlation function for an infinite system (with $t = 2$). O_i^A acts on site i and O_j^B at site j, and there are $d = \lfloor |i-j|/t \rfloor$ TMs between site i and j. We can expand the TM between the sites i and j which yields a constant term and exponential decaying terms.

$\boldsymbol{\eta}_1^{\mathrm{R\ (L)}}$. This is shown in figure 1.15. Note that if $|\eta_1| < 1$ then the state is not symmetric under the symmetry operation Σ, since the overlap $\langle\psi| \prod \Sigma |\psi\rangle$ would vanish for an infinite system. Furthermore, note that if $|\psi\rangle$ is invariant under the symmetry Σ it was shown [23] that there must be a projective representation of the symmetry Σ for the A tensors

$$\sum_{s'} \Sigma_{s,s'} A^{s'} = \mathrm{e}^{\mathrm{i}\theta_\Sigma} U_\Sigma^\dagger A^s U_\Sigma \,, \tag{1.38}$$

which is also shown in figure 1.16. U_Σ is a unitary matrix, that commutes with $\Lambda^{[0]}$. By inserting this projective representation to the eigenvalue equations (see figure 1.15) and comparing to the left and right eigenvector of the TM (see figure 1.11) we find for a symmetric state $|\eta_1| = 1$ that the eigenvectors are given as following. The left eigenvector to the eigenvalue $\mathrm{e}^{\mathrm{i}\theta_\Sigma}$ is the matrix U_Σ and the right eigenvector is $\Lambda^{[0]} U_\Sigma^\dagger \Lambda^{[0]}$, as can bee also seen in the last equations of figure 1.11.

By comparing this projective representation with the eigenvalue equations (see figure 1.15), we find that the projective symmetry representation U_Σ is simply given by the left eigenvector of the gTM T^Σ. Once we obtained the projective representation U_Σ for all symmetry operations of a symmetry group, we can look at the projective phase factors to distinguish different topological phases. This means we can look for all elements of the symmetry group, with $\Sigma^a \Sigma^b = \Sigma^{ab}$ at their projective representations $U_a U_b = \mathrm{e}^{\mathrm{i}\phi(a,b)} U_{ab}$. If there are projective phases $\phi(a,b) \neq 0$ that cannot be gauged away, we found a topological phase. For more details the reader is again referred to the original work [22] by Pollmann and Turner.

Finally, let us also have a look at the string order parameter in the iMPS formalism. As

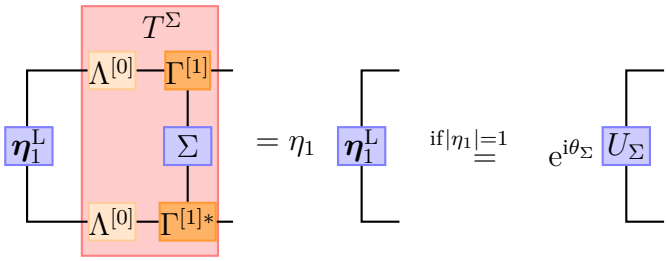

(a) Left eigenvector of the gTM T^Σ.

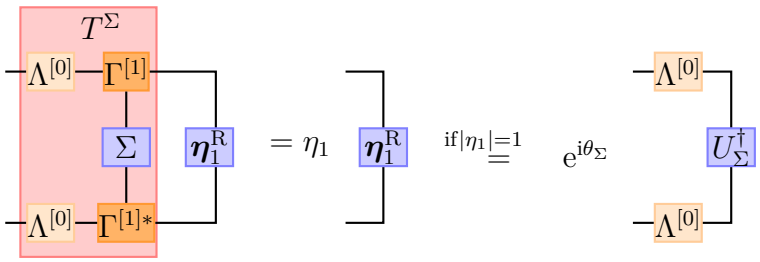

(b) Right eigenvector of the gTM T^Σ.

Figure 1.15: Graphical representation of the left and right eigenvectors with the largest eigenvalue η_1 of the gTM T^Σ (for simplicity we choose a unit cell $t = 1$). If the state is invariant under the symmetry Σ the eigenvalue is $\eta_1 = \mathrm{e}^{\mathrm{i}\theta_\Sigma}$ (with $|\eta_1| = 1$) and we can express the eigenvectors be the unitary matrix U_Σ.

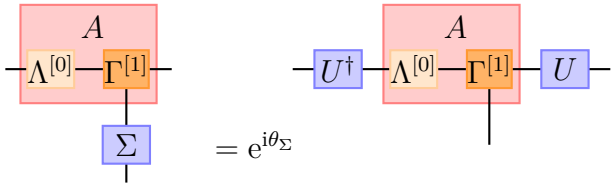

Figure 1.16: Graphical representation of the projective representation of a symmetry Σ applied to a symmetric tensor A.

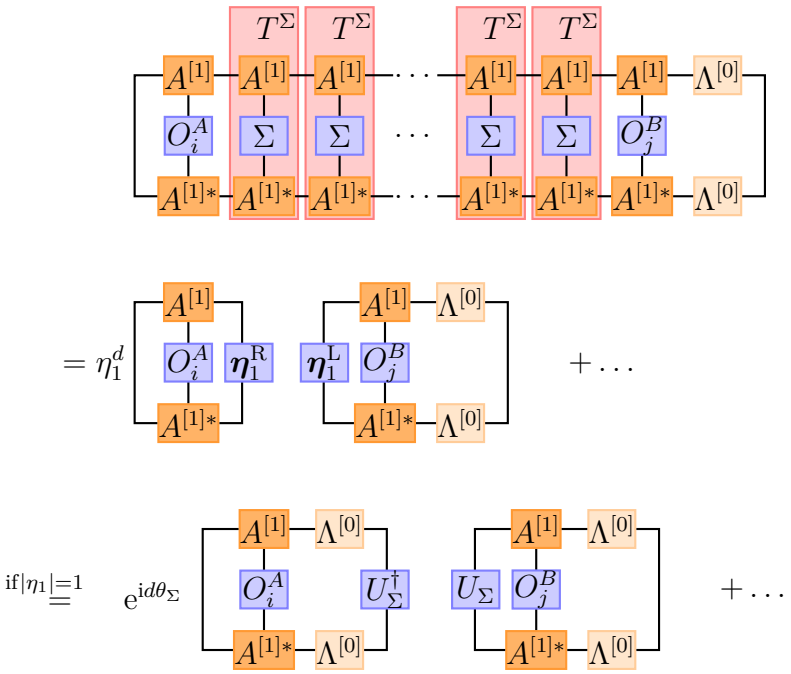

Figure 1.17: Graphical representation of the string order for an infinite system (with $t = 1$). O_i^A acts on site i and O_j^B at site j, and there is a string of Σ operators acting on the $d = |i - j - 1|$ sites in between (we choose $t = 1$). We can expand the gTM T^Σ between the sites i and j which yields for large d only one term with the dominant eigenvalue η_1. Only if the state is symmetric under Σ ($|\eta_1| = 1$) it does not vanish for $d \to \infty$. In this case the right and left eigenvectors can be expressed by the matrix U_Σ, see figure 1.15.

for the correlation function we consider two operators O_i^A and O_j^B acting at two distant sites i and j with $d = \lfloor |i - j| / t \rfloor$ unit cells between the two sites (for simplicity we again consider $t = 1$). But additionally we now apply a string of Σ operators at all sites between site i and j (see figure 1.17). As for the correlation function we can simplify the string of d unit cells between the outer local operators by now not taking the gTM to the d-th power, instead of the TM. Hence, we end up with the eigenvalues and eigenvectors of the gTM instead of the TM (as can bee seen in figure 1.17). For large d we see that the string order is only nonzero if $|\eta_1| = 1$, which means that the state is symmetric under the Σ. Furthermore, if the state is symmetric the string order simplifies for large d as can be seen in figure 1.17.

1.2.3 Density matrix renormalization group

After we now learned how to profit from a MPS and use it to calculate expectation values and other properties, we still do not know how to find the ground states of a Hamiltonian in the first place. Therefore, we will shortly explain the famous and powerful tool of the density matrix renormalization group (DMRG), which was introduced by White in 1992 [24, 25]. Nowadays, one can understand the DMRG method also within the MPS formalism, which we will also use to illustrate the DMRG method.

First, let us consider a Hamiltonian H which acts on a system of N sites and can be represented as MPO $H = \sum_{\boldsymbol{s},\boldsymbol{s}'} W^{[1]s_1 s'_1} W^{[2]s_2 s'_2} \ldots W^{[N]s_N s'_N} |\boldsymbol{s}\rangle \langle \boldsymbol{s}'|$. Furthermore, we expect the ground state of the system to be in a gapped phase.

We know that every quantum state $|\psi\rangle$ must fulfill

$$\langle\psi| H |\psi\rangle = E_\psi \geq E_0 = \langle\psi_0| H |\psi_0\rangle \ , \tag{1.39}$$

where E_0 is the energy of the ground state $|\psi_0\rangle$. We can therefore consider $|\psi\rangle$ as a variational ansatz, which we try to optimize by minimizing the energy E_ψ. However, a fully generic quantum state would have too many degrees of freedom to efficiently optimize the quantum state to finally find the ground state (or a state very close to the ground state). To circumvent this problem the basic idea of DMRG is to optimize the quantum state iteratively only at two neighboring sites and then sweeping over all sites, repeating this procedure until the energy converged. To be able to optimize a quantum state locally at two sites, it seems handy to treat the quantum state in the MPS formalism. In the following we are going to describe this optimization process in more detail within the MPS framework.

We start our optimization scheme with some initial guess $|\psi\rangle = \sum_{\boldsymbol{s}} M^{[1]s_1} M^{[2]s_2} \ldots M^{[N]s_N} |\boldsymbol{s}\rangle$ with a fixed maximal bond dimension χ of the matrices $M^{[i]s_i}$. The energy of this state is then simply given by the expectation value of the Hamiltonian, which we can calculate using the MPS and MPO notation like in figure 1.9. To optimize this energy locally at the first two sites, we calculate an effective Hamiltonian H^{eff}, that only acts on these two sites, by contracting all other legs of the Hamiltonian and our guess quantum state $|\psi\rangle$, as depicted in figure 1.18. We therefore end up with the effective two site Hamiltonian $(H^{\text{eff}})^{s_1,s_2,s'_1,s'_2}_{\alpha_0,\alpha_2,\alpha'_0,\alpha'_2}$.

To optimize the total E_ψ we can now simply calculate the smallest eigenvalue of H^{eff} and the corresponding eigenvector $\Theta^{s_1,s_2}_{\alpha_0,\alpha_2}$. Since we are only interested in the smallest eigenvalue and vector one can use an iterative algorithm, like the Lanczos algorithm, to calculate this ground state. And one can use the tensor $\Theta_{\text{init}} = M^{[1]} M^{[2]}$ as an initial guess, since after a few sweeps, this should already be close to the actual ground state.

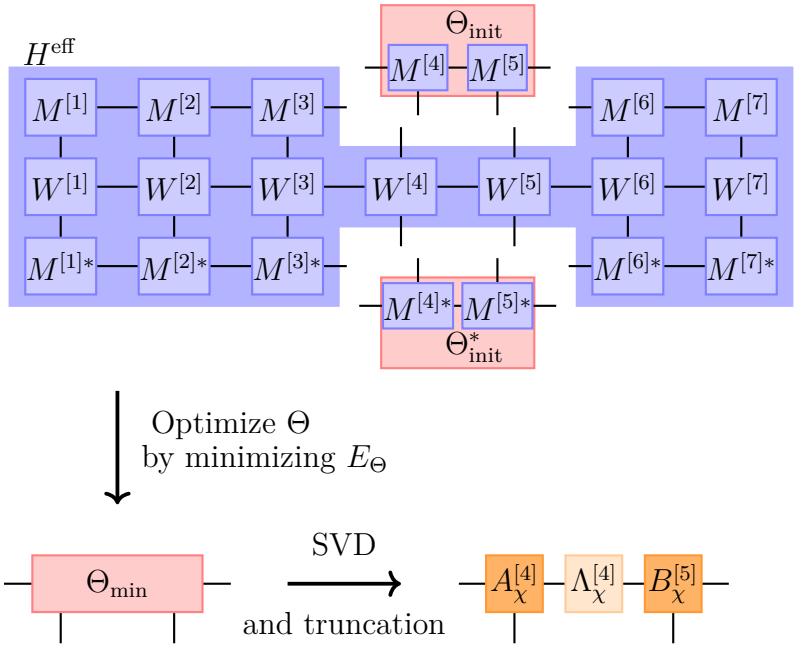

Figure 1.18: Schematic picture of one optimization process of the DMRG algorithm. After one successful step we optimize the MPS at the next sites (5 and 6) and sweep through the whole MPS, until the energy converges.

Note that this calculation of the smallest eigenvalue and vector is the computational most expensive part of the DMRG algorithm. After we found the smallest eigenvalue with eigenvector Θ_{min} we need to write our total quantum state $|\psi\rangle$ with the new Θ_{min} back as a MPS, which means that we need to decompose Θ_{min} into tensors corresponding to the two sites 1 and 2. We already know how to do that by applying a SVD

$$\Theta_{\text{min}} = A^{[1]}\Lambda^{[1]}B^{[2]} \approx A^{[1]}_\chi \Lambda^{[1]}_\chi B^{[2]}_\chi \,. \tag{1.40}$$

Importantly after the SVD the tensors $A^{[1]}$ and $B^{[2]}$ will likely have a higher dimension as our maximal chosen bond dimension χ. Thus, in the second step we truncate the matrices $A^{[1]}$, $\Lambda^{[1]}$ and $B^{[2]}$ to the χ largest singular values of $\Lambda^{[1]}$, since these also correspond to the largest Schmidt values.

Now we can repeat this optimization at site 2 and 3, and sweeping through all sites until the energy converges. One schematic DMRG optimization can also be seen in figure 1.18.

We conclude this discussion of the DMRG algorithm with some additional notes.
First, note that since we are applying a SVD every time we move from one to the next site we automatically find the MPS in a canonical form, which is quite convenient for

calculating expectation values and the entropy as discussed before (since we are then able to use the right and left eigenvalue equations for the A and B tensors, see figure 1.4). Secondly, note that we actually do not have to calculate all contractions for the effective Hamiltonian at each site, but can store and reuse them by storing left and right environments of a site, which correspond to a contraction of all legs from the Hamiltonian as well as the *bra* and *ket* vectors to the left or right of the given site. With this trick for every new effective Hamiltonian we only have to calculate the contraction of one site onto the right or left environment.
Furthermore, note that for an efficient algorithm it might be useful to start with a rather small maximal bond dimension and then increase the allowed bond dimension slowly up to the wanted maximal bond dimension. This makes the early sweeps much faster to roughly approximate the ground state and then slowly increases the accuracy of the MPS approximation.
Finally, we note that in the finite case the DMRG algorithm can actually also be used to calculate iteratively excited states, after one already found the ground state. This can be done by doing another DMRG simulation, where we orthogonalize the MPS against the already found ground state. For example, one could add an energy penalty to the Hamiltonian in the subspace of the already found ground (and lower excited) states.

Infinite DMRG

The DMRG method can indeed be generalized to find the ground state of an infinite system by using the iMPS representation. Since the basic idea remains the same we do not want to repeat a detailed explanation for the infinite DMRG (iDMRG) algorithm, the interested reader may look at [19]. But rather we shortly mention the key differences to the normal DMRG sweep. First, if we expect a t periodic ground state we only use t sites in our iDMRG sweep and start our algorithm with a t site periodic MPS (note that for a periodic MPS the first and last bond dimension can be larger than 1). After then again doing updates at the different sites we need to introduce one additional update, where we optimize the two sites t and 1. Furthermore, the way we achieve a convergence against the infinite ground state is by artificially growing the MPS by multiplying the periodic MPS once at the left edge and once at the right edge onto our t tensors and keeping only track of them by storing them as left and right environments, but only sweeping through the middle t tensors and updating them. Once the algorithm converged we can use the t tensors as building blocks for our iMPS like in the form of equation (1.30).

Note that one has to be very careful to keep track of what the energy of this growing system actual means to find a useful convergence criteria, see [19] for more details.

1.3 Spin algebra

In this section we are going to recap some basics about spin. Furthermore, we will introduce some important operators and symmetry groups. Finally, we will then define the for our model important order parameters, which will become very helpful when discussing the phase diagrams.

1.3.1 Basics

Generally the spin of a particle can be described by the spin operator $\hat{\boldsymbol{S}} = \left(\hat{S}^x, \hat{S}^y, \hat{S}^z\right)^{\mathrm{T}}$. Every component of this vector is a self-adjoint operator, and they satisfy the following commutation relations

$$\left[\hat{S}^\alpha, \hat{S}^\beta\right] = \mathrm{i} \sum_\gamma \epsilon_{\alpha\beta\gamma} \hat{S}^\gamma \,, \tag{1.41}$$

where $\epsilon_{\alpha\beta\gamma}$ is the Levi-Civita symbol. Furthermore, two spin operators acting on different spins always commute

$$\left[\hat{S}_i^\alpha, \hat{S}_j^\beta\right] = 0 \text{ for all } i \neq j \,. \tag{1.42}$$

We can also define the raising and lowering operators

$$\hat{S}^\pm = \hat{S}^x \pm \mathrm{i}\hat{S}^y \,. \tag{1.43}$$

From equation (1.41) we then find the following relations

$$\begin{aligned} \left[\hat{S}^z, \hat{S}^\pm\right] &= \pm \hat{S}^\pm \\ \left[\hat{S}^+, \hat{S}^-\right] &= 2\hat{S}^z \,. \end{aligned} \tag{1.44}$$

The spin quantum number S is given by $\hat{\boldsymbol{S}}^2 = S(S+1)$. It is a positive (half) integer value. The spin operators act on the Hilbert space $\mathcal{H}_{\text{local}}$, which is of the dimension $d = 2S + 1$. A convenient basis choice are the eigenstates of the $\hat{S}^z$ operator $\mathcal{B} = \{|s\rangle\}_{s=S,S-1,\ldots,-S}$. For this basis states one can find the following relations

$$\begin{aligned} \hat{S}^z |s\rangle &= s\,|s\rangle \\ \hat{S}^\pm |s\rangle &= \sqrt{S(S+1) - s(s\pm 1)}\,|s\pm 1\rangle \,. \end{aligned} \tag{1.45}$$

Spin 1/2

For spin $S = 1/2$ particles one usually calls the basis states

$$\begin{aligned} &\mathcal{B}_{S=1/2} = \{|\uparrow\rangle, |\downarrow\rangle\} \\ &\text{with} \quad S^z|\uparrow\rangle = \frac{1}{2}|\uparrow\rangle \quad \text{and} \quad S^z|\downarrow\rangle = -\frac{1}{2}|\downarrow\rangle . \end{aligned} \tag{1.46}$$

Furthermore, the spin operators for $S = 1/2$ particles can then be written in this basis as

$$S^{(x,y,z)}_{S=1/2} = \frac{1}{2}\sigma^{(x,y,z)} \quad \text{and} \quad S^{\pm} = \sigma^{\pm}, \tag{1.47}$$

where σ are the Pauli matrices

$$\begin{aligned} \sigma^x = \begin{pmatrix} 0 & 1 \\ 1 & 0 \end{pmatrix}, \quad \sigma^y = \begin{pmatrix} 0 & -\mathrm{i} \\ \mathrm{i} & 0 \end{pmatrix}, \quad \sigma^z = \begin{pmatrix} 1 & 0 \\ 0 & -1 \end{pmatrix}, \\ \sigma^+ = \begin{pmatrix} 0 & 1 \\ 0 & 0 \end{pmatrix} \quad \text{and} \quad \sigma^- = \begin{pmatrix} 0 & 0 \\ 1 & 0 \end{pmatrix}. \end{aligned} \tag{1.48}$$

Spin 1

However, for the most part of this work, we will be interested in the spin $S = 1$ case, where there are three basis states

$$\begin{aligned} &\mathcal{B}_{S=1} = \{|s\rangle\}_{s=+1,0,-1} = \{|+\rangle, |0\rangle, |-\rangle\} \\ &\quad \text{with } S^z|+\rangle = |+\rangle , \quad S^z|0\rangle = 0 \quad \text{and} \quad S^z|-\rangle = -|-\rangle . \end{aligned} \tag{1.49}$$

The spin operators for $S = 1$ particles in this basis are written as following

$$\begin{aligned} S^x = \frac{1}{\sqrt{2}}\begin{pmatrix} 0 & 1 & 0 \\ 1 & 0 & 1 \\ 0 & 1 & 0 \end{pmatrix}, \quad S^y = \frac{1}{\sqrt{2}}\begin{pmatrix} 0 & -\mathrm{i} & 0 \\ \mathrm{i} & 0 & -\mathrm{i} \\ 0 & \mathrm{i} & 0 \end{pmatrix}, \quad S^z = \begin{pmatrix} 1 & 0 & 0 \\ 0 & 0 & 0 \\ 0 & 0 & -1 \end{pmatrix}, \\ S^+ = \sqrt{2}\begin{pmatrix} 0 & 1 & 0 \\ 0 & 0 & 1 \\ 0 & 0 & 0 \end{pmatrix} \quad \text{and} \quad S^- = \sqrt{2}\begin{pmatrix} 0 & 0 & 0 \\ 1 & 0 & 0 \\ 0 & 1 & 0 \end{pmatrix}. \end{aligned} \tag{1.50}$$

Note that whenever we just write S^γ instead of $S^\gamma_{S=1}$ we refer to spin 1 operators.

Projection operators

We will encounter at different places the need to use projection operators, which is why we will introduce here all the projection operators we might need at a later point.

First, when introducing the AKLT model in the next section, we will encounter the projection operator to the spin $S = 2$ subspace $P^{S=2}$. Here we are going to show how to derive a representation of this projection operator in the basis of two spin $S = 1$ particles i and j, which we will then write as $P^{S=2}_{i,j}$. The total spin of the two spin $S = 1$ particles can be $S_{\text{total}} = 0, 1, 2$. Furthermore, this total spin is given by $\left(\hat{\boldsymbol{S}}_{\text{i}} + \hat{\boldsymbol{S}}_{\text{j}}\right)^2 = \hat{\boldsymbol{S}}^2_{\text{total}} = S_{\text{total}}(S_{\text{total}} + 1)$.

This also means that the action of the operator $\hat{\boldsymbol{S}}^2_{\text{total}}$ in the subspaces $S_{\text{total}} \in \{0, 1, 2\}$ is just given by a scalar multiplication. These scalars are given in table 1.1,

Table 1.1: Relations for the spin $S = 2$ projector.

S_{total}	$\hat{\boldsymbol{S}}^2_{\text{total}}$	$P^{S=0}_{i,j}$	$P^{S=1}_{i,j}$	$P^{S=2}_{i,j}$
0	0	1	0	0
1	2	0	1	0
2	6	0	0	1

Since $\hat{\boldsymbol{S}}^2_{\text{total}}$ is different in each subspace we can multiply different terms like $\left(\hat{\boldsymbol{S}}^2_{\text{total}} - J(J+1)\right)$, where J is the value of the subspaces we do not want to project to (i.e. 0 and 1). Thus, for $P^{S=2}_{i,j}$ by properly normalizing we end up with

$$\begin{aligned} P^{S=2}_{i,j} &= \frac{1}{6}\hat{\boldsymbol{S}}^2_{\text{total}}\frac{1}{4}\left(\hat{\boldsymbol{S}}^2_{\text{total}} - 2\right) \\ &= \frac{1}{2}\left(\hat{\boldsymbol{S}}_i\hat{\boldsymbol{S}}_j + \frac{1}{3}(\hat{\boldsymbol{S}}_i\hat{\boldsymbol{S}}_j)^2 + \frac{2}{3}\right), \end{aligned} \tag{1.51}$$

where we used for the spin 1 particles $\hat{\boldsymbol{S}}^2_{i(j)} = S_{i(j)}(S_{i(j)} + 1) = 2$.

For describing the ground state of the AKLT model, we will also need the projector to the spin $S = 1$ space. This we will need to project the total Hilbert space of two spin $S = 1/2$ particles to the subspace of $S_{\text{total}} = 1$ (ignoring the spin $S_{\text{total}} = 0$ subspace of the addition of two spin 1/2 particles). We could follow the same procedure as for the spin $S = 2$ projector. However, we are not interested in the representation of this projector with spin $S = 1/2$ operators, but rather want to write the projection operator in *bra-ket* notation. For that we use the knowledge, that the antisymmetric combination of two spin $S = 1/2$ particles forms the spin $S_{\text{total}} = 0$ sector ($|S_{\text{total}} = 0, s = 0\rangle = (\langle\uparrow\downarrow| - \langle\downarrow\uparrow|)/\sqrt{2}$).

And moreover the other three symmetric combinations form the spin $S_{\text{total}} = 1$ sector as follows

$$|S_{\text{total}} = 1, s = +1\rangle = |+\rangle = \langle\uparrow\uparrow| \ , \quad |S_{\text{total}} = 1, s = -1\rangle = |-\rangle = \langle\downarrow\downarrow| \ ,$$
$$|S_{\text{total}} = 0, s = 0\rangle = |0\rangle = \left(\langle\uparrow\downarrow| + \langle\downarrow\uparrow|\right)/\sqrt{2} \, . \tag{1.52}$$

Thus, we can write the $S_{\text{total}} = 1$ projector as follows

$$P_{i,j}^{S=1} = |+\rangle \langle\uparrow_i\uparrow_j| + |0\rangle \frac{\langle\uparrow_i\downarrow_j| + \langle\downarrow_i\uparrow_j|}{\sqrt{2}} + |-\rangle \langle\downarrow_i\downarrow_j| \ . \tag{1.53}$$

Furthermore, for convenience of notation we will later also use the projectors of two spin 1 particles to their different total magnetization $S_i^z + S_j^z = s_{\text{total}}$. These projection operators we will denote by $P^{s_{\text{total}}}$ and we can write their representation for two spin $S = 1$ particles i and j as following

$$\begin{aligned}
P_{i,j}^{\pm 2} &= |\pm_i \pm_j\rangle \langle\pm_i \pm_j| \\
&= \frac{1}{4}\left(S_i^z S_j^z \pm S_i^z S_j^z (S_i^z + S_j^z) + (S_i^z S_j^z)^2\right) \ , \\
P_{i,j}^{\pm 1} &= |\pm_i 0_j\rangle \langle\pm_i 0_j| + |0_i \pm_j\rangle \langle 0_i \pm_j| \\
&= \frac{1}{2}\left(\pm(S_i^z + S_j^z) + (S_i^z)^2 + (S_j^z)^2 \mp S_i^z S_j^z (S_i^z + S_j^z) - 2(S_i^z S_j^z)^2\right) \ , \\
P_{i,j}^{0} &= |+_i -_j\rangle \langle+_i -_j| + |0_i 0_j\rangle \langle 0_i 0_j| + |-_i +_j\rangle \langle-_i +_j| \\
&= 1 - \left((S_i^z)^2 + (S_j^z)^2\right) - \frac{1}{2} S_i^z S_j^z + \frac{3}{2}\left(S_i^z S_j^z\right)^2 \ .
\end{aligned} \tag{1.54}$$

Note that the operator representations can be obtained similar to the spin $S = 2$ projector, by making a table for the operator $\hat{S}_{\text{total}}^z = \hat{S}_i^z + \hat{S}_j^z = s_{\text{total}}$ and the different subspaces $s_{\text{total}} \in \{+2, +1, 0, -1, -2\}$.

1.3.2 Symmetries

The Haldane phase is a symmetry protected topological phase. There are three symmetry groups to consider as protective symmetries of the Haldane phase. Thus, we will introduce these symmetries here as well as their relevant representation for our spin 1 chain.

D_2 symmetry

The D_2 symmetry group describes all possible combinations of π rotations around any of the three x, y or z axis. The D_2 symmetry group has four elements, which we will

denote by $\{e, X, Z, XZ\}$. Note that the combined π rotations about the x and z axis is equivalent to a π rotation around the y axis.

The representations $R^{(x,y,z)}$ of the π rotations in the spin $S = 1$ Hilbert space are given by $R^{(x,y,z)} = \mathrm{e}^{\mathrm{i}\pi S^{(x,y,z)}}$ and can be written in the usual basis $\mathcal{B}_{S=1} = \{|+\rangle, |0\rangle, |-\rangle\}$ as following

$$R^x = \begin{pmatrix} 0 & 0 & -1 \\ 0 & -1 & 0 \\ -1 & 0 & 0 \end{pmatrix}, \quad R^y = \begin{pmatrix} 0 & 0 & 1 \\ 0 & -1 & 0 \\ 1 & 0 & 0 \end{pmatrix} \quad \text{and} \quad R^z = \begin{pmatrix} -1 & 0 & 0 \\ 0 & 1 & 0 \\ 0 & 0 & -1 \end{pmatrix}. \tag{1.55}$$

Again it is sufficient to only use R^x and R^z, since $R^y = R^x R^z$. Therefore, the D_2 symmetry group is given in the $S = 1$ representation by the following elements $\{\mathbb{1}, R^x, R^z, R^x R^z\}$.

Time reversal symmetry

The time reversal (TR) symmetry group only has two elements $\{e, \mathrm{TR}\}$. Time reversal acts on spins by flipping their sign

$$\mathrm{TR}\, \hat{S}^{(x,y,z)}\, \mathrm{TR} = -\hat{S}^{(x,y,z)}. \tag{1.56}$$

The TR operation can be represented in the $S = 1$ Hilbert space as anti-unitary operator T

$$T = \mathrm{e}^{\mathrm{i}\pi S^y} K = R^y K, \tag{1.57}$$

where K denotes the complex conjugation operator. Therefore, the TR symmetry group is given in the spin $S = 1$ representation by the following elements $\{\mathbb{1}, T\}$.

Inversion symmetry

The inversion symmetry group also has two elements $\{e, \mathcal{I}\}$. Inversion symmetry is only defined for a chain of spins. For a chain of length N inversion about the center is defined as

$$\mathcal{I}\, \hat{S}_i^{(x,y,z)}\, \mathcal{I} = \hat{S}_{N+1-i}^{(x,y,z)}. \tag{1.58}$$

1.3.3 Order parameters

In this subsection we are going to introduce and define all important quantities and order parameters, which we will later use to discuss the different phases.

Local order parameter

Let us start with local long range order parameters, which are used to characterize symmetry broken phases. A general local order parameter can be defined as the expectation value of two operators O^A and O^B acting on two sites i and j

$$\mathcal{O}_{i,j}(O^A, O^B) = \langle\psi| O_i^A O_j^B |\psi\rangle \ . \tag{1.59}$$

For translational invariant systems only the site distance $d = |i - j|$ is important for the expectation value, and thus we will replace in these cases the index (i, j) by d. Furthermore, if we consider a local order parameter with $O = O^A = O^B$ we will only write $\mathcal{O}_d(O)$.

To discuss different phases and phase transitions one normally is interested in the thermodynamic limit of the long range order parameter by taking the limit $d \to \infty$. However, for the numerical discussion we are restricted to finite distances d. Nevertheless, most local order parameters in gapped phases are converging fast, and there convergence to the thermodynamic value is given by a typical correlation length ξ, which also can be numerically determined in the iMPS formalism (see equation (1.36)). Thus, using finite distances is fine to discuss the local order parameters in gapped phases, for gapless phases (where the correlation length typically is diverging) one should however be careful whether these order parameters already converged at the chosen finite distance.

In particular, we will often be interested in the ferromagnetic order parameter, and will refer to it by

$$\mathcal{O}_d^{\mathrm{FM},\alpha} = \mathcal{O}_d(S^\alpha) = \langle\psi| S_i^\alpha S_{i+d}^\alpha |\psi\rangle \ . \tag{1.60}$$

String order parameter

The string order parameter is a non-local order parameter, which in addition to the local order parameter also acts on all the sites between the site i and j with a symmetry operator Σ [23, 26]. We define the string order parameter as following

$$\mathcal{S}_{i,j}(\Sigma, O^{\mathrm{A}}, O^{\mathrm{B}}) = -\langle\psi| O_i^{\mathrm{A}} \left(\prod_{k=i+1}^{j-1} \Sigma_k \right) O_j^{\mathrm{B}} |\psi\rangle \ . \tag{1.61}$$

Note that the minus sign is just convention (it is chosen such that the string order parameters for the AKLT state are positive). Again we use the shorthand notation $\mathcal{S}_d(\Sigma, O) = \mathcal{S}_{1,1+d}(\Sigma, O, O)$ for translational invariant systems and if both operators acting on site $i = 1$ and $j = 1 + d$ are the same.

In particular, we will mainly be interested in two kinds of string order parameters. First, the original introduced string order parameter $\mathcal{S}_d(R^\alpha, S^\alpha)$, which we will also refer to as odd string order parameter and if we do not specify odd or even we will also always refer to this odd string order parameter. Moreover, to distinguish different symmetric phases it is also useful to look at the even string order parameter $\mathcal{S}_d(R^\alpha, \mathbb{1})$. The names *odd* and *even* refer to the parity of the operators at site i and j. It has been discussed [22], that actually the vanishing of one of these string order parameters and the non-vanishing of the other is what characterizes a SPT. The selection rule, which string order parameter vanishes in which phase depends on the projective symmetry phase factors, which we already discussed in section 1.2 and will also be defined below (see equation (1.65)). For more details on this the interested reader is referred to the original work [22] by Pollmann and Turner.

Symmetry factor and phase factor

Additional to the string order parameters we will also use two other quantities to characterize a SPT.

First, we define a symmetry factor $\mathcal{R}^\Sigma$, which tells us if a state is invariant under a certain symmetry. We define the symmetry factor for an iMPS state as largest (in terms of absolute value) eigenvalue of the generalized transfer matrix T^Σ

$$\mathcal{R}^\Sigma = \eta_1 = \max_{\eta,|\star|} \left[\boldsymbol{\eta}^{\mathrm{L}}_{\alpha_0,\alpha_0'} T^\Sigma_{(\alpha_0,\alpha_0'),(\alpha_t,\alpha_t')} \boldsymbol{\eta}^{\mathrm{R}}_{\alpha_t,\alpha_t'} \right] . \tag{1.62}$$

If this symmetry factor is $\left|\mathcal{R}^\Sigma\right| = 1$, the state is invariant under the symmetry Σ. If $\left|\mathcal{R}^\Sigma\right| < 1$ the state is not invariant under Σ and breaks the symmetry. Furthermore, if it is smaller than one, all string order parameters with Σ as string operator will decay exponentially for large distances $d = |i - j|$ with $\left|\mathcal{R}^\Sigma\right|^d$.

Secondly, we will define the phase factor $\mathcal{P}$ for the three symmetry groups D_2, TR and inversion (see again [22]). This phase factor reflects the phase of the projective representation of the symmetry group to the iMPS. It is defined to be zero if the

symmetry factor is $\left|\mathcal{R}^{\Sigma}\right| < 1$ and else given by the following expressions

$$\mathcal{P}^{\mathrm{D}_2} = \begin{cases} \frac{1}{\chi} \operatorname{tr}\left(U_{R^x} U_{R^z} U_{R^x}^{\dagger} U_{R^z}^{\dagger}\right) & \text{if } \left|\mathcal{R}^{R^x}\right| = \left|\mathcal{R}^{R^z}\right| = 1 \\ 0 & \text{else} \end{cases}, \tag{1.63}$$

$$\mathcal{P}^{\mathrm{TR}} = \begin{cases} \frac{1}{\chi} \operatorname{tr}\left(U_{\mathrm{TR}} U_{\mathrm{TR}}^{*}\right) & \text{if } \left|\mathcal{R}^{\mathrm{TR}}\right| = 1 \\ 0 & \text{else} \end{cases}, \tag{1.64}$$

$$\mathcal{P}^{\mathcal{I}} = \begin{cases} \frac{1}{\chi} \operatorname{tr}\left(U_{\mathcal{I}} U_{\mathcal{I}}^{*}\right) & \text{if } \left|\mathcal{R}^{\mathcal{I}}\right| = 1 \\ 0 & \text{else} \end{cases}, \tag{1.65}$$

where the projective representations U_{Σ} is the left eigenvector $\boldsymbol{\eta}_1^{\mathrm{L}}$ of the eigenvalue $|\eta_1| = 1$, see also equation (1.38). Thus, for this three symmetry groups $\mathcal{P}$ is either 0 for a symmetry broken phase, $+1$ for a symmetric but trivial phase and -1 for a symmetric topological phase (the Haldane phase).

1.4 AKLT model

In 1987 Affleck, Kennedy, Lieb and Tasaki proposed a state, which we will also refer to as AKLT state, that does not break any symmetry and also is not in a trivial phase [16]. This state is in the same phase as the earlier by Haldane proposed spin $S = 1$ antiferromagnetic Heisenberg model in 1D [2]. Nowadays, this phase is known to be a symmetry protected topological phase and called the Haldane phase. The AKLT state is a prime example for this Haldane phase, since it is an analytically solvable exact ground state of the AKLT model and also provides a lot of useful insight and understanding for the properties of the Haldane phase.

Therefore, in this section we are going to study the famous AKLT state. We will first introduce the AKLT model Hamiltonian. Then we discuss how to find its ground state and how to write the ground state as MPS. And furthermore we will discuss the characteristic properties of this AKLT ground state.

1.4.1 Model and ground state

Let us consider an infinite one-dimensional chain of spin $S = 1$ particles. The Hamiltonian of the AKLT model is then build from projection operators onto the spin $S = 2$ space for each neighboring pair of spin $S = 1$ sites. Thus, with equation (1.51) we can write the Hamiltonian as

$$H^{\mathrm{AKLT}} = \sum_i P^{S=2}_{i,i+1} = \sum_i \frac{1}{2}\boldsymbol{S}_i\boldsymbol{S}_{i+1} + \frac{1}{6}\left(\boldsymbol{S}_i\boldsymbol{S}_{i+1}\right)^2 + \frac{1}{3}\,. \tag{1.66}$$

The idea of this Hamiltonian is that its ground state must have a zero or positive energy, since the eigenvalues of the projector operators are 0 and +1. Thus, if we can construct a state, where two neighboring sites cannot have a total spin of $S = 2$, therefore all the projection operators will evaluate to 0, we found the ground state of this model with the energy being 0. This construction can be done in a clever way by picturing each spin 1 particle as symmetrized product of two spin 1/2 particles. If we now combine for each pair of neighboring sites i and $(i + 1)$ one of the spin 1/2 particles of site i and one spin 1/2 particle of site $(i + 1)$ to a singlet state $(|S = 0, s = 0\rangle = (|{\downarrow_i}{\uparrow_{i+1}}\rangle - |{\uparrow_i}{\downarrow_{i+1}}\rangle)/\sqrt{2})$, such that their total spin is $S = 0$, the remaining two spin 1/2 particles of site i and $(i+1)$ can only have a total spin of $S_{\mathrm{total}} \in \{0, 1\}$ (and not $S_{\mathrm{total}} = 2$). Thus, this constructed state is a ground state of the Hamiltonian (1.66). This state and its construction are also visualized in figure 1.19.

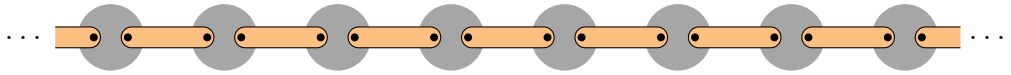

Figure 1.19: Illustration of the AKLT ground state. The black dots represent spin 1/2 particles, the gray circles depict the symmetrizing the two inner spin 1/2 particles (by applying the $P_{i,j}^{S=1}$ projector) resulting in a spin 1 particle (these are the actual sites). And the bond between two spin 1/2 particles represent the antisymmetrization of these particles, resulting in a singlet $S = 0$ state $\left(\left(|{\downarrow_i}{\uparrow_{i+1}}\rangle - |{\uparrow_i}{\downarrow_{i+1}}\rangle\right)/\sqrt{2}\right)$.

From this qualitative and pictorial description of the AKLT ground state we are also able to construct the ground state within the iMPS formalism. For this we start by writing a singlet state of two spin 1/2 particles as MPS

$$|S=0, s=0\rangle = \frac{1}{\sqrt{2}}\left(|{\downarrow_1}{\uparrow_2}\rangle - |{\uparrow_1}{\downarrow_2}\rangle\right) = \sum_{s_1,s_2} M^{[1]s_1} M^{[2]s_2} \, |s_1, s_2\rangle \ , \tag{1.67}$$

with the matrices

$$\begin{aligned} M^{[1]\uparrow} &= \begin{pmatrix} 0 & 1 \end{pmatrix} , \quad M^{[1]\downarrow} = \begin{pmatrix} 1 & 0 \end{pmatrix} \\ M^{[2]\uparrow} &= \begin{pmatrix} 1/\sqrt{2} \\ 0 \end{pmatrix} , \quad M^{[2]\downarrow} = \begin{pmatrix} 0 \\ -1/\sqrt{2} \end{pmatrix} . \end{aligned} \tag{1.68}$$

By inserting the matrices in equation (1.67) one can easily check this statement. Furthermore, we can now write a product of such singlet states in an infinite system of spin 1/2 particles as iMPS

$$\begin{aligned} |\psi_{\text{singlets}}\rangle = &\quad \ldots \quad \otimes \frac{1}{\sqrt{2}}\left(|{\downarrow}{\uparrow}\rangle - |{\uparrow}{\downarrow}\rangle\right) \otimes \frac{1}{\sqrt{2}}\left(|{\downarrow}{\uparrow}\rangle - |{\uparrow}{\downarrow}\rangle\right) \otimes \quad \ldots \\ = &\sum_{\boldsymbol{s}} \operatorname{tr}\left[\ldots M^{[1]s_{i-1}} M^{[2]s_i} M^{[1]s_{i+1}} M^{[2]s_{i+2}} \ldots\right] |\boldsymbol{s}\rangle \ , \end{aligned} \tag{1.69}$$

where at all odd sites the tensor for the iMPS is given by $M^{[1]}$, and at all even sites by $M^{[2]}$.

From this we gain the AKLT state by applying the projection operator to the spin $S = 1$ sector ($P_{i,j}^{S=1}$, see equation (1.53)) at all neighboring spin 1/2 sites, that are not combined to a singlet state (so at all even sites i with the tensor $M^{[2]}$ and their right neighbor site $(i+1)$ with the tensor $M^{[1]}$). Thus, for every two spin 1/2 particles corresponding two

one spin 1 site we get the following expression

$$\begin{aligned} & P_{i,i+1}^{S=1} \sum_{s_i, s_{i+1}} M^{[2]s_i} M^{[1]s_{i+1}} |s_i, s_{i+1}\rangle \\ & = |+\rangle M^{[2]\uparrow} M^{[1]\uparrow} + |0\rangle \frac{M^{[2]\uparrow} M^{[1]\downarrow} + M^{[2]\downarrow} M^{[1]\uparrow}}{\sqrt{2}} + |-\rangle M^{[2]\downarrow} M^{[1]\downarrow} \\ & = \frac{1}{\sqrt{2}} \sigma^+ |+\rangle + \frac{1}{2} \sigma^z |0\rangle - \frac{1}{\sqrt{2}} \sigma^- |-\rangle \,. \end{aligned} \tag{1.70}$$

Due to the projection operators this state is not normalized anymore. We can calculate the normalization by looking at the eigenvalues of the transfer matrix, which we will do in equation (1.75). For now, we will just state the correct left normalized tensors

$$A^+ = \sqrt{\frac{2}{3}} \sigma^+ \,, \quad A^0 = \sqrt{\frac{1}{3}} \sigma^z \quad \text{and} \quad A^- = -\sqrt{\frac{2}{3}} \sigma^- \,. \tag{1.71}$$

Hence, with these tensors we can now write the AKLT ground state for an infinite system as iMPS

$$|\psi_{\text{AKLT}}\rangle = \sum_{\boldsymbol{s}} \text{tr} \left[\dots A^{s_i} \dots \right] |\boldsymbol{s}\rangle \,, \tag{1.72}$$

where now the spin indices s are the spin indices for a spin 1 state $s \in \{+, 0, -\}$. Note that this state is translation invariant.

1.4.2 Ground state properties

Let us first comment at the form of the A tensor. We remember the left and right normalized conditions for tensors in equation (1.20) and equation (1.23). By inserting our A tensor of the AKLT state we find, that the A tensor is indeed left normalized and at the same time also right normalized. This then means that the Λ matrix, which contains the Schmidt values, must be proportional to the two-dimensional identity $\mathbb{1}$, and since Λ must satisfy $\sum_\alpha \Lambda_{\alpha,\alpha} = 1$ we find the Schmidt values, as well as the Γ matrices (remember $A^s = \Lambda \Gamma^s$)

$$\Lambda = \frac{1}{\sqrt{2}} \mathbb{1} \quad \text{and} \quad \Gamma^s = \sqrt{2} A^s \,. \tag{1.73}$$

Therefore, we can calculate the entanglement entropy of a bipartition at any bond

$$S = -\sum_\alpha \Lambda_{\alpha,\alpha}^2 \log \Lambda_{\alpha,\alpha}^2 = \log 2 \approx 0.69 \,. \tag{1.74}$$

Note that the Schmidt values (and thus also the entanglement spectrum) are degenerate, which is a necessary condition for a symmetry protected topological state, as discussed in detail in [27].

Also, due to this degeneracy of the entanglement spectrum the canonical form is not uniquely defined (e.g. we could just swap the first and second right/left singular vectors and ending up with $\tilde{A}^+ = \sqrt{2/3}\sigma^-$, $\tilde{A}^0 = -\sqrt{1/3}\sigma^z$, $\tilde{A}^- = -\sqrt{2/3}\sigma^+$). However, in the following we will stick to the convention of the left normalized A tensor given by equation (1.71).

Instead of just checking equations (1.20) and (1.23) to see whether the A tensors are (left/right) normalized, we can also explicitly calculate the TM and its eigenvalues and eigenvectors. We start with the TM

$$T_{(\alpha_0,\alpha_0'),(\alpha_1,\alpha_1')} = \sum_{s\in\{+,0,-\}} A^s_{\alpha_0\alpha_1}\left(A^s_{\alpha_0'\alpha_1'}\right)^*$$

$$T = \sum_s A^s \otimes (A^s)^* = \frac{1}{3}\begin{pmatrix} 1 & & & 2 \\ & -1 & & \\ & & -1 & \\ 2 & & & 1 \end{pmatrix}, \tag{1.75}$$

where the left (right) basis of the final matrix representation of T is

$$\mathcal{B}_{\mathrm{L\,(R)}} = \{\left(\alpha_{0(1)} = 1, \alpha'_{0(1)} = 1\right)\left(\alpha_{0(1)} = 1, \alpha'_{0(1)} = 2\right)$$
$$\left(\alpha_{0(1)} = 2, \alpha'_{0(1)} = 1\right)\left(\alpha_{0(1)} = 2, \alpha'_{0(1)} = 2\right)\}. \tag{1.76}$$

Since the matrix is symmetric, the left and right eigenvectors are each others transpose, and thus we will only focus on the right eigenvectors.

Diagonalizing the matrix yields the eigenvalues $\eta_1 = 1$, $\eta_{2,3,4} = -1/3$. The corresponding (not normalized) eigenvectors are

$$\boldsymbol{\eta}_1^{\mathrm{R}} = \begin{pmatrix}1\\0\\0\\1\end{pmatrix}, \quad \boldsymbol{\eta}_2^{\mathrm{R}} = \begin{pmatrix}-1\\0\\0\\1\end{pmatrix}, \quad \boldsymbol{\eta}_3^{\mathrm{R}} = \begin{pmatrix}0\\1\\0\\0\end{pmatrix} \quad \text{and} \quad \boldsymbol{\eta}_4^{\mathrm{R}} = \begin{pmatrix}0\\0\\1\\0\end{pmatrix}. \tag{1.77}$$

We can reshape them into matrices corresponding to a mapping from α_1 to α_1'

$$\boldsymbol{\eta}_1^{\mathrm{R}} = \begin{pmatrix}1 & 0\\0 & 1\end{pmatrix}, \quad \boldsymbol{\eta}_2^{\mathrm{R}} = \begin{pmatrix}-1 & 0\\0 & 1\end{pmatrix}, \quad \boldsymbol{\eta}_3^{\mathrm{R}} = \begin{pmatrix}0 & 1\\0 & 0\end{pmatrix} \quad \text{and} \quad \boldsymbol{\eta}_4^{\mathrm{R}} = \begin{pmatrix}0 & 0\\1 & 0\end{pmatrix}. \tag{1.78}$$

and thus found our right eigenvector $\boldsymbol{\eta}_1^{\mathrm{R}} \propto \delta_{\alpha_1,\alpha_1'} \propto \Lambda_{\alpha_1,\alpha_1'}$ for the largest eigenvalue $\eta_1 = 1$. And similar one also finds the left eigenvector $\boldsymbol{\eta}_1^{\mathrm{L}} \propto \delta_{\alpha_0,\alpha_0'}$. Thus, we confirmed

that the TM is in normalized and canonical form. One note about the normalization of the eigenvectors. One could choose $\boldsymbol{\eta}_1^{\mathrm{R}} = \boldsymbol{\eta}_1^{\mathrm{L}} = \sqrt{1/2} \cdot \mathbb{1}$. However, to end up with the familiar form of the left and right eigenvectors like in figure 1.11 we can also choose $\boldsymbol{\eta}_1^{\mathrm{L}} = \mathbb{1}$ and $\boldsymbol{\eta}_1^{\mathrm{R}} = (1/2) \cdot \mathbb{1} = \Lambda^2$.

From the second-largest eigenvalues we can read of the correlation length (see equation (1.36)) $\xi = R/\log 3$.

Since the AKLT state is in a SPT phase we expect all local order parameters to vanish. Let us demonstrate this explicitly for the ferromagnetic order parameter $\lim_{d\to\infty} \mathcal{O}_d^{\mathrm{FM},z}$. From figure 1.14 we can already read off that in the thermodynamic limit ($d \to \infty$) only one constant term survives

$$\begin{aligned}
\lim_{d\to\infty} \mathcal{O}_d^{\mathrm{FM},z} &= \lim_{|i-j|\to\infty} \langle\psi_{\mathrm{AKLT}}| S_i^z S_j^z |\psi_{\mathrm{AKLT}}\rangle = \langle\psi_{\mathrm{AKLT}}| S_i^z |\psi_{\mathrm{AKLT}}\rangle \langle\psi_{\mathrm{AKLT}}| S_j^z |\psi_{\mathrm{AKLT}}\rangle \\
&= \langle\psi_{\mathrm{AKLT}}| S_i^z |\psi_{\mathrm{AKLT}}\rangle^2 = \left(A^s_{\alpha_0,\alpha_1} \Lambda_{\alpha_1,\alpha_1} S^z_{s,s'} \left(A^{s'}_{\alpha_0,\alpha_1}\right)^* \Lambda_{\alpha_1,\alpha_1}\right)^2 \\
&= \left[\frac{1}{2}\operatorname{tr}\left(A^+ \left(A^+\right)^\dagger\right) - \frac{1}{2}\operatorname{tr}\left(A^- \left(A^-\right)^\dagger\right)\right]^2 = 0\,. \qquad (1.79)
\end{aligned}$$

This also holds true for the x and y component.

Moreover, instead of local order parameters we are rather interested in the symmetry and topological properties of this state. For that let us consider the D_2 symmetry group and first look at how the π rotations R^α act on the AKLT state. We can do so by examine the generalized transfer matrix (see equation (1.37)) for a π rotation around the z axis

$$\begin{aligned}
T^{R^z}_{(\alpha_0,\alpha_0'),(\alpha_1,\alpha_1')} &= \sum_{s,s'} A^s_{\alpha_0,\alpha_1} R^z_{s,s'} \left(A^{s'}_{\alpha_0',\alpha_1'}\right)^* \\
T^{R^z} &= \sum_s R^z_{s,s'} \cdot A^s \otimes \left(A^{s'}\right)^* = \frac{1}{3}\begin{pmatrix} 1 & & & -2 \\ & -1 & & \\ & & -1 & \\ -2 & & & 1 \end{pmatrix}. \qquad (1.80)
\end{aligned}$$

We find again a largest eigenvalue of $\kappa_1 = 1$ (and thus $\mathcal{R}^{R^z} = 1$, see equation (1.62)), which means that the AKLT state is, as expected, invariant under this rotation. Furthermore, we find the corresponding left (and right) eigenvectors $\boldsymbol{\kappa}_1^{\mathrm{L\,(R)}} = (1,0,0,-1)^{(T)}$ which we again can reshape as matrix acting on the indices α_0 and α_0' (respectively α_1 and α_1')

$$\kappa_1^{\mathrm{L\,(R)}} = \begin{pmatrix} 1 & 0 \\ 0 & -1 \end{pmatrix} = \sigma^z\,. \qquad (1.81)$$

As discussed earlier (see at equation (1.38)) the left eigenvector corresponds to the projective representation U_{R^z} of the R^z rotation acting on the tensors of the MPS. Thus, we found $U_{R^z} = \sigma^z$.

Doing the same calculation for a π rotation around the x axis, yields that the AKLT state is also invariant under this rotation ($\mathcal{R}^{R^x} = 1$) and we find the eigenvector and projective representation $U_{R^x} = \sigma^x$.

The trivial elements $\mathbb{1}$ of the D_2 group will also act trivially on the MPS tensors ($U_{\mathbb{1}} = \mathbb{1}$) and the last element of the D_2 group (the combined rotation around the x axis and z axis) we define as $U_{R^xR^z} = U_{R^x}U_{R^z} = -\mathrm{i}\sigma^y$. However, keep in mind that the U matrices form a projective representation. While we already choose a convenient form for the U_{R^x} and U_{R^z} matrices, such that $U_{R^x}U_{R^x} = \mathbb{1}$ and $U_{R^z}U_{R^z} = \mathbb{1}$, we cannot gauge the phase for the $U_{R^z}U_{R^x} = \mathrm{e}^{\mathrm{i}\phi}U_{R^x}U_{R^z} = \mathrm{e}^{\mathrm{i}\phi}U_{R^xR^z}$ element away. By inserting we find $\mathrm{e}^{\mathrm{i}\phi} = -1$, this corresponds to a topological phase factor of $\mathcal{P}^{\mathrm{D}_2} = -1$ (see also equation (1.65)), and confirms that the AKLT state is in the topological Haldane phase.

One can apply a similar scheme to also determine the phase factors for the inversion as well as the TR symmetry and also finds a nontrivial phase factor $\mathcal{P}^{\mathrm{TR}} = \mathcal{P}^{\mathcal{I}} = -1$.

Last but not least, we can now also calculate the string order parameter for the AKLT state. Since we already found the representation of the π rotations U_{R^α}, we can use figure 1.17 for calculating the odd string order parameters $\mathcal{S}_d(R^\alpha, S^\alpha)$. In the thermodynamic limit $d \to \infty$ again only the first term of figure 1.17 survives, yielding

$$\begin{aligned}
\lim_{d\to\infty} \mathcal{S}_d(R^z, S^z) &= -\lim_{|i-j|\to\infty} \langle\psi_{\mathrm{AKLT}}| S_i^z \left(\prod_{k=i+1}^{j-1} R_k^z\right) S_j^z |\psi_{\mathrm{AKLT}}\rangle \\
&= -\left(A^s_{\alpha_0,\alpha_1}\Lambda_{\alpha_1,\alpha_1}(U^*_{R^z})_{\alpha_1,\alpha_1'}S^z_{s,s'}\left(A^{s'}_{\alpha_0,\alpha_1'}\right)^*\Lambda_{\alpha_1',\alpha_1'}\right) \\
&\qquad \cdot \left(A^s_{\alpha_0,\alpha_1}\Lambda_{\alpha_1,\alpha_1}(U_{R^z})_{\alpha_0,\alpha_0'}S^z_{s,s'}\left(A^{s'}_{\alpha_0',\alpha_1}\right)^*\Lambda_{\alpha_1,\alpha_1}\right) \\
&= -\frac{1}{2}\left[\mathrm{tr}\left(A^+U^*_{R^z}(A^+)^\dagger\right) - \mathrm{tr}\left(A^-U^*_{R^z}(A^-)^\dagger\right)\right] \\
&\qquad \cdot \frac{1}{2}\left[\mathrm{tr}\left(A^+(A^+)^\dagger U^T_{R^z}\right) - \mathrm{tr}\left(A^-(A^-)^\dagger U^T_{R^z}\right)\right] \\
&= \frac{4}{9}\,.
\end{aligned} \tag{1.82}$$

Doing the same calculations for the x and y odd string order parameter will also yield the same result of $\mathcal{S}_\infty(R^x, S^x) = \mathcal{S}_\infty(R^y, S^y) = 4/9$.

In fact, there is also a nice pictorial representation for the non-vanishing string order parameter of the AKLT state. Thus, let us again consider the pictorial AKLT state in figure 1.19 and let us choose one possible state of this complex AKLT state, see figure 1.20 (the actual AKLT state is build from a superposition of all different states similar to the one presented in figure 1.20). Since two neighboring spin 1/2 particles of different spin $S = 1$ sites form a singlet state, we can make an interesting observation.
If at any site both spin 1/2 pointing up (thus forming a spin $S = 1$ $|+\rangle$ state) at the next

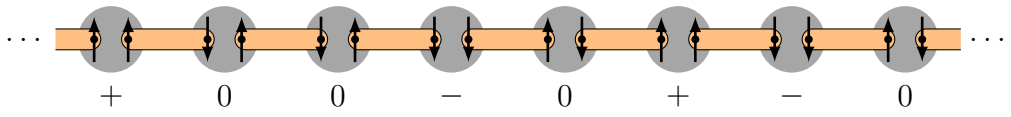

Figure 1.20: One possible spin configuration of the AKLT state. The complete AKLT state is a superposition of this and similar spin configurations. Note the hidden antiferromagnetic order (explained in the text).

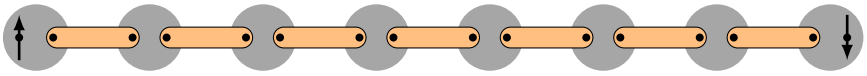

Figure 1.21: One of the four possible finite AKLT ground states with total spin magnetization 0. Note the fractional spin excitations at the edges.

spin site one of the spin 1/2 must point down (due to the singlet condition). Thus, the next site can either form a spin $S = 1$ $|0\rangle$ or $|-\rangle$ state.
In fact, at all following sites there can only be again a spin $S = 1$ $|+\rangle$ state if at some site before that there was a $|-\rangle$ state.
This is also true vise versa (exchanging $|+\rangle$ and $|-\rangle$). Thus, the overall pattern of the possible AKLT state configurations are chains, where $|+\rangle$ and $|-\rangle$ alternate (like in an antiferromagnet), but with an arbitrary number of $|0\rangle$ states in between (we will call that hidden antiferromagnetic order [28]). This arbitrary number of $|0\rangle$ states destroys the long range antiferromagnetic order. Note that the antiferromagnetic order parameter would be given as $(-1)^{|i-j|} \langle\psi| S_i^z S_j^z |\psi\rangle$. However, if instead of counting a prefactor of -1 for each site between sites i and j we only count a minus sign for each $|+\rangle$ or $|-\rangle$ state between the sites i and j we could check for the hidden antiferromagnetic order. This is exactly what the string operator $\prod_{k=i+1}^{j-1} R_k^z$ in the string order parameter is doing.

We could also calculate the even string order parameters, by replacing the S^z operators in equation (1.82) by identities $\mathbb{1}$, which for all three even string order parameters yields $\mathcal{S}_d(R^x, \mathbb{1}) = \mathcal{S}_d(R^y, \mathbb{1}) = \mathcal{S}_d(R^z, \mathbb{1}) = 0$.

Last but not least, let us also comment on the finite AKLT state. We can construct the AKLT state in a finite chain similar as for an infinite chain, see figure 1.21. This however leaves at each edge a spin 1/2 particle, which state ($|\uparrow\rangle$ or $|\downarrow\rangle$) can be chosen freely without changing the energy. Since there are four configurations to choose the two spin 1/2 degrees of freedom we find a fourfold degenerate ground state manifold, where the ground states can be distinguished by their fractional edge excitations.

1.5 Rydberg atoms

Rydberg atoms gain an increasing interest for realizing quantum many body phenomena as well as quantum information processes. One main reason for this are the strong and tunable interactions between Rydberg atoms.

In this section we are going to recap some theoretical background on the topic of Rydberg atoms. We will start with a brief discussion of the single atom energy levels as well as the effect of electric and magnetic fields. After this we will introduce the dipole-dipole interactions between two Rydberg atoms. A much more detailed introduction to Rydberg atoms can be found in [29] or [30].

To actually calculate the energies and interaction strengths for the later proposed three Rydberg states (see chapter 4) we will employ the *pairinteraction* software [31], which is a powerful tool to calculate Rydberg states, energies and interactions.

Energy spectrum and quantum defect

Rydberg atoms are atoms with one highly excited outer electron. Most commonly used are alkali atoms (e.g. Rubidium), since they already only have one electron in the outmost shell.

The highly excited electron will have a large principal quantum number n. For large n the electron will in average have a large distance to the inner electrons and the atom nucleus. Therefore, the effective potential is that of a screened nucleus with only one positive charge, and in first approximation we can treat Rydberg atoms like Hydrogen atoms, where the energy can be described by the Balmer formula $E_n = -Ry/n^2$, with the Rydberg constant $Ry \approx 13.6\,\mathrm{eV}$. For large angular momenta l this formula is accurate. However, for small angular momenta l the excited electron will also feel the inner structure of the atom, which can be taken into account by introducing the effective principal quantum number $n^* = n - \delta_{nlj}$, where δ_{nlj} is the quantum defect, that is strongly dependent on the angular momentum quantum number l (for small l the δ_{nlj} are positive, and they vanish for larger l). In addition, δ_{nlj} also accounts for the fine structure energy offsets. Thus, the energy level of Rydberg atoms can be sufficiently described by the adjusted formula

$$E = -Ry \frac{1}{(n - \delta_{nlj})^2} \,. \tag{1.83}$$

Stark effect

Adding an external electric field $\boldsymbol{E}$ will result in an additional electric interaction

$$\hat{V}_{\boldsymbol{E}} = -\hat{\boldsymbol{d}} \cdot \boldsymbol{E}\,, \tag{1.84}$$

where $\hat{\boldsymbol{d}} = e\hat{\boldsymbol{r}}$ is the electric dipole operator, which does not couple states with the same angular momentum quantum number l (due to parity reasons). Thus, for non-degenerate subspaces of l (which is the case for small l and small electric fields) we can treat the electric interaction in second order non-degenerate perturbation theory, leading to a quadratic Stark shift

$$\Delta E_{\text{Stark}} = -\frac{1}{2}\alpha \left|\boldsymbol{E}\right|^2\,, \tag{1.85}$$

where α is the polarizability, which only depends on the absolute value of the magnetic moment $|m_j|$.

However, this second order perturbation theory is only valid for small electric fields and no other interactions. The *pairinteraction* software [31] we are going to use for calculating Rydberg energies and interactions will use the exact electric interaction term (1.84) and calculates all matrix elements of it by expressing it in a spherical basis.

Zeeman effect

Adding a magnetic field $\boldsymbol{B}$ will also yield an additional magnetic interaction term

$$\hat{V}_{\boldsymbol{B}} = -\hat{\boldsymbol{\mu}} \cdot \boldsymbol{B}\,, \tag{1.86}$$

where $\hat{\boldsymbol{\mu}}$ is the magnetic dipole operator.

In weak magnetic fields and by applying first order perturbation theory this results in a linear Zeeman shift

$$\Delta E_{\text{Zeeman}} = g_j m_j \mu_{\text{B}} B\,, \tag{1.87}$$

where μ_{B} is the Bohr magneton and g_j is the Landé g-factor.

Again the *pairinteraction* software will use the exact magnetic interaction (1.86), and also includes the diamagnetic interaction term $\frac{1}{8m_e}\left|\hat{\boldsymbol{d}} \times \boldsymbol{B}\right|^2$.

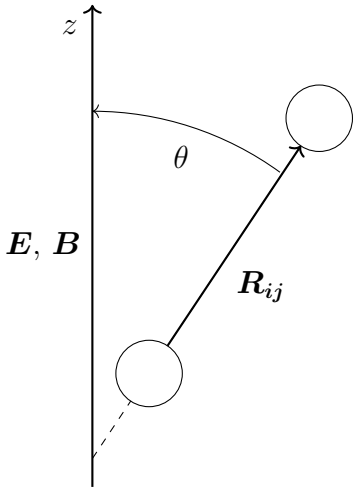

Figure 1.22: Setup of two interacting Rydberg atoms in an electric and magnetic field. We choose the quantization axis parallel to the fields.

Dipole-dipole interactions

Next we want to give a brief introduction to interactions occurring between two Rydberg atoms. For that we start with the dipole-dipole interaction operator between two Rydberg atoms i and j

$$\hat{H}_{ij}^{\mathrm{dd}} = \frac{1}{4\pi\epsilon_0}\frac{1}{R^3}\left[\hat{\boldsymbol{d}}_i \cdot \hat{\boldsymbol{d}}_j - 3\left(\hat{\boldsymbol{d}}_i \cdot \boldsymbol{r}_{ij}\right)\left(\hat{\boldsymbol{d}}_j \cdot \boldsymbol{r}_{ij}\right)\right], \tag{1.88}$$

where ϵ_0 is the electric constant, $R = |\boldsymbol{R}_{ij}|$ the interatomic distance between the two atoms and $\boldsymbol{r}_{ij} = \boldsymbol{R}_{ij}/R$ the normalized form of the relative vector $\boldsymbol{R}_{ij}$.

We can express everything in spherical coordinates

$$\boldsymbol{r}_{ij} = \begin{pmatrix} \sin\theta\cos\phi \\ \sin\theta\sin\phi \\ \cos\theta \end{pmatrix},$$
$$\hat{d}_i^0 = \hat{d}_i^z\,, \quad \hat{d}_i^{\pm} = \mp\frac{1}{\sqrt{2}}\left(\hat{d}_i^x \pm \mathrm{i}\hat{d}_i^y\right). \tag{1.89}$$

Note that we will always choose the quantization axis parallel to the electric and magnetic fields and label this axis as z axis (thus $\boldsymbol{B} = B_z\boldsymbol{e}_z$ and $\boldsymbol{E} = E_z\boldsymbol{e}_z$). The angle θ corresponds to the angle between the interatomic relative vector $\boldsymbol{R}_{ij}$ and the quantization axis, see also figure 1.22.

With that we can rewrite the dipole-dipole Hamiltonian as following [30]

$$\begin{aligned}\hat{H}_{ij}^{\mathrm{dd}} = \frac{1}{4\pi\epsilon_0}\frac{1}{R^3}\Big[&(1-3\cos^2\theta)[\hat{d}_i^0\hat{d}_j^0 + \frac{1}{2}(\hat{d}_i^+\hat{d}_j^- + \hat{d}_i^-\hat{d}_j^+)] \\ &-\frac{3}{\sqrt{2}}\sin(\theta)\cos(\theta)[\mathrm{e}^{+\mathrm{i}\phi}(\hat{d}_i^0\hat{d}_j^- + \hat{d}_i^-\hat{d}_j^0) - \mathrm{e}^{-\mathrm{i}\phi}(\hat{d}_i^0\hat{d}_j^+ + \hat{d}_i^+\hat{d}_j^0)] \\ &-\frac{3}{2}\sin^2\theta[\mathrm{e}^{+2\mathrm{i}\phi}\hat{d}_i^-\hat{d}_j^- + \mathrm{e}^{-2\mathrm{i}\phi}\hat{d}_i^+\hat{d}_j^+]\Big] \,. \end{aligned} \tag{1.90}$$

Note that the dipole operators $\hat{d}^{\pm}$ increases/decreases the magnetic quantum number m_j by 1, while $\hat{d}^0$ does not change m_j. Thus, the terms in the first row of equation (1.90) conserve the total magnetic moment $\sum m_j$, while the second (third) row corresponds to a change of the total magnetic moment by ± 1 (± 2). Furthermore, note that the terms in the second and third line are only non-vanishing if $\theta \neq 0$, which means if the interatomic axis and the electric/magnetic fields are not parallel aligned. Finally, note that the phase ϕ is only important for two-dimensional systems, where one cannot gauge them away by properly choosing the x axis. For one-dimensional chains of Rydberg atoms, which is what we are looking at in this work, one can always choose the x axis, such that angle is zero ($\phi = 0$).

2 Effective spin 1 model

In this chapter we are going to consider three energetically isolated Rydberg states to build an effective three level system. We can then map this three level system to a spin 1 particle. In doing so we will show that by using appropriate Rydberg states near to a Förster resonance the resulting energy terms and allowed interactions between the Rydberg atoms describe a variety of energy and coupling terms in the spin 1 picture.

2.1 Effective three level system

We are going to consider the following three Rydberg states, defined by there quantum numbers $|n, l, j, m_j\rangle$, and map them to the three basis states of a spin 1 particle $|s\rangle$ with $s \in \{+1, 0, -1\}$

$$\begin{aligned} |+\rangle &= \left|n^+, l^+, j^+, m_j^+\right\rangle \\ |0\rangle &= \left|n^0, l^0, j^0, m_j^0\right\rangle \\ |-\rangle &= \left|n^-, l^-, j^-, m_j^-\right\rangle . \end{aligned} \tag{2.1}$$

To energetically isolate the three Rydberg states from other states we apply homogeneous electric ($\boldsymbol{E}$) and magnetic ($\boldsymbol{B}$) fields resulting in the above discussed Zeeman and Stark shifts.

The natural spin conservation $\sum_i s_i = const$ can be enforced in the Rydberg system by choosing large energy offsets between the three different states, thus the spin conservation will correspond to energy conservation in our Rydberg system. To allow for spin conserving two particle couplings like $|00\rangle \leftrightarrow |+-\rangle$ we have to choose three Rydberg states close to a Förster resonance, i.e. the detuning $\left(2E_{|0\rangle} - E_{|+\rangle} - E_{|-\rangle}\right)$ must be small. We can summarize this by the following parameters (see also figure 2.1). We define the energy of state $|0\rangle$ as zero energy $E_{|0\rangle} = 0$ and then define the asymmetric and symmetric energy offset $\omega = (E_{|+\rangle} - E_{|-\rangle})/2$ and $D = (E_{|+\rangle} + E_{|-\rangle})/2$, such that the Rydberg energies are given as $E_{|+\rangle} = \omega + D$ and $E_{|-\rangle} = -\omega + D$. Now the spin conservation translates to having a large value of ω, which we will typically choose on the order of tens of GHz.

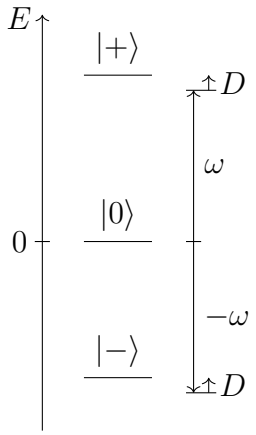

Figure 2.1: Effective three level system with the energy offsets ω and D.

And the Förster resonance condition translates to having a small value of D, which will be on the order of MHz and can be tuned by the electric and magnetic fields. We can simply translate this energy terms into spin operators yielding $\omega S^z + D(S^z)^2$, where D might be an interesting parameter, while ω does not change any physics if we already consider spin conservation.

2.2 Dipole-dipole interactions

Now we can think of how to add spin couplings by adding interactions between two atoms in the Rydberg framework. The most natural idea is to employ the dipole-dipole interactions of the Rydberg states to allow for two particle interactions.
The simplest Rydberg interaction terms are hopping terms $|+0\rangle \leftrightarrow |0+\rangle$ (respectively $|-0\rangle \leftrightarrow |0-\rangle$), which we will describe by their hopping amplitude J^{+0} (J^{-0}). To allow for such hoppings we have to choose $l^0 - l^+ = \pm 1$ ($l^0 - l^- = \pm 1$) and $\Delta m_j = 0, \pm 1$. These kinds of configuration will in general then also allow for more complicated interaction terms like $|00\rangle \leftrightarrow |+-\rangle$ (and $|00\rangle \leftrightarrow |-+\rangle$), which interaction strength we will denote by J^{00}.
Note that we want to construct a spin 1 Hamiltonian with a D_2 (as well as TR and inversion) symmetry, since we are trying to construct a Hamiltonian in the Haldane phase, which is protected by these three symmetries. To satisfy the symmetry of the R^x operator, which swaps the $|+\rangle$ and $|-\rangle$ states, a reasonable approach is to also construct the three Rydberg states symmetrically. Meaning that we only look at configurations with $\left|m_j^+ - m_j^0\right| = \left|m_j^- - m_j^0\right|$. This excludes all configurations, where $|0\rangle$ and only one of the $|+\rangle$ or $|-\rangle$ states have the same magnetic quantum number.

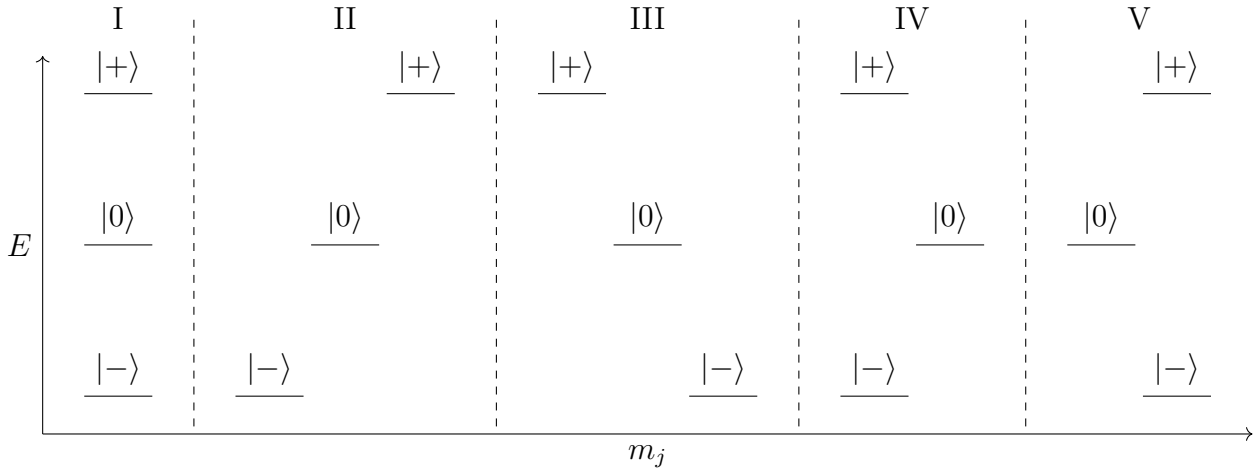

Figure 2.2: Schematic picture of the possible configurations for realizing an interacting three level system with Rydberg states. We constrain ourselves to three level systems with two approximately equal energy gaps and ignore configurations, where $|0\rangle$ and only one of the $|+\rangle$ or $|-\rangle$ states have the same magnetic quantum number.

With this in mind there are 5 possibilities to choose the m_j^s quantum numbers of the three states, which are shown in figure 2.2. Let us now discuss the resulting Rydberg interactions of these configurations. For this discussion we are going to look at the dipole-dipole interaction terms from the interaction Hamiltonian (1.90) and will ignore any effect of the electric and magnetic field to these interactions. Therefore, this is just a qualitative discussion of possible interactions, to motivate all interesting spin coupling terms we will look at in the next chapter. For the experimental proposal in chapter 4 we will calculate the interactions using the *pairinteraction* software [31], which will also take into account the effect of the electric and magnetic field. However, these later results will be in good agreement with the simplified picture presented here.

Configuration I

The first possibility is to choose all magnetic quantum numbers the same $m_j^+ = m_j^0 = m_j^-$. Therefore, the only important dipole-dipole interaction operator is $\hat{d}_i^0 \hat{d}_j^0$. This results in

the following interaction strengths

$$J^{+0} = -\frac{1}{4\pi\epsilon_0 R^3}\left(3\cos^2\theta - 1\right)\langle +0|\,\hat{d}_i^0\hat{d}_j^0\,|0+\rangle$$
$$= -\frac{1}{4\pi\epsilon_0 R^3}\left(3\cos^2\theta - 1\right)\left|\langle +|\,\hat{d}^0\,|0\rangle\right|^2 , \tag{2.2a}$$
$$J^{-0} = -\frac{1}{4\pi\epsilon_0 R^3}(3\cos^2\theta - 1)\left|\langle -|\,\hat{d}^0\,|0\rangle\right|^2 , \tag{2.2b}$$
$$J^{00} = -\frac{1}{4\pi\epsilon_0 R^3}\left(3\cos^2\theta - 1\right)\langle +-|\,\hat{d}_i^0\hat{d}_j^0\,|00\rangle$$
$$= -\frac{1}{4\pi\epsilon_0 R^3}\left(3\cos^2\theta - 1\right)\langle +|\,\hat{d}^0\,|0\rangle\cdot\langle -|\,\hat{d}^0\,|0\rangle\ . \tag{2.2c}$$

Note that to realize the Haldane phase we are trying to build a D_2 symmetric Hamiltonian. From the R^x rotation symmetry we would expect the two parameters J^{+0} and J^{-0} to be the same. For different principle quantum numbers n^s of the three states (which we will need to find a Förster resonance), J^{+0} and J^{-0} will not be exactly the same. However, for large n, and typically the same l for the $|+\rangle$ and $|-\rangle$ state the difference between J^{+0} and J^{-0} will be small. We will also study the impact of this small symmetry breaking term, which we will call $\delta = (J^{+0} - J^{-0})/2$, in the next chapter, for now let us assume these two interactions are roughly similar. Then also J^{00} will have the same absolute value $|J^{00}| = |J^{+0}| = |J^{-0}|$, and we can only tune the overall interaction strength in this configuration.

Configuration II and III

The next possibility is to choose all magnetic quantum numbers increasingly $m_j^0 = m_j^- + 1 = m_j^+ - 1$. Therefore, the important dipole-dipole interaction operators are $(\hat{d}_i^+\hat{d}_j^- + \hat{d}_i^-\hat{d}_j^+)$. This yields the following interaction strengths

$$J^{+0} = -\frac{1}{4\pi\epsilon_0 R^3}\frac{3\cos^2\theta - 1}{2}\langle +0|\,\hat{d}_i^+\hat{d}_j^-\,|0+\rangle$$
$$= \frac{1}{4\pi\epsilon_0 R^3}\frac{3\cos^2\theta - 1}{2}\left|\langle +|\,\hat{d}^+\,|0\rangle\right|^2 , \tag{2.3a}$$
$$J^{-0} = \frac{1}{4\pi\epsilon_0 R^3}\frac{3\cos^2\theta - 1}{2}\left|\langle -|\,\hat{d}^-\,|0\rangle\right|^2 , \tag{2.3b}$$
$$J^{00} = -\frac{1}{4\pi\epsilon_0 R^3}\frac{3\cos^2\theta - 1}{2}\langle +-|\,\hat{d}_i^+\hat{d}_j^-\,|00\rangle$$
$$= -\frac{1}{4\pi\epsilon_0 R^3}\frac{3\cos^2\theta - 1}{2}\langle +|\,\hat{d}^+\,|0\rangle\cdot\langle -|\,\hat{d}^-\,|0\rangle\ . \tag{2.3c}$$

We again can argue that we want J^{+0} and J^{-0} as similar as possible, which also in this configuration means, that all three parameters would have the same θ dependence and thus roughly the same absolute value $|J^{00}| = |J^{+0}| = |J^{-0}|$. Note the different sign of J^{+0} and J^{-0} for $\theta = 0$ compared to the first configuration is due to $(\hat{d}^{+})^{\dagger} = -\hat{d}^{-}$.

Configuration III, where the magnetic quantum numbers are chosen decreasingly $m_j^0 = m_j^- - 1 = m_j^+ + 1$ is analog to this configuration II.

Configuration IV and V

Now we chose the same magnetic quantum numbers for the $|+\rangle$ and $|-\rangle$ state $m_j^+ = m_j^-$ and a larger magnetic quantum number for the $|0\rangle$ state $m_j^0 = m_j^+ + 1$.

The J^{+0} and J^{-0} hopping amplitudes behave similar to the last case (note that now $\hat{d}^{+} |+\rangle \propto |0\rangle$, since the dipole operators act on the magnetic quantum number and not the mapped spin). However, the J^{00} amplitude corresponds now to a dipole-dipole interaction, where the total magnetic quantum number changes by ± 2, and is given by the dipole operators $(\hat{d}_i^{+}\hat{d}_j^{+} + \hat{d}_i^{-}\hat{d}_j^{-})$ (as explained earlier for a one-dimensional chain we can set the angle $\phi = 0$). This yields

$$
\begin{aligned}
J^{+0} &= -\frac{1}{4\pi\epsilon_0 R^3}\frac{3\cos^2\theta - 1}{2} \langle +0|\, \hat{d}_i^{-}\hat{d}_j^{+}\, |0+\rangle \\
&= \frac{1}{4\pi\epsilon_0 R^3}\frac{3\cos^2\theta - 1}{2} \left|\langle +|\, \hat{d}^{-}\, |0\rangle\right|^2 , && \text{(2.4a)} \\
J^{-0} &= \frac{1}{4\pi\epsilon_0 R^3}\frac{3\cos^2\theta - 1}{2} \left|\langle -|\, \hat{d}^{-}\, |0\rangle\right|^2 , && \text{(2.4b)} \\
J^{00} &= -\frac{1}{4\pi\epsilon_0 R^3}\frac{3}{2}\sin^2\theta \, \langle +-|\, \hat{d}_i^{-}\hat{d}_j^{-}\, |00\rangle \\
&= -\frac{1}{4\pi\epsilon_0 R^3}\frac{3}{2}\sin^2\theta \, \langle +|\, \hat{d}^{-}\, |0\rangle \cdot \langle -|\, \hat{d}^{-}\, |0\rangle \ . && \text{(2.4c)}
\end{aligned}
$$

Interestingly we find a different dependence on the angle θ for the J^{00} parameter compared to the J^{+0} and J^{-0} parameters. This will allow us to tune not only the overall strength, but also the ratio of these parameters.

Analog results can be derived for configuration V, where the magnetic quantum number of state $|0\rangle$ is chosen smaller $m_j^0 = m_j^+ - 1$ and again $m_j^+ = m_j^-$.

To summarize the dipole-dipole interactions we found three possible interactions between two Rydberg atoms J^{+0} ($|+0\rangle \leftrightarrow |0+\rangle$), J^{-0} ($|-0\rangle \leftrightarrow |0-\rangle$) and J^{00} ($|+-\rangle \leftrightarrow |00\rangle$ and $|-+\rangle \leftrightarrow |00\rangle$). We can translate these also to spin couplings. For convenience

reasons we will express these terms in the spin language dependent on the following three parameters

$$J^{xy} = \frac{J^{+0} + J^{-0}}{2}\,, \quad \delta = \frac{J^{+0} - J^{-0}}{2} \quad \text{and} \quad \delta_0 = J^{00} - \frac{J^{+0} + J^{-0}}{2}\,. \tag{2.5}$$

With these definitions the Rydberg interactions map to the following spin couplings

$$\begin{aligned} H_{ij}^{J^{xy}} &= J^{xy}\Big(|+0\rangle\langle 0+| + |+-\rangle\langle 00| + |-+\rangle\langle 00| + |-0\rangle\langle 0-|\Big) + \text{H.c.} \\ &= J^{xy}\left(S_i^x S_j^x + S_i^y S_j^y\right) = \frac{J^{xy}}{2}\left(S_i^+ S_j^- + S_i^- S_j^+\right)\,, \end{aligned} \tag{2.6}$$

$$\begin{aligned} H_{ij}^{\delta} &= \delta\Big(|+0\rangle\langle 0+| + |0+\rangle\langle +0| - |-0\rangle\langle 0-| - |0-\rangle\langle -0|\Big) \\ &= \frac{\delta}{2}\left[P_{ij}^{+1}\left(S_i^+ S_j^- + S_i^- S_j^+\right)P_{ij}^{+1} - P_{ij}^{-1}\left(S_i^+ S_j^- + S_i^- S_j^+\right)P_{ij}^{-1}\right] \\ &= \frac{\delta}{2}\left(S_i^z S_i^+ S_j^- S_j^z + \text{H.c.}\right) - \frac{\delta}{2}\left(S_i^+ S_i^z S_j^z S_j^- + \text{H.c.}\right)\,, \end{aligned} \tag{2.7}$$

$$\begin{aligned} H_{ij}^{\delta_0} &= \delta_0\Big(|+-\rangle\langle 00| + |-+\rangle\langle 00| + |00\rangle\langle +-| + |00\rangle\langle -+|\Big) \\ &= \frac{\delta_0}{2}P_{ij}^0\left(S_i^+ S_j^- + S_i^- S_j^+\right)P_{ij}^0 \\ &= \frac{\delta_0}{2}\left[-S_i^z S_i^+ S_j^z S_j^- - S_i^z S_i^- S_j^z S_j^+\right] + \text{H.c.}\,, \end{aligned} \tag{2.8}$$

where $P_{ij}^{s_{\text{total}}}$ are projection operators to the total magnetization $s_{\text{total}} = S_i^z + S_j^z$, see equation (1.54). To end up with the final form using only spin operators one can insert the equations of the projectors. However, we can also verify the equation by a simple calculation. Let us consider the $S_i^z S_i^+ S_j^- S_j^z$ term. We find $S_i^z S_i^+ |+_i\rangle = 0$ and $S_i^z S_i^+ |-_i\rangle \propto S_i^z |0_i\rangle = 0$ (and similar $S_j^- S_j^z |0_j\rangle = 0$ and $S_j^- S_j^z |-_j\rangle = 0$). Thus, the only contributing term of this operator is $S_i^z S_i^+ S_j^- S_j^z |0_i +_j\rangle = 2\,|+_i 0_j\rangle$. Similar considerations can also be done for all other terms.

Note that we did not find a dipole-dipole interaction term to mimic the spin $S_i^z S_j^z$ coupling, which would allow us to realize a spin 1 Heisenberg model. Nevertheless, as we will discuss in the next chapter it is also possible to realize the Haldane phase without a $S_i^z S_j^z$ coupling.

2.3 Van der Waals interactions

Additional to the dipole-dipole interaction terms there might also appear van der Waals interactions (second order processes) between two Rydberg atoms. In general the allowed van der Waals terms are complicated and depend on the precise choice of the Rydberg

states and the electric and magnetic fields. As second order processes the van der Waals terms scale with $1/R^6$ in the interatomic distance and also with $1/\Delta E$, where ΔE is the energy detuning of an auxiliary Rydberg state, that is used as in-between state of the second order process. For all these general van der Waals terms we assume, that they are small enough to neglect them for now (in the experimental proposal in chapter 4 we will also take these terms into account).

However, there are two van der Waals terms, which we want to discuss her in more detail. As we will see these terms can for a three level system of configuration IV be stronger than the other van der Waals interactions, because the energy gap to the involved auxiliary states is small.

To do so we will look at only one example auxiliary state, which gives rise to these two van der Waals terms via second order processes. In reality there are more than this one auxiliary state, that allows for similar second order process, we will discuss this also again in section 4.1.

In configuration IV we defined $m_j^+ = m_j^-$ and $m_j^0 = m_j^+ + 1$. For the sake of simplicity let us consider in this example $l^+ = 0, m_j^+ = 1/2$, $l^- = 0, m_j^- = 1/2$ and $l^0 = 1, m_j^0 = 3/2$. Let us also define the auxiliary Rydberg state $|v\rangle = \left|n^0, l^0, j^0, m_j^0 - 1\right\rangle$ (for example this means $l^v = 1, m_j^v = 1/2$), which is the same state as $|0\rangle$ except for a reduced magnetic moment, which is now equal to the magnetic moment of the $|+\rangle$ and $|-\rangle$ states.

By applying electric and magnetic fields we assume that we tuned the states $|00\rangle$ and $|+-\rangle$ close to resonance. However, this means also that the state $|vv\rangle$ will be nearby. For appropriate fields the energy detuning will be still large enough to treat interactions with this state in second order perturbation theory, but since the detuning ΔE will be rather small compared to other van der Waals processes this term can have a much larger amplitude then the other typical van der Waals terms.

Van der Waals interactions involving this auxiliary state $|vv\rangle$ will lead to two additional terms. First, an additional coupling of the $|+-\rangle$ and $|-+\rangle$ states, which strength we will call B, occurs via the following second order process

$$|+-\rangle \xrightarrow{\hat{d}_i^0 \hat{d}_j^0} |vv\rangle \xrightarrow{\hat{d}_i^0 \hat{d}_j^0} |-+\rangle \ . \tag{2.9}$$

The interaction strength $B_{|vv\rangle}$ resulting from this process scales like

$$B_{|vv\rangle} \propto \frac{1}{E_{|+-\rangle} - E_{|vv\rangle}} \frac{1}{R^6} \left(1 - 3\cos^2\theta\right)^2 \tag{2.10}$$

Second, similar second order processes give also rise to additional diagonal van der Waals energy terms of the state $|+-\rangle$ (respectively $|-+\rangle$), which strength we will call V^{+-}.

The corresponding second order processes are

$$\begin{aligned} |+-\rangle &\xrightarrow{\hat{d}_i^0 \hat{d}_j^0} |vv\rangle \xrightarrow{\hat{d}_i^0 \hat{d}_j^0} |+-\rangle \ , \\ |-+\rangle &\xrightarrow{\hat{d}_i^0 \hat{d}_j^0} |vv\rangle \xrightarrow{\hat{d}_i^0 \hat{d}_j^0} |-+\rangle \ . \end{aligned} \tag{2.11}$$

We find that for this specific auxiliary state $|vv\rangle$ the parameters $B_{|vv\rangle}$ and $V^{+-}_{|vv\rangle}$ are exactly the same.

As mentioned before there are other possible auxiliary states, which might even couple via different dipole operator terms, e.g. also the state $|v0\rangle$ (and $|0v\rangle$) are energetically nearby and contribute via the dipole operators $\hat{d}_i^0 \hat{d}_j^+$ and $\hat{d}_i^0 \hat{d}_j^-$. Calculating all these interactions we will leave to the *pairinteraction* software, however note that the parameters B and V^{+-} will always be nearly the same, and compared to the dipole-dipole interaction parameters J^{+0}, J^{-0} and J^{00} (scaling with $1/R^3$) the second order interactions B and V^{+-} will scale with $1/R^6$.

We will summarize these two additional van der Waals interactions by writing them in the spin 1 language

$$\begin{aligned} H_{ij}^B &= B \left(|+-\rangle \langle -+| + |-+\rangle \langle +-| \right) \\ &= \frac{B}{4} \left(S_i^+ S_i^+ S_j^- S_j^- + S_i^- S_i^- S_j^+ S_j^+ \right) \end{aligned} \tag{2.12}$$

$$\begin{aligned} H_{ij}^{V^{+-}} &= V^{+-} \left(|+-\rangle \langle +-| + |-+\rangle \langle -+| \right) \\ &= \frac{V^{+-}}{2} (S_i^z S_j^z - 1) S_i^z S_j^z \, . \end{aligned} \tag{2.13}$$

Note that we found a term involving the coupling $S_i^z S_j^z$. However, this term also includes a $S_i^z S_i^z S_j^z S_j^z$ interaction with an opposite sign, and as discussed before also the B term will have a similar strength as V^{+-}.

We will discuss how these different van der Waals terms and also the different dipole-dipole interactions (2.6) – (2.8) effect the Haldane phase in the next chapter.

3 Haldane phase discussion

In this section we want to have a detailed discussion about the Haldane phase diagram for the above introduced different interaction parameters. For that we will first introduce the Hamiltonians resulting from the couplings introduced in the last section. Then we start the discussion with a simple one-dimensional well know phase diagram, where we vary the parameter J^z of the spin coupling $S_i^z S_j^z$, which we cannot tune in our three level Rydberg system. Nevertheless, we use this phase diagram to introduce and explain the properties, which can characterize the Haldane phase and distinguish it from other phases. Once we introduced these properties we will continue by discussing two-dimensional phase diagrams for the Haldane phase, where we additionally to J^z vary a parameter which can also be tuned in the Rydberg level scheme. We will find that there are indeed other couplings than the J^z term that can stabilize the Haldane phase even for $J^z = 0$. Thus, we will end this chapter by looking at phase diagrams with $J^z = 0$ to find an optimal parameter set that we can use to realize the Haldane phase with experimentally realizable interactions.

3.1 Hamiltonian

Hamiltonian terms

In chapter 2 we introduced a three level system of Rydberg states and their energies, as well as a variety of two atom interactions for these states. We also already mapped this three level system to a spin 1 particle, and translated the Rydberg two atom interactions to spin couplings of two particles, which we expressed with spin operators.

From here on we are going to look at a chain of N spin 1 particles with a spacing R between two neighboring spins. In particular, in this chapter we will consider an infinite chain $N \to \infty$. The Hamiltonian for this spin 1 chain can then be written as sum over all single particle energies and sum over all two particle interactions. Note that for infinite systems we will consider periodic boundary conditions, while for finite systems (which we will discuss in the next chapter) we consider open boundary conditions.

The starting point for our phase discussion will be the spin 1 XXZ model, which is described by the Hamiltonian

$$H^{\mathrm{XXZ}} = \sum_{i>j} \frac{1}{|i-j|^{\alpha}} \left[\frac{J^{xy}}{2} (S_i^+ S_j^- + S_i^- S_j^+) + J^z S_i^z S_j^z \right] . \tag{3.1}$$

Here the sum runs over all pairs (i, j) of the chain with $i > j$ and the decay of the spin couplings is described by the exponent α. For $\alpha = \infty$ the model does only have nearest neighbor interactions. For Rydberg atoms we expect dipole-dipole interaction decaying with $\alpha = 3$ and van der Waals interactions with $\alpha = 6$. A detailed study of the effect of the interaction range for the spin 1 XXZ model was done in [32].

The parameter J^{xy} describes the nearest neighbor interaction strength. In chapter 2 we already discussed the possibility to realize such a term with Rydberg atoms via dipole-dipole interactions, which then would correspond to a decay with $\alpha = 3$. The term of J^z is the only coupling, that we will consider in this chapter, that cannot be realized by our three level Rydberg system. However, since the Haldane phase in the XXZ model appears for finite J^z parameters, it is a good starting point to also consider J^z. In the last part of this chapter we are then focusing on phase diagrams, where we choose $J^z = 0$.

Next we are adding the single particle energy terms to our system. We again choose the energy of state $|0\rangle$ as zero energy $E_{|0\rangle}$. Thus, leaving us with the antisymmetric energy shift described by

$$H^{\omega} = \sum_i \omega S_i^z . \tag{3.2}$$

But as discussed before, we are considering total spin conservation $\sum_i S_i^z$ and therefore this term only describes an energy offset of the nevertheless decoupled different spin sectors and does not change the phase diagram.

Additional we also apply a symmetric energy shift

$$H^{D} = \sum_i D \left(S_i^z\right)^2 . \tag{3.3}$$

We are also adding all the different interactions we found for the three Rydberg states. First, the detuning of the $|+0\rangle \leftrightarrow |0+\rangle$ and the $|-0\rangle \leftrightarrow |0-\rangle$ coupling, which we called δ and is described by

$$\begin{aligned} H^{\delta} &= \sum_{i>j} \frac{1}{|i-j|^{\alpha}} \left[\frac{\delta}{2} P_{i,j}^{+1} \left(S_i^+ S_j^- + S_i^- S_j^+ \right) P_{i,j}^{+1} - \frac{\delta}{2} P_{i,j}^{-1} \left(S_i^+ S_j^- + S_i^- S_j^+ \right) P_{i,j}^{-1} \right] \\ &= \sum_{i>j} \frac{1}{|i-j|^{\alpha}} \left[\frac{\delta}{2} \left(S_i^z S_i^+ S_j^- S_j^z + \mathrm{H.c.} \right) - \frac{\delta}{2} \left(S_i^+ S_i^z S_j^z S_j^- + \mathrm{H.c.} \right) \right] . \end{aligned} \tag{3.4}$$

Second we also consider a detuning of the $|+-\rangle \leftrightarrow |00\rangle$ (respectively the $|-+\rangle \leftrightarrow |00\rangle$) coupling from the J^{xy} parameter, which is given by

$$\begin{aligned} H^{\delta_0} &= \sum_{i>j} \frac{1}{|i-j|^{\alpha}} \frac{\delta_0}{2} P^0_{i,j} \left(S^+_i S^-_j + S^-_i S^+_j \right) P^0_{i,j} \\ &= \sum_{i>j} \frac{1}{|i-j|^{\alpha}} \frac{\delta_0}{2} \left[-S^z_i S^+_i S^z_j S^-_j - S^z_i S^-_i S^z_j S^+_j \right] + \text{H.c.}\,. \end{aligned} \tag{3.5}$$

Where both this detuning parameters δ and δ_0 describe the detuning for nearest neighbors. Since these also originate from dipole-dipole interactions the decay of these interaction strengths is typically also given by the same $\alpha = 3$ as for the J^{xy} interactions.

Last but not least, we also look at the terms, which stem from the second order processes, and therefore will have a different decay of the interaction strengths, described by α_{vdw}. For the realistic case these van der Waals interactions will decay with $\alpha_{\text{vdw}} = 6$.

First, there is the additional term, coupling the states $|+-\rangle \leftrightarrow |-+\rangle$, which is described by

$$H^B = \sum_{i>j} \frac{1}{|i-j|^{\alpha_{\text{vdw}}}} \frac{B}{4} \left(S^+_i S^+_i S^-_j S^-_j + S^-_i S^-_i S^+_j S^+_j \right) . \tag{3.6}$$

And additionally the diagonal energy term for the states $|+-\rangle$ and $|-+\rangle$, given by

$$H^{V^{+-}} = \sum_{i>j} \frac{1}{|i-j|^{\alpha_{\text{vdw}}}} \frac{V^{+-}}{2} (S^z_i S^z_j - 1) S^z_i S^z_j \,. \tag{3.7}$$

Hamiltonian symmetries

Before diving into the phase diagrams let us shortly comment on the symmetries of the above terms. The results are summarized in table 3.1 can be easily obtained by applying the symmetry rules, see section 1.3, to the different terms.

Table 3.1: Symmetries of the Hamiltonians

Hamiltonian	D_2	TR	Inversion
H^{XXZ}	✓	✓	✓
H^D	✓	✓	✓
H^{δ}			✓
H^{δ_0}	✓	✓	✓
H^B	✓	✓	✓
$H^{V^{+-}}$	✓	✓	✓

We note that only H^{δ} breaks the TR and D_2 symmetry. It has been argued for the Haldane phase, that only the D_2 symmetry protects the string order, while TR or D_2 symmetry protect the ground state degeneracy and either of TR, D_2 or inversion symmetry protect the degeneracy of the entanglement spectrum [27, 33]. Therefore, to see the string order parameter of the Haldane phase one will probably need a vanishing (or at least small) detuning δ, while we can hope to stabilize the Haldane phase by tuning the other parameters.

3.2 Phase diagram discussion

All phase diagrams have been created by running simulations, which used the TeNPy library [19] at its core to perform (i)DMRG sweeps for finding the ground state of a given Hamiltonian. In appendix B you can find some more information about the code used in this work. Note that some simulations have also been run with the ITensors library [34], which qualitatively produced the same results. Due to the lack of handling infinite systems with the iMPS and iDMRG approach, in this work only results produced with TeNPy are shown for consistency reasons. Nevertheless, the ITensors library gives a very easy and straightforward way to do DMRG calculations, and is therefore a good and instructive way to learn about DMRG simulations.

3.2.1 XXZ model - an instructive example

We start our phase diagram discussion by looking at the simple spin 1 XXZ Hamiltonian (3.1) with only nearest neighbor interactions ($\alpha = \infty$). We will choose $J^{xy} > 0$ as our energy scale and therefore this Hamiltonian only has one free parameter J^z. This model has already often been studied to have four different phases [32, 35–37], as depicted in figure 3.1. For a large positive (negative) coupling strength $J^z > 0$ ($J^z < 0$) the system belongs to the gapped antiferromagnetic (AFM) (ferromagnetic (FM)) phase. In between one can find a gapless phase, called the XY phase and our phase of interest, the gapped Haldane phase.

It seems to be a nice opportunity to show and explain the properties, which were already introduced analytically for the AKLT state in section 1.4, for an already known phase diagram, since then we can focus more on these properties. Therefore, in the following we will explore which properties we can numerically study and give some insights of how to possibly interpret these results.

Energy

The first result we get from a DMRG ground state calculation is the energy of this ground state. The ground state energies for different values of J^z can be seen in figure 3.1, where also the expected phase boundaries are already plotted, as dashed vertical lines. We will discuss these phase transition at the end of this subsection.

Note that at the phase transition from the FM to the XY phase the energy is not smooth, but the first derivate seems to be discontinuous. This is a hint at a phase transition at

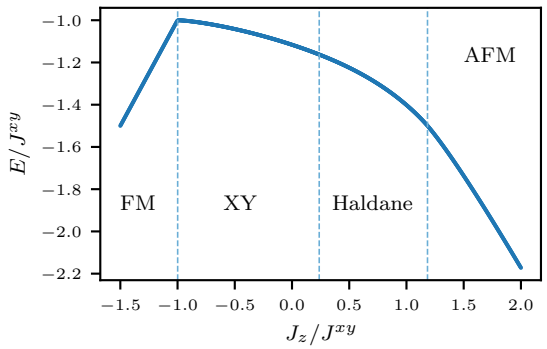

Figure 3.1: Ground state energy E for varying coupling strengths J^z. The dashed lines indicate the expected phase transitions.

this point and furthermore it suggests that this is a phase transition of first order, which corresponds to a level crossing in the energy spectrum.

Entanglement entropy

As already discussed in section 1.2 the entanglement entropy S is an important quantity to look at for doing DMRG calculations and approximating quantum states by a MPS with limited bond dimension χ. For an iMPS one takes the entanglement entropy at bond 0 (left of the first site) of the unit cell as entanglement entropy of a bipartition of the system into two half infinite chains. For finite systems (which we will look at in the next chapter) we cut the system simply at the center bond $\lfloor (N-1)/2 \rfloor$. The entanglement entropy for a maximal allowed bond dimension of $\chi = 200$ is plotted in figure 3.2a.

We already discussed that gapped one-dimensional ground states follow an area law behavior of the entanglement entropy for increasing system sizes (thus a constant value) and therefore the entanglement entropy even for infinite systems is finite. Furthermore, this finite entangled states can be approximated with a finite bond dimension, and thus we expect the entanglement entropy to quickly converge with increasing bond dimension in the gapped phases.

This is exactly what we can see in figure 3.2b, where we plotted the entanglement entropy for different maximal bond dimensions χ. If points cannot be seen they are hidden behind the points with higher bond dimension, and hence the entropy at these points already converged. As expected in the gapless XY phase the entropy does not converge at all, even for bond dimensions up to $\chi = 200$. Note that these maximal bond dimensions χ are the maximally *allowed* bond dimensions. If however the ground state

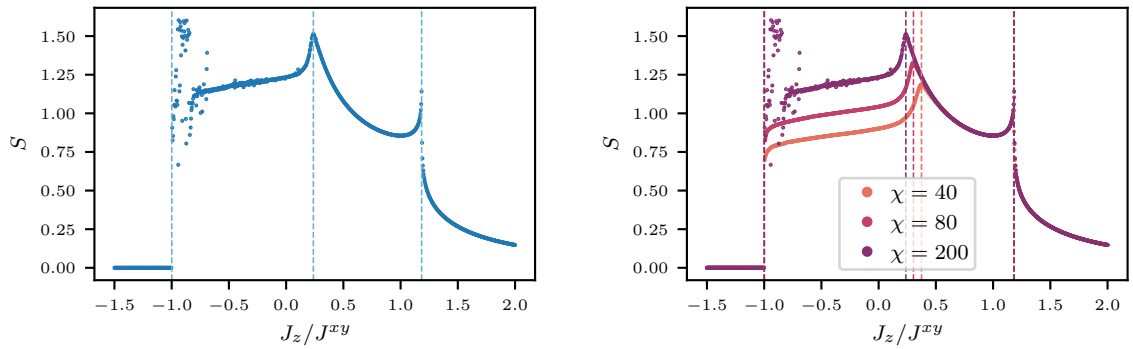

(a) Fixed bond dimension $\chi = 200$.

(b) Different bond dimensions $\chi \leq 200$.

Figure 3.2: The entanglement entropy S for varying J^z for a bipartition of the iMPS at bond 0. The dashed lines indicate the phase transitions (determined for different bond dimensions), which is discussed at the end of this subsection.

can be approximated good enough with a smaller bond dimension (because we discard all Schmidt values smaller than some tolerance), the actual bond dimensions can also be smaller, which for comparison is plotted in figure 3.3.

Interestingly one finds that at the phase transitions from the Haldane phase to the XY and the AFM phase the entropy seems to diverge and has a local maxima. Therefore, the entanglement entropy could be used to find phase transition points. Also, one can see that this local peeks in the entanglement entropy at the phase transition from the Haldane to the XY phase shifts with increasing bond dimension. This phase transition is a Berezinsky Kosterlitz Thouless (BKT) transition from a gapless to a gapped phase [38]. Thus, it will be rather challenging to find the exact phase transition point, which we will discuss later in more detail.

Finally, note that the data points in the gapless XY phase near to the FM transition do not properly converge. As already mentioned DMRG is designed to find area law ground states. In the XY phase and near to the FM transition this breaks down twice. The XY phase is gapless, which already results in a volume law ground state, and furthermore at the phase transition to the FM phase there is an energy level crossing, meaning an additional energy level coming close to the gapless ground state. This non converging data points will not only be a problem in the entanglement entropy but also in other plots. However, we will not be interested in the XY phase and therefore ignore these points.

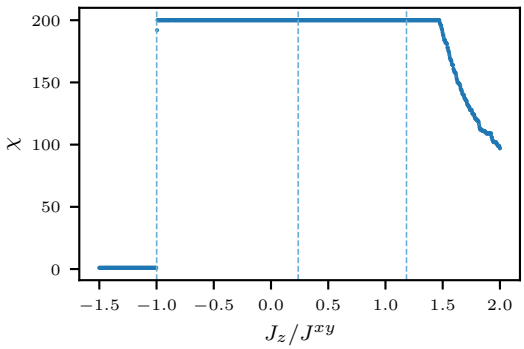

Figure 3.3: The actual bond dimension used to describe the ground state iMPS. The maximal allowed bond dimension was $\chi = 200$.

Entanglement spectrum and Schmidt degeneracy

Closely related to the entanglement entropy is the entanglement spectrum ϵ_α. While the entanglement entropy is calculated as sum over all Schmidt values $S = -\sum_\alpha \Lambda_\alpha^2 \log \Lambda_\alpha^2$ the entanglement spectrum represents the Schmidt values $\epsilon_\alpha = -\log \Lambda_\alpha^2$. Note that the smallest entanglement spectrum values ϵ_α correspond to the largest Schmidt values Λ_α. As for the entanglement entropy we again calculate the entanglement spectrum for infinite systems at bond 0 and for finite systems at bond $\lfloor (N-1)/2 \rfloor$.

In figure 3.4a the smallest entanglement spectrum values are plotted, where the color indicates the degeneracy of the points. Values $\epsilon_\alpha > 8$, which correspond to Schmidt values $\Lambda_\alpha^2 \lesssim 0.0003$, are not shown.

First, we see that the entanglement spectrum in the FM phase only consists of one value $\epsilon_1 = 0$. This can be explained because the ground state in the FM phase is a simple product state ($|\psi_{\mathrm{FM},\pm}\rangle = |\pm \pm ... \pm\rangle$) and thus can be exactly written as MPS with bond dimension 1 (see also figure 3.3), where all Λ matrices in the canonical form (1.28) are also simply matrices with only one entry 1. One can already see this also in the entanglement entropy, where $S = 0$ in the FM phase, corresponding to an unentangled product state.

Furthermore, we find a twofold degeneracy of the two smallest values in the Haldane phase. Moreover, all the entanglement spectrum values in the Haldane phase are at least double and always even degenerate. This is a feature of the symmetry protected Haldane phase and can also be generalized to other SPTs [27]. Instead of plotting the full entanglement spectrum, we can also only plot the difference of the two largest Schmidt values $\Lambda_1 - \Lambda_2$, as in figure 3.4b, and refer to it as Schmidt degeneracy. Note that if the bond dimension is 1 and there is only one Schmidt value $\Lambda_1 = 1$ we define $\Lambda_2 = 0$ to make the Schmidt degeneracy well-defined in all phases.

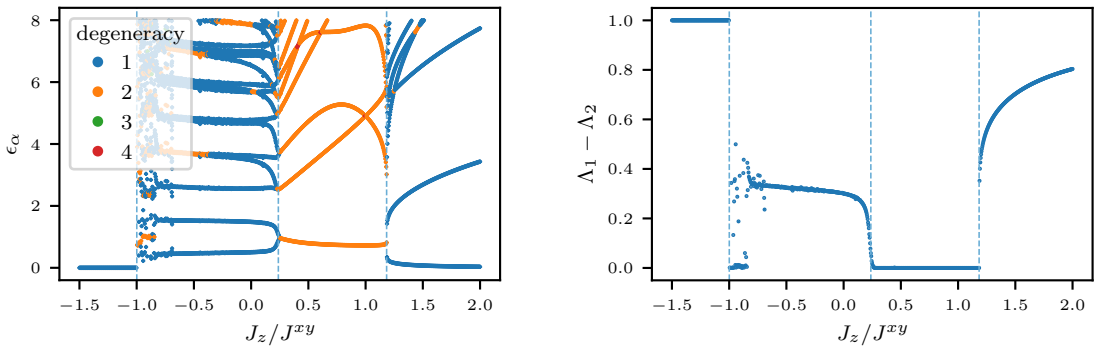

(a) Entanglement spectrum (values $\epsilon_\alpha > 8$ are not shown). The degeneracy of the entanglement spectrum is shown by different colors.

(b) Schmidt degeneracy.

Figure 3.4: Entanglement spectrum ϵ_α and Schmidt degeneracy $\Lambda_1 - \Lambda_2$ plotted for varying J^z for a bipartition of the iMPS at bond 0.

Correlation length

Next we will have a look at the correlation length ξ, as defined in equation (1.36). This is only well-defined for an translation invariant infinite system and can be calculated by simply evaluating the second-largest eigenvalue of the transfer matrix.

The correlation lengths for the XXZ model can be seen in figure 3.5a for a bond dimension of $\chi = 200$. Similar to the entanglement entropy the correlation length only converges for a gapped ground state and keeps increasing with the bond dimension in the gapless XY phase, which can be seen in figure 3.5b. We also find a local peek of the correlation length at the phase transition from the Haldane to the AFM phase. This indicates, that this phase transition is a second order phase transition.

Central charge

In fact, the divergence of the entropy and the correlation length in a gapless phase are related to each other by the central charge c [39, 40] with the following relation

$$S = \frac{c}{6} \log \frac{\xi}{R} \,. \tag{3.8}$$

By comparing the scaling of the correlation length and the entanglement entropy dependent on the bond dimension one can thus determine the central charge in the XY phase. This can be seen in figure 3.6. The central charge of the XY phase is $c \approx 1$.

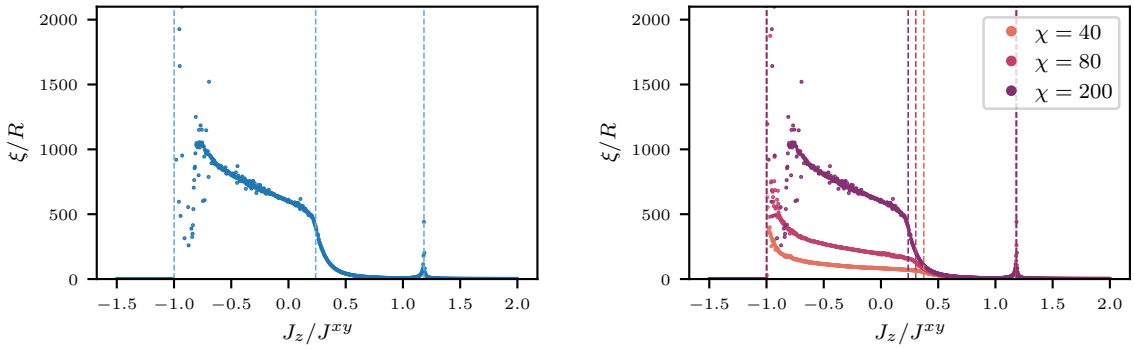

(a) Fixed bond dimension $\chi = 200$.

(b) Different bond dimensions $\chi \leq 200$.

Figure 3.5: Correlation length ξ in units of R (the distance between two neighboring spins).

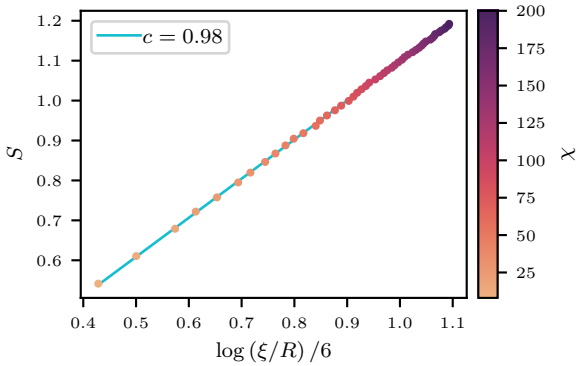

Figure 3.6: The entanglement entropy S plotted over the correlation length $\log(\xi/R)/6$ in the XY phase (at $J^z/J^{xy} = -0.3$). Thus, the gradient of the points correspond to the central charge c. We determined the value for c by fitting a linear function ($S = \frac{c}{6}\log(\xi/R) + b$) to the data points.

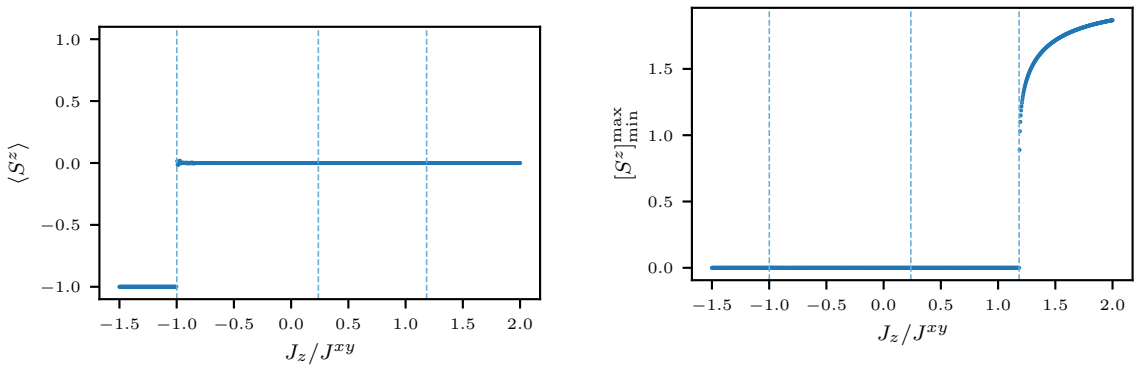

(a) $\langle S^z \rangle$ magnetization.

(b) Difference of maximal and minimal magnetization at different sites.

Figure 3.7: Onsite expectation values for varying J^z.

Magnetization

Let us continue by looking at expectation values of the ground state. We start with simple onsite expectation values, in particular by looking at the averaged magnetization $\left\langle S^{(x,y,z)} \right\rangle = \frac{1}{N} \sum_{i=1}^{N} \langle \psi | S_i^{(x,y,z)} | \psi \rangle$ of the ground state, where the expectation value $\langle \psi | S_i^{(x,y,z)} | \psi \rangle$ was averaged over all sites i. For infinite systems we averaged over the $t = 2$ sites of one unit cell. The $\langle S^x \rangle$ and $\langle S^y \rangle$ magnetization is 0 everywhere. The results for $\langle S^z \rangle$ can be seen in figure 3.7a, it is only nonzero in the FM phase, as expected since the FM phase has a symmetry broken ground state with all spins pointing in the same direction. To see the antiferromagnetic character of the AFM phase we plotted in figure 3.7b also the difference of maximal and minimal magnetization at different sites

$$[S^z]^{\max}_{\min} = \max_i(\langle \psi | S_i^z | \psi \rangle) - \min_i(\langle \psi | S_i^z | \psi \rangle) \,. \tag{3.9}$$

Clearly $\langle S^z \rangle$ and $[S^z]^{\max}_{\min}$ could be used to determine the phase transitions of the FM and AFM phase.

For the symmetric ground state of the Haldane phase but also for the gapless XY phase all the onsite expectation values are 0.

Ferromagnetic order parameter

Let us continue by looking at expectation values of local order parameters. To detect the symmetry broken FM and AFM phase it is useful to look at the ferromagnetic local order parameter $\mathcal{O}_d^{\mathrm{FM},\alpha}$ as defined in equation (1.60). However, although we are treating

infinite system sizes and have the ground state as iMPS, we are numerically limited to calculate all order parameters not in the limit $|i-j| \to \infty$, but only for a finite distance $|i-j| = d$. We will in the following always choose a site distance of $d = 500$, at which distance the local order parameters already converged to a constant value for all gapped phases. Note that the typical decay length is given by the correlation length, see figure 3.5. Since this decay length is diverging in gapless phases for increasing bond dimensions it might be that in the gapless phases the order parameters did not fully converge even for distances of $d = 500$ sites.

The results for the ferromagnetic order parameters $\mathcal{O}_d^{\mathrm{FM},\alpha}$ as function of J^z can be seen in figure 3.8. As expected the order parameter $\mathcal{O}_d^{\mathrm{FM},z}$ is a good indicator for the FM and AFM phase. Note that the sign of the ferromagnetic z order parameter in the AFM phase actually jumps for odd and even distances. The proper antiferromagnetic order parameter is therefore defined with an additional $(-1)^d$ compared to the ferromagnetic order parameter. However, since we are looking at a fixed even distance $d = 500$ we do not have to take this into account. Furthermore, note that at the first order phase transition from the FM to the XY phase the order parameter is discontinuous, while it is continuous at the second order phase transition from the Haldane to the AFM phase, as expected for first and second order phase transitions.

We find only in the Haldane phase that all local order parameters are vanishing, hinting at a SPT. In the gapless XY phase the x and y ferromagnetic order parameters seem not to vanish. However, as can be seen in figure 3.9 the order parameters in the XY phase depend on the bond dimension, and due to the large correlation lengths in this gapless phase one needs also to study larger distanced d. In [36] this has been discussed in more detail, and they also introduced a pseudo order parameter $\mathcal{O}_d^{\mathrm{FM},t}(\chi) = \mathcal{O}_d^{\mathrm{FM},x}(\chi) + \mathcal{O}_d^{\mathrm{FM},y}(\chi)$, which for finite bond dimensions χ can be used to specify the XY phase.

String order parameter

Also for the string order parameters $\mathcal{S}_d(\Sigma, O)$ we choose a distance $d = 500$ for all evaluations. In figure 3.10 the original, odd string order parameters $\mathcal{S}_d(R^\alpha, S^\alpha)$ are plotted.

As expected all three (x, y and z) odd string order parameters are nonzero in the topological Haldane phase, while only the z string order parameter is non-vanishing in the symmetry broken ferromagnetic and antiferromagnetic phases. The z string order parameter is 0 in the XY phase, but is only smoothly and slowly increasing in the Haldane phase, which makes it difficult to determine the phase transition point between the XY and Haldane phase with this parameter. The x and y string order parameters

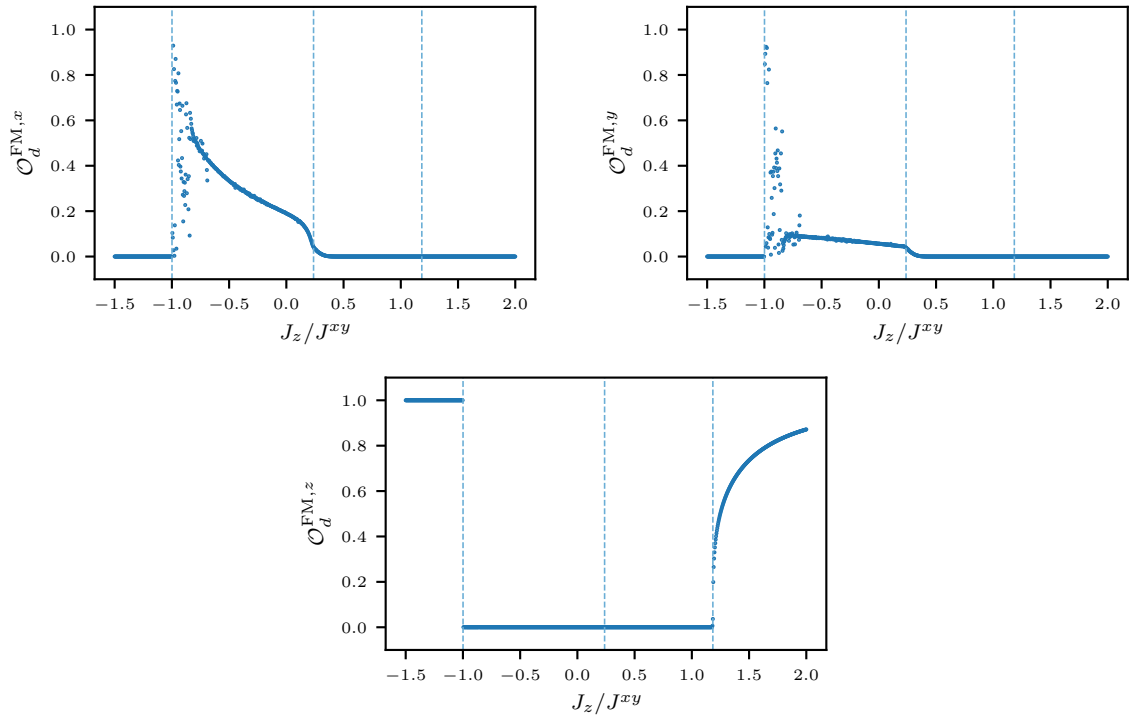

Figure 3.8: Ferromagnetic order parameters $\mathcal{O}_d^{\mathrm{FM},\alpha}$ for a site distance $d = 500$ and all three directions $\alpha \in \{x, y, z\}$. $\mathcal{O}_d^{\mathrm{FM},z}$ characterizes the FM and AFM phase.

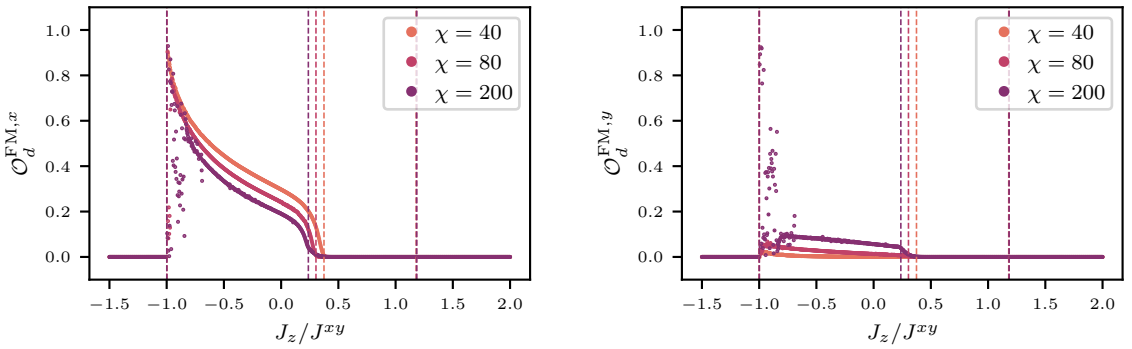

Figure 3.9: Ferromagnetic order parameters $\mathcal{O}_d^{\mathrm{FM},\alpha}$ ($\alpha \in \{x, y\}$) for different bond dimensions χ showing the χ dependence of the x and y order parameters in the gapless XY phase.

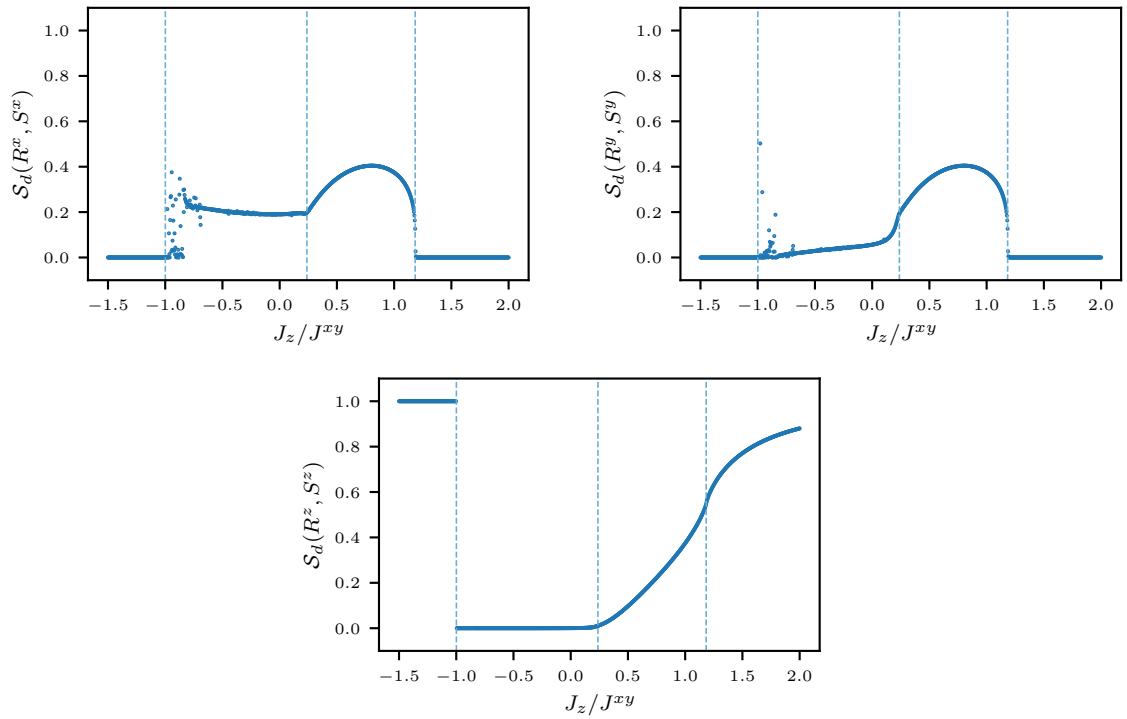

Figure 3.10: String order parameters $\mathcal{S}_d(R^\alpha, S^\alpha)$ for a site distance $d = 500$ and all three directions $\alpha \in \{x, y, z\}$. The finite value of all three parameters indicates the Haldane phase.

are non-vanishing for the fixed bond dimension χ and distance d in the XY phase. Again in [36] it has been studied in more detail, that for larger distances and also dependent on the bond dimension the x and y string order parameters are also vanishing in the XY phase, which would allow for a better distinction of the XY and Haldane phase. However, we will not focus on this here, but rather want to introduce later another parameter, the symmetry (and phase) factor, which also allows us to distinguish these two phases. Before doing so let us also have a look at the even string order parameters $\mathcal{S}_d(R^\alpha, \mathbb{1})$ in figure 3.11. As discussed in [22] the vanishing of this even string order parameters, while the odd string order parameters are finite, is what characterizes a SPT and can also be seen for the Haldane phase here. On the other hand the even z string order parameter in the symmetry broken phases are non-vanishing, while also the odd z string order parameter is non-vanishing, which demonstrates that these are symmetry broken phases. Similar this is true for the x and y string order parameters in the XY phase, where also the odd and even string order parameters are nonzero (but still both depend on the chosen bond dimension χ and distance d).

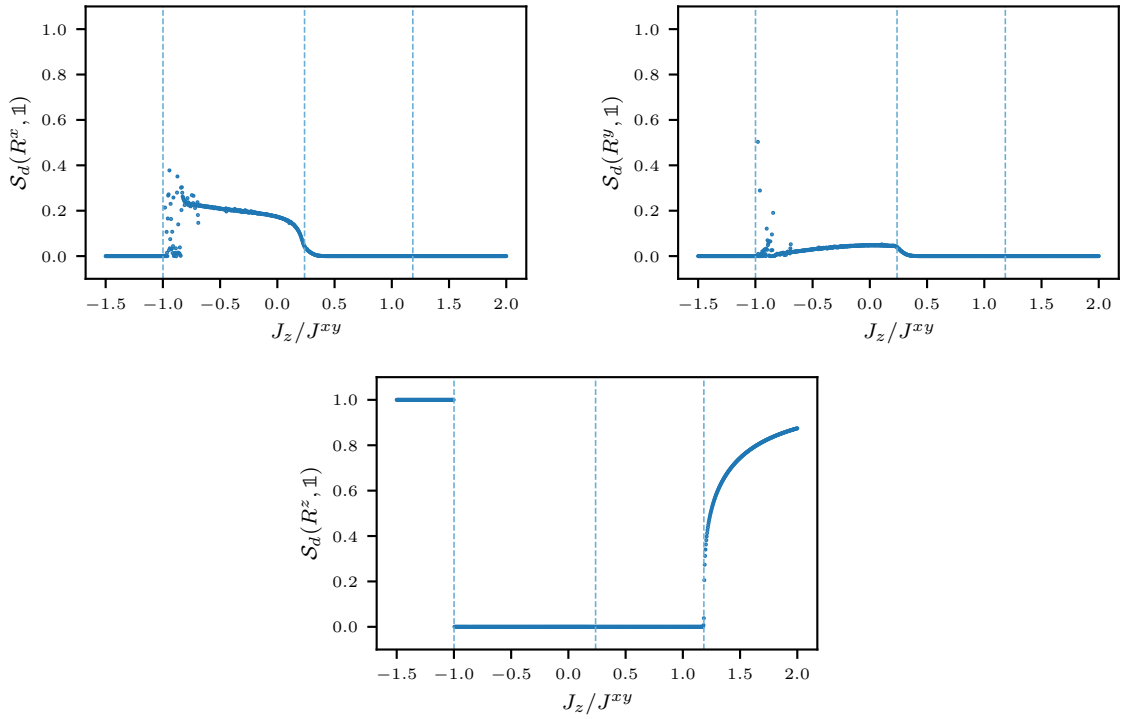

Figure 3.11: Even string order parameters $\mathcal{S}_d(R^\alpha, \mathbb{1})$ for a site distance $d = 500$ and all three directions $\alpha \in \{x, y, z\}$. In the Haldane phase these are vanishing in agreement with the expectation for a SPT.

Symmetry factor

Now let us have a look at the symmetry factors $\mathcal{R}^\Sigma$ for the different symmetries introduced in section 1.3.2, which is determined by calculating the largest eigenvalue of the generalized transfer matrix T^Σ. We will also only look at the absolute value of this eigenvalue, since we are only interested in the invariance of the ground states under the symmetries, where an absolute value of 1 corresponds to an invariant ground state.

Let us start with the D_2 symmetry group, and in particular with the π rotations around the x and z axis (R^x and R^z). The corresponding symmetry factors $\mathcal{R}^{R^x}$ and $\mathcal{R}^{R^z}$ are plotted in figure 3.12. In figure 3.12a one can see the symmetry breaking of the ferromagnetic and antiferromagnetic ground states, while all phases (except for phase transition points) seem to be almost invariant under the R^z rotation. However, by looking at the difference $1 - \left|\mathcal{R}^\Sigma\right|$ from the perfect symmetry invariant value 1 and plotting it in a logarithmic scale (see figure 3.12d) we can find further differences between the XY and the other phases. The ground states of all other phases are numerically perfectly invariant under the R^z rotation (note that the machine precision for normal *float* values, which were mostly used in this calculation, is of the order of 10^{-16}). In contrast, in the XY phase we can clearly see that the ground state is not perfectly symmetric (for the fixed bond dimension $\chi = 200$). The transition point, as well as the exact value still depends on the bond dimension, but compared to the x and y string order parameters of the XY phase it does not depend on a distance $|i - j|$, which is why it seems to be an easier parameter to distinguish the XY and the Haldane phase.

In figure 3.13 also the symmetry factors (in logarithmic scale) for the TR and inversion symmetries are shown. In total, we find that the Haldane phase is invariant for all symmetry operators. The FM phase is invariant for a R^z rotation and inversion symmetry. The AFM phase is only symmetric under the R^z rotation. And the XY ground state for a finite bond dimension is only symmetric under the R^x rotation.

Phase factor

Finally, we want to look yet at another order parameter, the phase factor $\mathcal{P}$, as discussed in equation (1.65) and originally introduced in [22]. It distinguishes symmetric from non-symmetric phases and furthermore classifies in topological and trivial phases. To distinguish non-symmetric phases it relies on the observations of the symmetry factor and is defined to be 0 if the ground state breaks one element of the symmetry group (meaning if the symmetry factor for one element is not 1). Note that numerically we will set the tolerance for a state not being invariant under a symmetry operation at $1 - \left|\mathcal{R}^\Sigma\right| > 10^{-5}$.

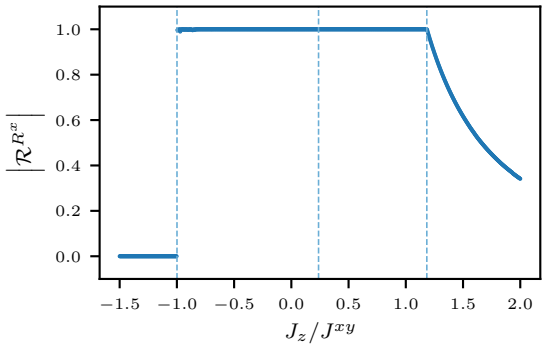

(a) Symmetry factor $\mathcal{R}^{R^x}$ for a R^x rotation.

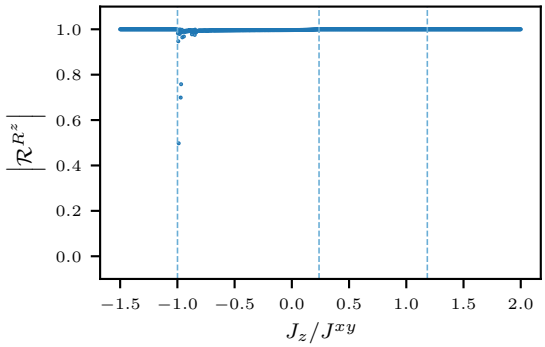

(b) Symmetry factor $\mathcal{R}^{R^z}$ for a R^z rotation.

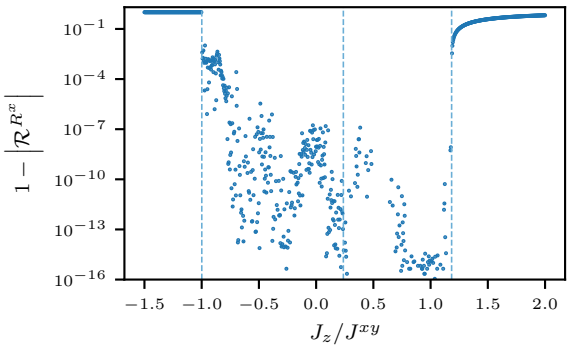

(c) Symmetry factor $\mathcal{R}^{R^x}$ for a R^x rotation in logarithmic scale as difference from the perfect value 1.

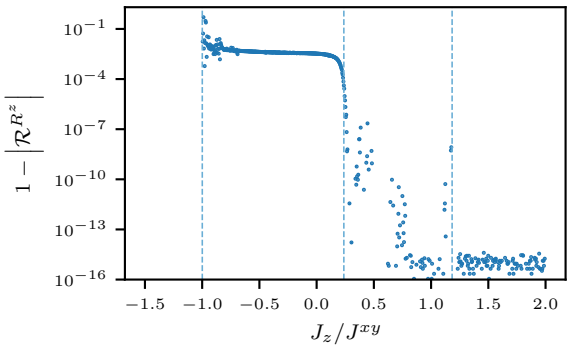

(d) Symmetry factor $\mathcal{R}^{R^z}$ for a R^z rotation in logarithmic scale as difference from the perfect value 1.

Figure 3.12: Symmetry factors for the generators of the D_2 symmetry group (R^x and R^z). Plotted as absolute value and in a logarithmic scale as difference from the perfect value 1.

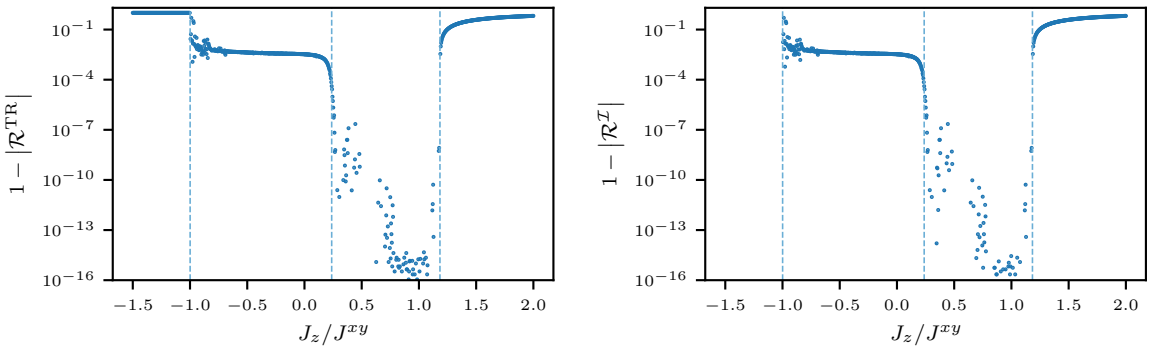

(a) Symmetry factor for TR.

(b) Symmetry factor for inversion.

Figure 3.13: Symmetry factors for the TR and inversion symmetries. Plotted in a logarithmic scale as difference from the perfect value 1.

In figure 3.14a we see that for the D_2 and TR symmetries the Haldane phase is the only invariant phase and the projective phase is -1 revealing the topological character of this phase. For the inversion symmetry we can see two invariant phases. The FM phase has a projective phase factor of $+1$, indicating a trivial phase, while the Haldane phase has again a topological phase factor of -1.

Phase transitions

Let us end this discussion of the XXZ phase diagram by looking at the phase transitions.

The phase transition of the FM to XY phase is a first order phase transition, indicated by the discontinuous ferromagnetic order parameter $\mathcal{O}_d^{\mathrm{FM},z}$ and the bump in the ground state energy. Therefore, it can easily be obtained by looking at the ferromagnetic order parameter and determining the J^z parameter of the discontinuous jump. Doing so results in a phase transition point at $J^z/J^{xy} \approx 1.00$.

The phase transition from Haldane to AFM phase is a second order phase transition, that does not have a discontinuous jump in the ferromagnetic order parameter and is indicated by the diverging peek of the correlation length. Since the ferromagnetic order parameter is nevertheless increasing very sharp at the phase transition one could in principle define a cutoff value for the ferromagnetic order below/above which we define the Haldane/AFM phase. But this would slightly depend on the cutoff value we choose. We define the exact phase transition point at the peek in the entanglement entropy, such that it does not depend on any cutoff. This results in a phase transition point at $J^z/J^{xy} \approx 1.18$.

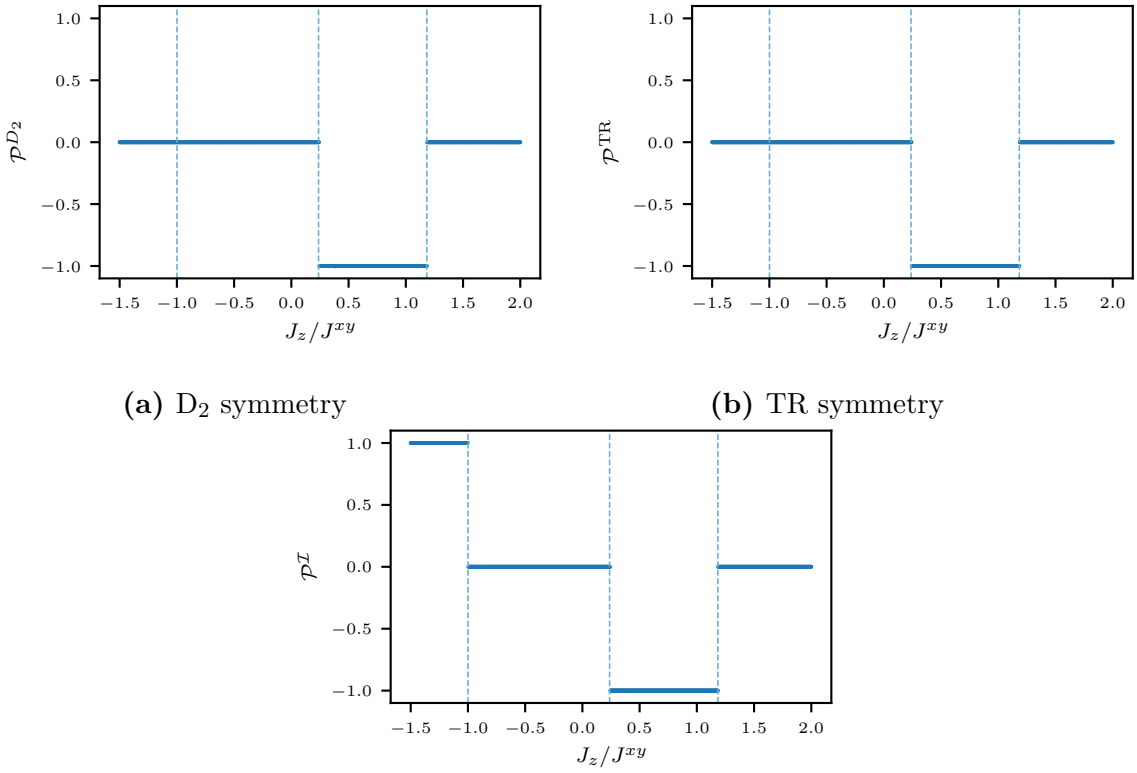

(a) D_2 symmetry

(b) TR symmetry

(c) Inversion symmetry

Figure 3.14: Phase factors $\mathcal{P}$ for the D_2, TR and inversion symmetries.

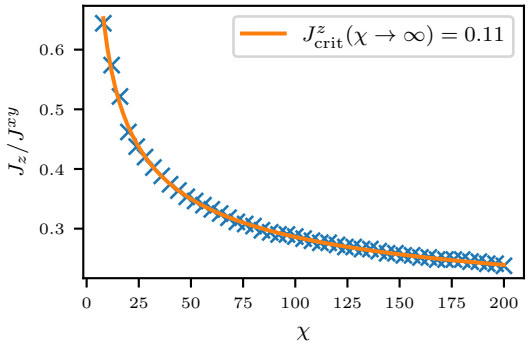

Figure 3.15: Phase transition point $J^z{}_{\text{crit}}$ from XY to Haldane phase extrapolation for increasing χ. We used the fit function $J^z{}_{\text{crit}}(\chi) = a + b\chi^{-c}$ to extrapolate the phase transition point for an infinite bond dimension $J^z{}_{\text{crit}}(\chi \to \infty)$.

Finally, let us discuss the BKT transition from the XY to the Haldane phase. In principle, we can use the jump of the phase factors $\mathcal{P}$ as phase transition point. However, this jump numerically depends on the ambiguous choice of the cutoff which ground states to consider as symmetric invariant (we choose $1 - \left|\mathcal{R}^{\Sigma}\right| > 10^{-5}$ as cutoff for symmetry broken states). Therefore, we again use the entanglement entropy peek closest to this phase boundary as phase transition point. This phase transition point does still strongly depend on the bond dimension, as already seen in figure 3.2b. In figure 3.15 one can see the phase transition points plotted over the bond dimension. The data suggest an asymptotic behavior for larger bond dimensions. This motivates the possibility to extrapolate a physical transition point for an infinite bond dimension by fitting an asymptotic function to the data [36]. The heuristic fit function of our choice is $J^z{}_{\text{crit}}(\chi) = a + b\chi^{-c}$, from which we can extrapolate the phase transition point for an infinite bond dimension $J^z{}_{\text{crit}}(\chi \to \infty)$. Doing this, as it can be seen in figure 3.15 for bond dimensions from $\chi = 8$ up to $\chi = 200$ in steps of 4 results in a phase transition point $J^z{}_{\text{crit}}(\chi \to \infty) \approx 0.11$. This is reasonably closer to the analytically expected phase transition point $J^z = 0$ [41]. However, the exact value of this extrapolation does also depend on the range of the used bond dimensions χ for the extrapolation (e.g. by only using larger values of χ, to minimize the error of to small bond dimensions we also find extrapolation values even closer to zero ($J^z{}_{\text{crit}}(\chi \to \infty) \approx 0.04$)).

To summarize this phase transition discussion of the XY to the Haldane phase, one can say, that iDMRG together with infinite bond dimension extrapolation is a useful tool to better approximate such a BKT phase transition and probably can even be further improved. Another approach to treat BKT phase transition is to look at energy crossing of the ground state energy manifold at the phase transition point. With this method one can find more accurate phase boundaries also for the XXZ model, as it was done in [35,

42].

In this work however we will focus more on finding the Haldane phase and good parameter sets (away from phase transitions), that strongly feature the Haldane phase properties rather than looking at phase transitions. Therefore, in all following phase diagrams the plotted phase boundaries are obtained for a fixed bond dimension and serve as qualitatively line for the eye (although for first and second order phase transitions they might be quite accurate).

3.2.2 Detailed phase diagram discussion

After studying the instructive spin 1 XXZ model in the last subsection we can now look at the Haldane phase diagram for more complicated Hamiltonians by adding long range interactions ($\alpha < \infty$) as well as all the additional Hamiltonian terms described in section 3.1. Keep in mind that the goal of this phase diagram study is to find parameters, that stabilize the Haldane phase for a vanishing $J^z = 0$ spin coupling. To analyze how the different additional Hamiltonian terms effect the Haldane phase we start by examining two-dimensional phase diagrams with J^z as one parameter (always plotted on the x axis) and one of the following additional parameters: $\alpha, D, \delta_0, B, V^{+-}, \delta$, which Hamiltonians are described in equations (3.1) – (3.7). In the second part of this subsection we will focus on phase diagrams with $J^z = 0$, which corresponds to model parameters that we can implement experimentally with Rydberg atoms. Therefore, in this second part we will look for an optimal parameter set, which features the Haldane phase and has a good visibility of all its characteristic properties.

Phase diagrams with J^z

As mentioned above in this first part we are going to study the effect of the different parameters in the context of stabilizing the Haldane phase at $J^z = 0$. Therefore, if not mentioned otherwise we will study the XXZ Hamiltonian (3.1) with only nearest neighbor interactions ($\alpha = \infty$), where only one of the additional Hamiltonians (3.3) – (3.7) are added.

$J^z - \alpha$

Let us start our phase diagram discussion by adding long range interaction terms $\alpha < \infty$. An extensive study for this was also done in [32]. Therefore, we will only recap the important results for our model. Note that we will focus in this work only on the antiferromagnetic model ($J^{xy} > 0$). This is because in [32] it was shown, that in the antiferromagnetic model long range interactions can indeed stabilize the Haldane phase. On the other hand it was also shown in their work that in ferromagnetic models ($J^{xy} < 0$) long range interactions destabilize the Haldane phase and for values $\alpha \gtrsim 3$ the Haldane phase in the XXZ model disappears.

As before we will consider the interaction strength J^{xy} as energy scale. For the experimental implementation with Rydberg atoms we expect a dipole-dipole interaction with $\alpha = 3$, which we will not be able to tune. However, it is still interesting to know, how this affects the stability of the Haldane phase compared to only nearest neighbor interactions.

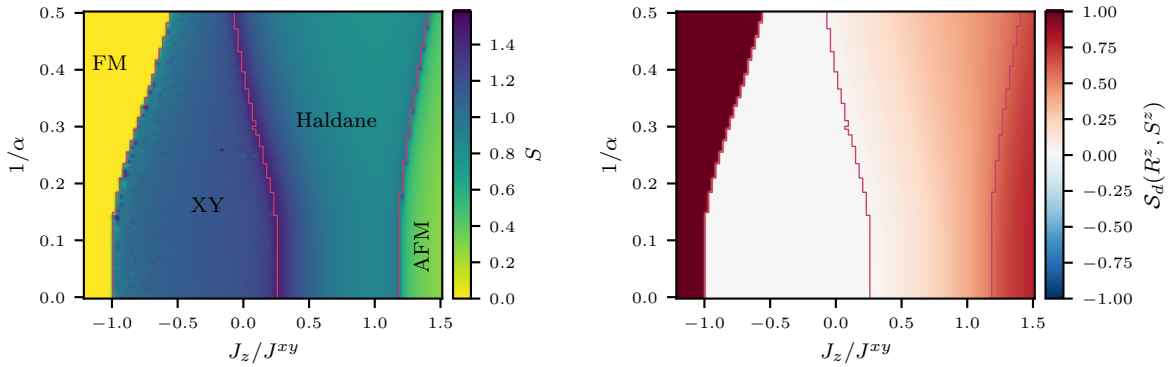

(a) Entanglement entropy S. **(b)** Odd z string order parameter $\mathcal{S}_d(R^z, S^z)$.

Figure 3.16: Phase diagram for varying the parameters J^z and $1/\alpha$. The phases are labelled in (a) and the boundaries (calculated for a bond dimension $\chi = 200$) are drawn as red lines.

In figure 3.16 we can see the entanglement entropy S and the odd z string order parameter. Similar to the nearest neighbor XXZ model we find again the four phases from negative J^z to positive J^z: FM, XY, Haldane and AFM phase. The lines drawn in all phase diagrams indicate the phase boundaries for a fixed bond dimension $\chi = 200$. As discussed for the XXZ model some phase transition strongly depend on the bond dimension, which means to determine the exact phase transitions one would require additional work (e.g. extrapolating these to infinite bond dimensions). However, we will use the plotted phase boundaries only as lines to guide the eye and will not investigate the exact phase transitions further in this work.

Most interestingly we find, that the Haldane phase gets larger for increasing interaction lengths (larger values of $1/\alpha$ corresponds to larger interaction lengths). By extrapolating the exact phase transition in [32] it was found, that for $1/\alpha = 0$ the phase transition is approximately at $J^z \approx 0$ and even shifts to small negative values for increasing values of $1/\alpha$.

$J^z - D$

Next we consider the onsite energy offset D (setting again $\alpha = \infty$). Adding an onsite energy offset D to the XXZ model has also already been discussed, e.g. with exact diagonalization of small systems [35], and also with iDMRG methods [37]. As we will later see this parameter is actually experimentally quite easy to tune for the three level Rydberg system.

Apart from the already introduced phases at $D = 0$ (FM, XY, Haldane and AFM phase), we find in figure 3.17 also two new phases. The Large-D phase appearing for large positive values $D/J^{xy} \gtrsim 1$. This phase is a gapped symmetric phase, which can be seen by the fast converging entropy as well as the symmetry factors, which are $\left|\mathcal{R}^{\Sigma}\right| = 1$ for all symmetry operators (R^z, R^x, TR and inversion) (not plotted here). Looking at the phase factor (see e.g. figure 3.17b) for this symmetric phase reveals, that this phase is a trivial symmetric phase with $\mathcal{P} = +1$, and thus this phase is the trivial counterpart to the Haldane phase. Due to this reversed sign of the phase factor in contrast to the Haldane phase, in this Large-D phase the odd string order parameters are zero ($\mathcal{S}_d(R^\alpha, S^\alpha) = 0$ see e.g. figure 3.17c) and the even string order parameters are nonzero ($\mathcal{S}_d(R^\alpha, \mathbb{1}) \neq 0$ see e.g. figure 3.17d). In the Haldane phase this is reversed. This behavior is also discussed in more detail in [22].

The second new phase, called the XY2 phase, is below the XY phase and similar to the XY phase, XY2 is also a gapless phase with central charge $c = 1$ (not plotted here).

Let us now focus on the Haldane phase. It seems like for negative D the Haldane phase shifts to smaller J^z. However, keep in mind that the Haldane to XY phase transition in the iMPS framework is strongly dependent on the bond dimension. Analytically for $D = 0$ and nearest neighbor interactions it was shown that the exact phase transition point is at $J^z = 0$ and also for negative D the phase transition stays constant at $J^z = 0$, this is discussed in [35] by exact diagonalization of small systems.

Nevertheless, it still might be that for long range interactions ($\alpha = 3$), and other additional parameters, where in principle there is already a Haldane phase at $J^z = 0$, the features of the Haldane phase might get more apparent for a nonzero value of D.

$J^z - \delta_0$

The next parameter we are going to consider is δ_0. We first note that the phase diagram seems to be symmetric for a reflection at the $\delta_0/J^{xy} = -1$ line. This behavior can be understood by noticing that a reflection at $\delta_0/J^{xy} = -1$ can be expressed as unitary transformation of the Hamiltonian, which we will discuss in more detail in appendix A.

We again can identify at the $\delta_0 = 0$ line the FM, XY, Haldane and AFM phase. Additional we find for large positive and negative δ_0 a symmetric phase, which has a trivial phase factor $\mathcal{P} = +1$ for all three symmetry groups (see e.g. figures 3.18c and 3.18d) and thus we identify this phase with the trivial Large-D phase (in figure 3.23 we can also see that this phase is indeed connected to the Large-D phase).

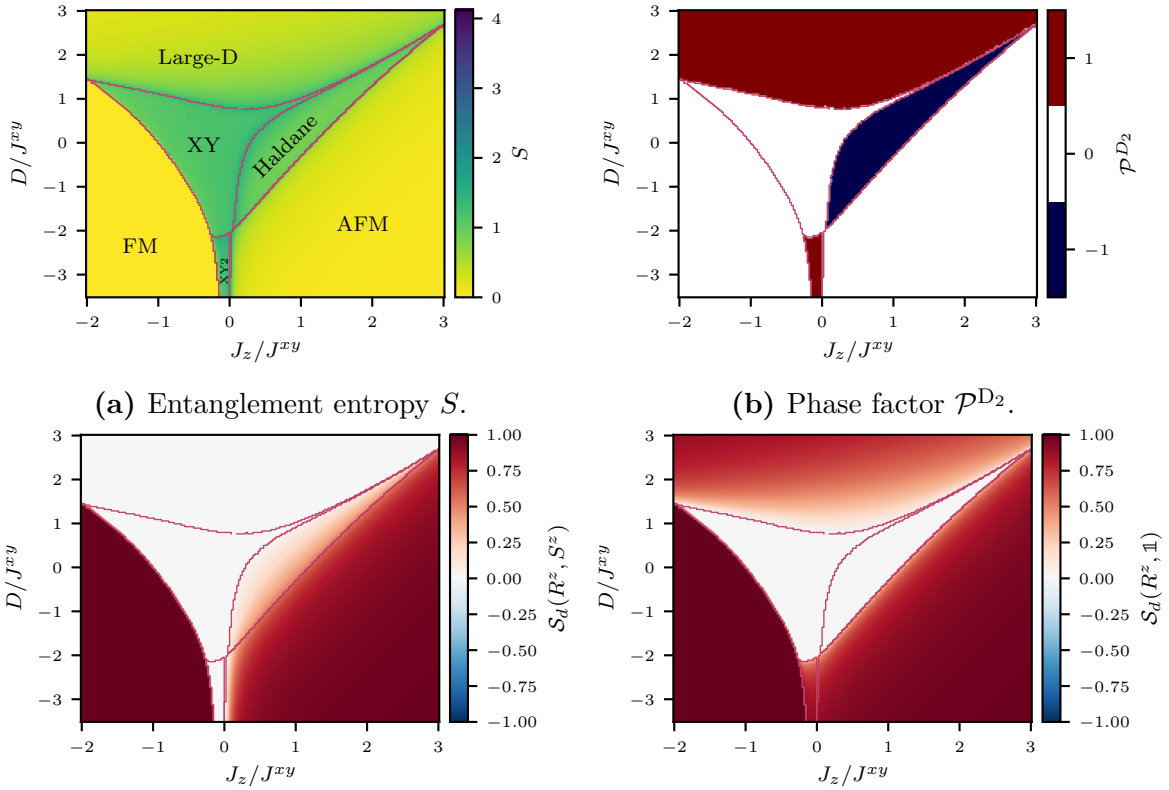

(a) Entanglement entropy S.

(b) Phase factor $\mathcal{P}^{\mathrm{D}_2}$.

(c) Odd z string order parameter $\mathcal{S}_d(R^z, S^z)$.

(d) Even z string order parameter $\mathcal{S}_d(R^z, \mathbb{1})$.

Figure 3.17: Phase diagram for varying the parameters J^z and D. The phases are labelled in (a) and the boundaries (calculated for a bond dimension $\chi = 200$) are drawn as red lines.

Below the XY phase we find a new gapless phase (again with central charge $c = 1$, which was determined similar as in figure 3.6) and the mirrored XY phase, which we will refer to as XY*.

Let us focus again at the Haldane phase and its mirrored phase (Haldane*). While the phase factors of the inversion and D_2 symmetries are topological ($\mathcal{P}^{D_2} = \mathcal{P}^{\mathcal{I}} = -1$) on both sides of $\delta_0/J^{xy} = -1$ (see e.g. figure 3.18d), the TR symmetry phase factor is only topological ($\mathcal{P}^{\mathrm{TR}} = -1$) in the Haldane phase and trivial ($\mathcal{P}^{\mathrm{TR}} = +1$) in the mirrored Haldane phase, see figure 3.18c. Also, only the odd z string order parameter is finite in both phases (see figure 3.18f) and the x (and y, which is not plotted here) string order parameters are only finite for $\delta_0/J^{xy} > -1$ (see figure 3.18e). All even string order parameters are vanishing $\mathcal{S}_d(R^\alpha, \mathbb{1}) = 0$ in both Haldane phases. We will do an additional discussion on this mirrored Haldane phase for the simpler case of the AKLT model in appendix A. In this section we will focus on the Haldane phase, where all symmetry phase factors are topological and we also find a finite z and x string order parameter.

We again find that for a fixed bond dimension ($\chi = 200$) the Haldane to XY phase transition moves closer to $J^z = 0$ if we decrease δ_0 from 0 to -1, at which point the XY phase disappears and the phase transition to the new gapless phase is exactly at $J^z = 0$. However, as discussed before the XY to Haldane transition is for infinite bond dimensions also already for δ_0 at $J^z = 0$, which leads to the assumption that also for $-1 < \delta_0/J^{xy} <= 0$ the Haldane to XY transition is at $J^z = 0$.

Nevertheless, we are not interested in the phase transitions here but continue by summarizing that small negative δ_0 might be able to stabilize a Haldane phase but for nearest neighbor interactions only the δ_0 term is not enough to feature a Haldane phase at $J^z = 0$.

$J^z - B$

Another tunable parameter in our Rydberg systems is B, which couples the states $|+-\rangle \leftrightarrow |-+\rangle$. Note that this coupling is one of the terms, that is also added in the AKLT model by the $(\boldsymbol{S_i}\boldsymbol{S_j})^2$ term, which however also adds other couplings. Thus, we might hope, that this coupling term, given by B can stabilize the Haldane phase. Although in the Rydberg states this interaction will be a van der Waals interaction, and thus decaying with $\alpha_{\mathrm{vdw}} = 6$, for simplicity we will consider here, similar to $\alpha = \infty$ also only nearest neighbor interactions $\alpha_{\mathrm{vdw}} = \infty$.

So let us look at the phase diagram in figure 3.19. At the reference line at $B = 0$ we again see the already known FM, XY, Haldane and AFM phase. For positive B we find three new gapless phases. At large $B \gtrsim 2$ there appears a gapless phase, which seems to

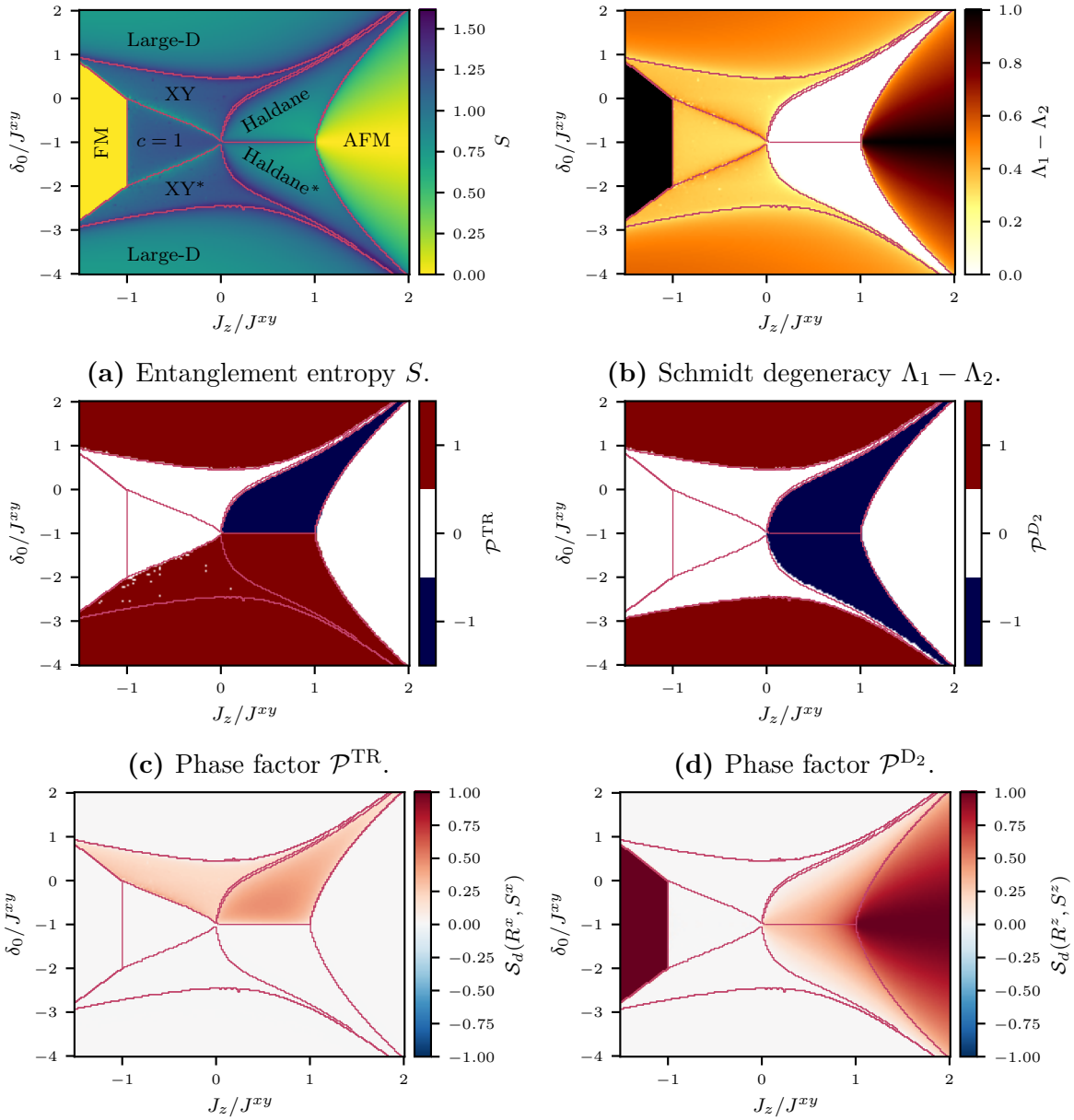

(a) Entanglement entropy S.

(b) Schmidt degeneracy $\Lambda_1 - \Lambda_2$.

(c) Phase factor $\mathcal{P}^{\mathrm{TR}}$.

(d) Phase factor $\mathcal{P}^{\mathrm{D}_2}$.

(e) Odd x string order parameter $\mathcal{S}_d(R^x, S^x)$.

(f) Odd z string order parameter $\mathcal{S}_d(R^z, S^z)$.

Figure 3.18: Phase diagram for varying the parameters J^z and δ_0. The phase labelled by $c = 1$ corresponds to a gapless phase with central charge $c = 1$. Phases mirrored at $\delta_0 = -1$ are denoted by a *.

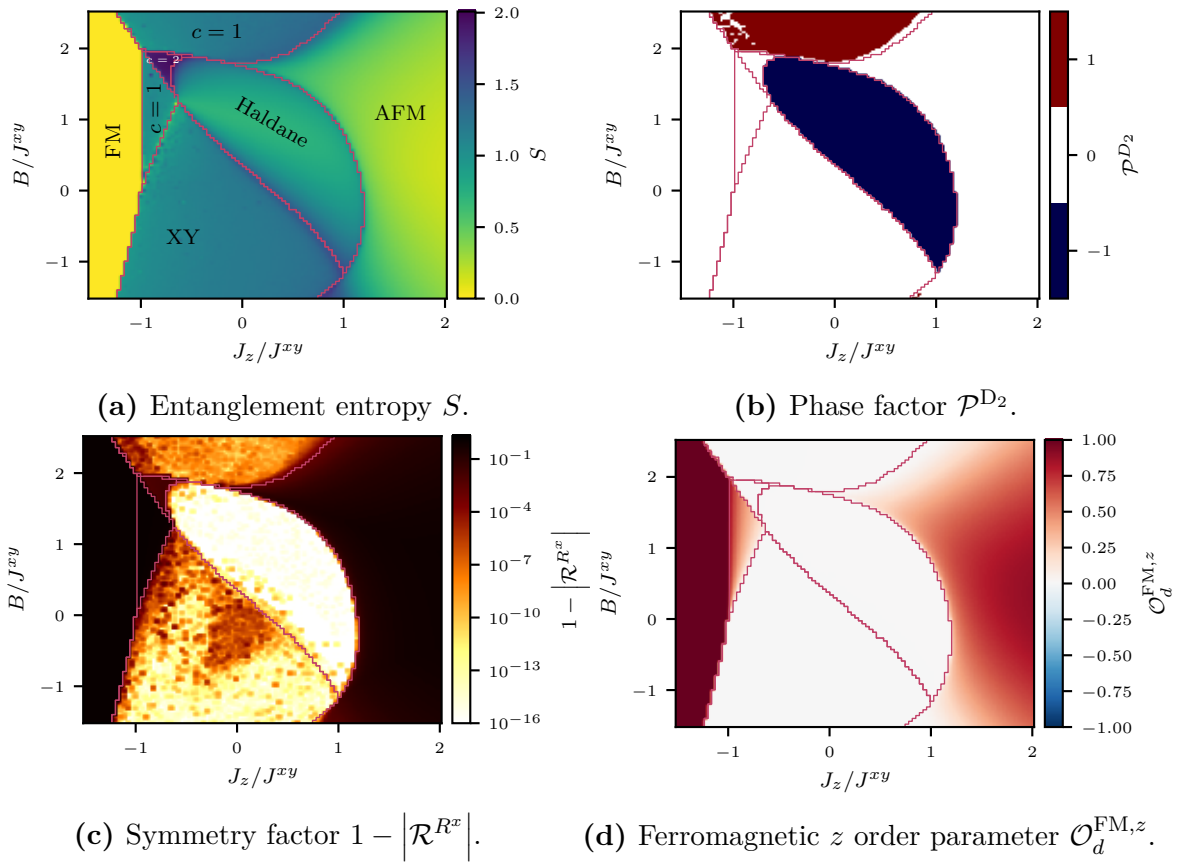

(a) Entanglement entropy S.

(b) Phase factor $\mathcal{P}^{\mathrm{D}_2}$.

(c) Symmetry factor $1 - \left|\mathcal{R}^{R^x}\right|$.

(d) Ferromagnetic z order parameter $\mathcal{O}_d^{\mathrm{FM},z}$.

Figure 3.19: Phase diagram for varying the parameters J^z and B. Additional to XY there are three more gapless phases labelled by their central charge c.

have a symmetric ground state under an arbitrary rotation R^α and for TR (but not for inversion) (see e.g. the symmetry factor for a R^x rotation in figure 3.19c). This phase has a central charge of $c = 1$. Also the gapless phase appearing between the FM and the XY phase for small positive B values has a central charge $c = 1$ and a non-vanishing ferromagnetic order in z direction (see figure 3.19d). Finally, there is the small gapless phase, between these two other gapless phases with a central charge $c = 2$.

If we focus again on the Haldane phase we find that for $B \approx 1$ the point $J^z = 0$ is clearly inside the Haldane phase. Thus, by being able to tune B we can stabilize the Haldane phase also for $J^z = 0$. However, as discussed in chapter 2, in the three level Rydberg system the interaction corresponding to B does not appear on its own, but together with an additional diagonal interaction term corresponding to V^{+-}, which we will look at next.

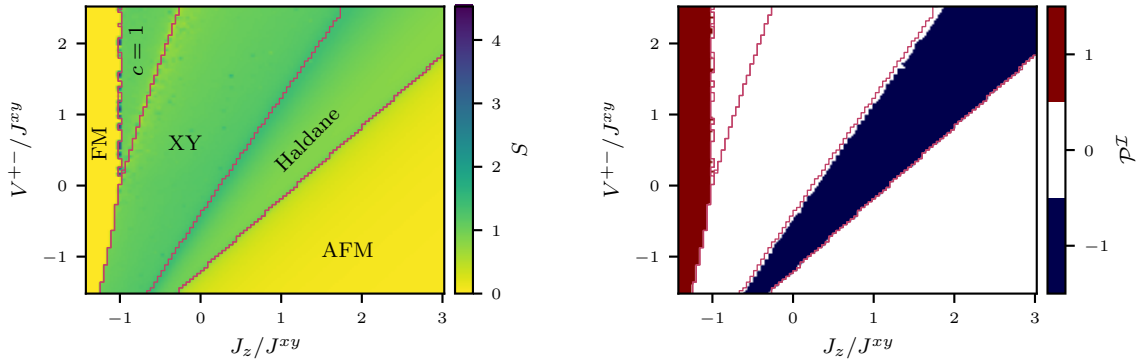

(a) Entanglement entropy S.

(b) Phase factor $\mathcal{P}^{\mathcal{I}}$.

Figure 3.20: Phase diagram for varying the parameters J^z and V^{+-}.

$J^z - V^{+-}$

The term corresponding to V^{+-}, written with spin operators, consist of two parts. First, a part $\propto -S_i^z S_j^z$ which would correspond to a negative J^z, and thus we expect the Haldane phase to shift for positive values of V^{+-} to even bigger J^z parameters (and also the other way around, for negative V^{+-} we expect the Haldane phase now also to appear at negative J^z). This linear shifting of the Haldane phase can also be seen in the phase diagrams, see figure 3.20.

However, there is also the second part of the V^{+-} term $\propto S_i^z S_i^z S_j^z S_j^z$ which seems to be responsible for an enlargement of the Haldane phase for positive V^{+-} and a shrinkage of the Haldane phase for negative V^{+-}. So although we find the Haldane phase for negative V^{+-} at $J^z = 0$ (see figure 3.20), the Haldane phase at this point also became smaller.

Furthermore, notice that we found the Haldane phase at $J^z = 0$ for positive values of B but now for negative values of V^{+-}. In our three level Rydberg system these two interactions will be approximately the same (with the same sign) and are, in our scheme, not independently tunable. Thus, we are actually interested in the phase diagram, where we tune B and V^{+-} together, to see which effect will gain the upper hand.

$J^z - B = V^{+-}$

In figure 3.21 we can see the phase diagram, where we tune $B = V^{+-}$ together. As for the phase diagram in figure 3.19, where we only tuned B we again find two gapless phases above the XY phase, one with central charge $c = 1$ and the other with $c = 2$. Additional there appears a gapless phase also below the XY phase, also with central charge $c = 1$

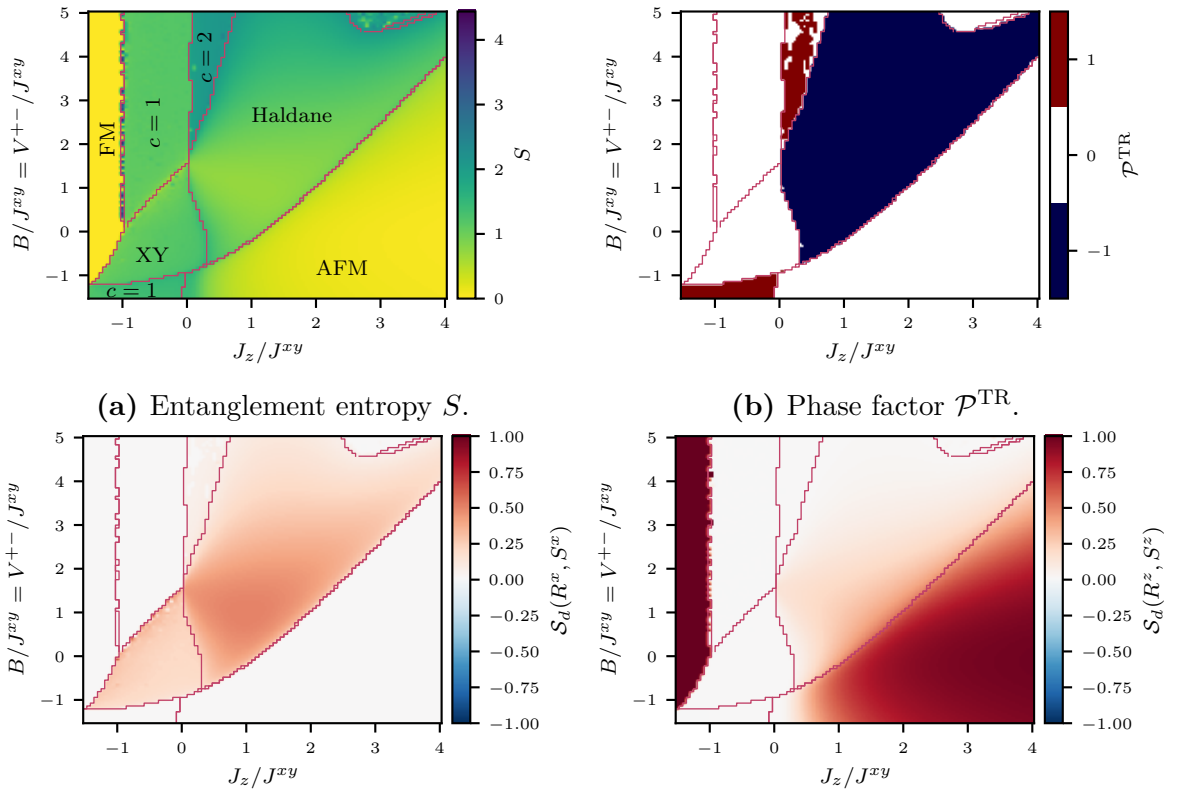

(a) Entanglement entropy S.

(b) Phase factor $\mathcal{P}^{\mathrm{TR}}$.

(c) Odd x string order parameter $\mathcal{S}_d(R^x, S^x)$.

(d) Odd z string order parameter $\mathcal{S}_d(R^z, S^z)$.

Figure 3.21: Phase diagram for varying the parameters J^z and $B = V^{+-}$, i.e. we varied B and V^{+-} identically.

and which ground state seems to be symmetric under any rotation R^α and also TR and inversion symmetry.

Focusing on the Haldane phase we find a large Haldane phase for positive values of $B = V^{+-}$. This however appears only for positive values of J^z, even though it does come quite close to $J^z = 0$. Remember that these simulations were performed for only nearest neighbor interactions $\alpha = \alpha_{\mathrm{vdw}} = \infty$. Fortunately the long range interactions will help us again. As we will see in the second part of this subsection for $\alpha = 3$ and $\alpha_{\mathrm{vdw}} = 6$ we will indeed also for $J^z = 0$ find the Haldane phase.

$J^z - \delta$

Before we continue our discussion for $J^z = 0$ let us also have a look at the symmetry breaking parameter δ, which does break the R^x rotation symmetry and therefore also the D_2 symmetry group (compare section 3.1). Since δ breaks the R^x symmetry we expect

also a symmetry broken ground state with respect to R^x. In figure 3.22c we see that indeed in the Haldane phase the ground state is no longer perfectly symmetric, however the symmetry factor $\left|\mathcal{R}^{R^x}\right|$ is still very close to 1. With respect to inversion symmetry this phase is still symmetric ($\left|\mathcal{R}^{\mathcal{I}}\right| = 1$) and also still has a topological phase factor of $\mathcal{P}^{\mathcal{I}} = -1$. Probably the most surprising result is that the x string order parameter is finite in the whole Haldane phase, although it breaks the R^x symmetry (see figure 3.22e). This might be explained by two arguments. First, as mentioned the R^x symmetry of the ground state in the Haldane phase is only slightly broken (meaning $1 - \left|\mathcal{R}^{R^x}\right| \approx 10^{-4}$). And second keep in mind that we are calculating the string order parameter at a finite distance $d = 500$, which is why the string order parameter can survive if the symmetry is only slightly broken.

Although the Haldane phase gets smaller for larger $|\delta|$, in total this is a promising result, because we are able to detect the Haldane phase also with experimental realistic parameters, where we cannot perfectly tune δ to be zero. Typical values will be $\delta/J^{xy} \approx \pm 0.02$ which will not affect the Haldane phase too much.

Phase diagrams at $J^z = 0$

In this second part we are now considering experimentally more realistic parameters. For that if not mentioned otherwise we will use the following parameters, where all parameters are used as defined in the Hamiltonians (3.1) – (3.7).

$$\begin{aligned} J^z = 0\,, \quad \delta_0 = 0\,, \quad \delta = 0\,, \quad \alpha = 3\,, \\ D = 0\,, \quad B = V^{+-} = 0\,, \quad \alpha_{\text{vdw}} = 6\,. \end{aligned} \tag{3.10}$$

Again we will use J^{xy} as energy scale. All the interaction lengths for the dipole-dipole interaction terms (J^{xy}, δ_0 and δ) are considered to be $\alpha = 3$, while for the van der Waals terms (B and V^{+-}) $\alpha_{\text{vdw}} = 6$.

$D - \delta_0$

We start by looking at the $D - \delta_0$ phase diagram in figure 3.23. Indeed, we do find in this phase diagram with $J^z = 0$ also the Haldane phase. Similar to before also this phase diagram is mirrored for a reflection at the $\delta_0/J^{xy} = -1$ line, where we again find the Haldane phase for $\delta_0/J^{xy} > -1$ and the mirrored Haldane phase, with a trivial phase factor for the TR symmetry ($\mathcal{P}^{\text{TR}} = +1$ not plotted here) at $\delta_0/J^{xy} < -1$. Above the Haldane and below the mirrored Haldane phase we again find the gapless XY and XY* phase. For large D or large $|\delta_0|$ the Hamiltonian is in the Large-D phase. For large

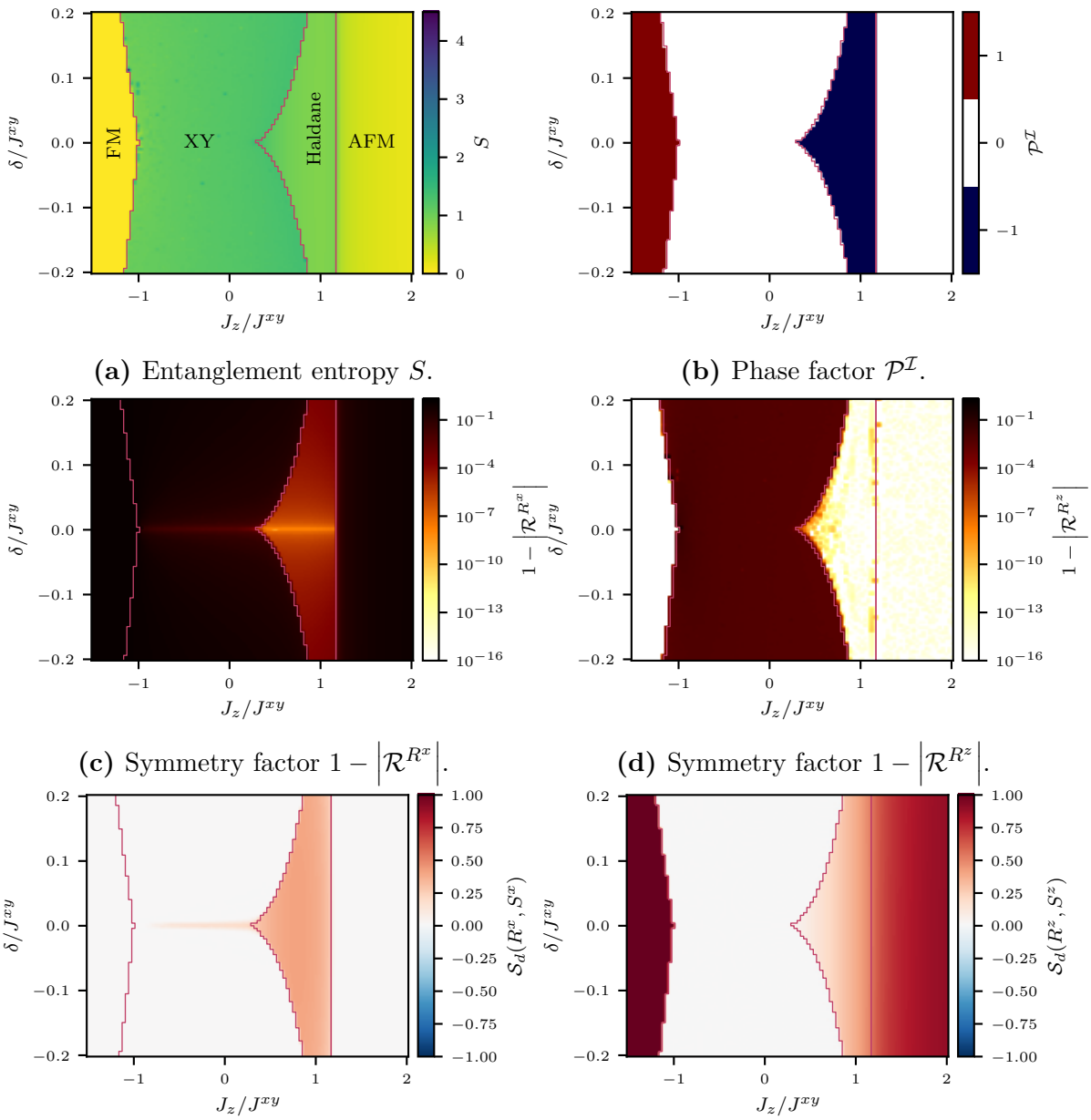

(a) Entanglement entropy S. **(b)** Phase factor $\mathcal{P}^{\mathcal{I}}$.

(c) Symmetry factor $1-\left|\mathcal{R}^{R^x}\right|$. **(d)** Symmetry factor $1-\left|\mathcal{R}^{R^z}\right|$.

(e) Odd x string order parameter $\mathcal{S}_d(R^x,S^x)$. **(f)** Odd z string order parameter $\mathcal{S}_d(R^z,S^z)$.

Figure 3.22: Phase diagram for varying the parameters J^z and the R^x symmetry breaking parameter δ.

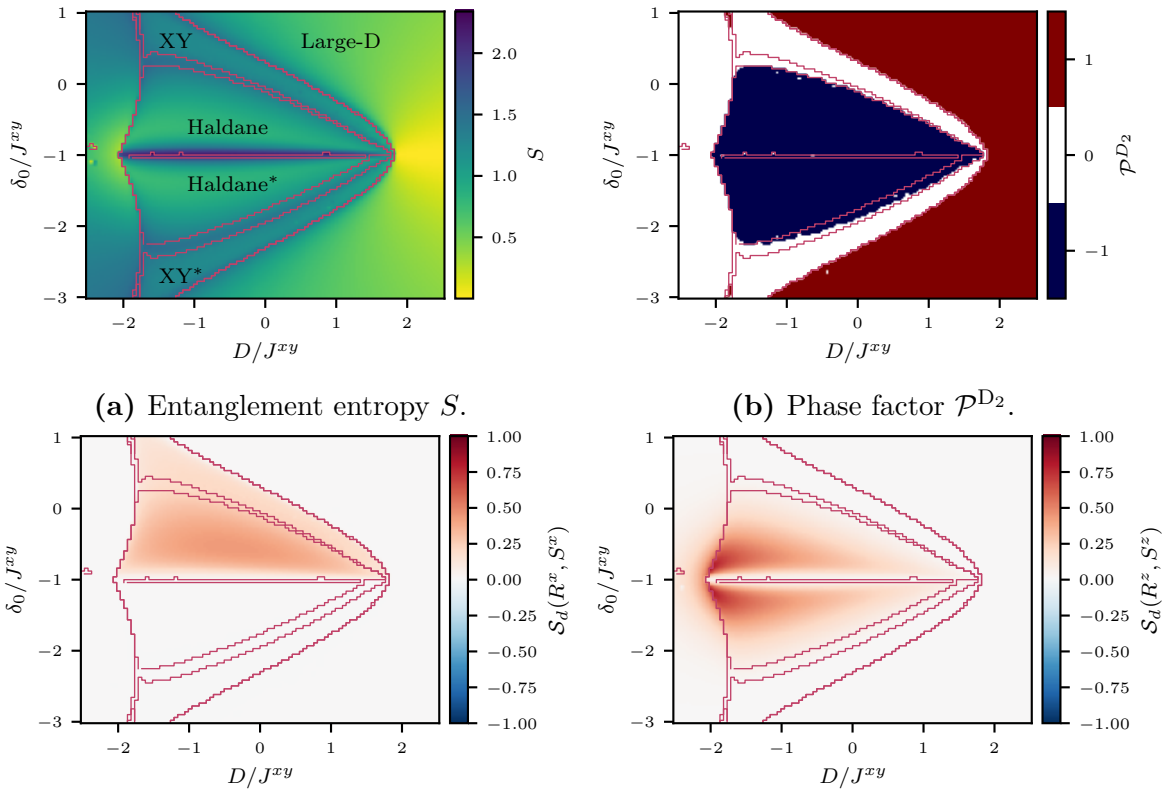

(a) Entanglement entropy S.

(b) Phase factor $\mathcal{P}^{\mathrm{D}_2}$.

(c) Odd x string order parameter $\mathcal{S}_d(R^x, S^x)$.

(d) Odd z string order parameter $\mathcal{S}_d(R^z, S^z)$.

Figure 3.23: Phase diagram for varying the parameters D and δ_0. Phases mirrored at $\delta_0 = -1$ are denoted by a *.

negative D it has similar properties as the AFM phase, but also large correlation lengths, thus further study needs to be done to characterize this phase.

If we are interested in realizing the Haldane phase we can now choose a point inside the Haldane phase, where the string order parameters are large. However, let us first look at the other last two phase diagrams.

$\delta_0 - B = V^{+-}$

Next we consider the $\delta_0 - B = V^{+-}$ phase diagram in figure 3.24. Note again the symmetry for a reflection at $\delta_0/J^{xy} = -1$. We find the already introduced phases: Large-D, XY, XY*, Haldane and Haldane* phase. Furthermore, we find two more gapless phases, one with central charge $c = 1$ for negative $B = V^{+-}$. And another for positive $B = V^{+-}$, for which phase we were not able to determine the central charge unambiguously. The

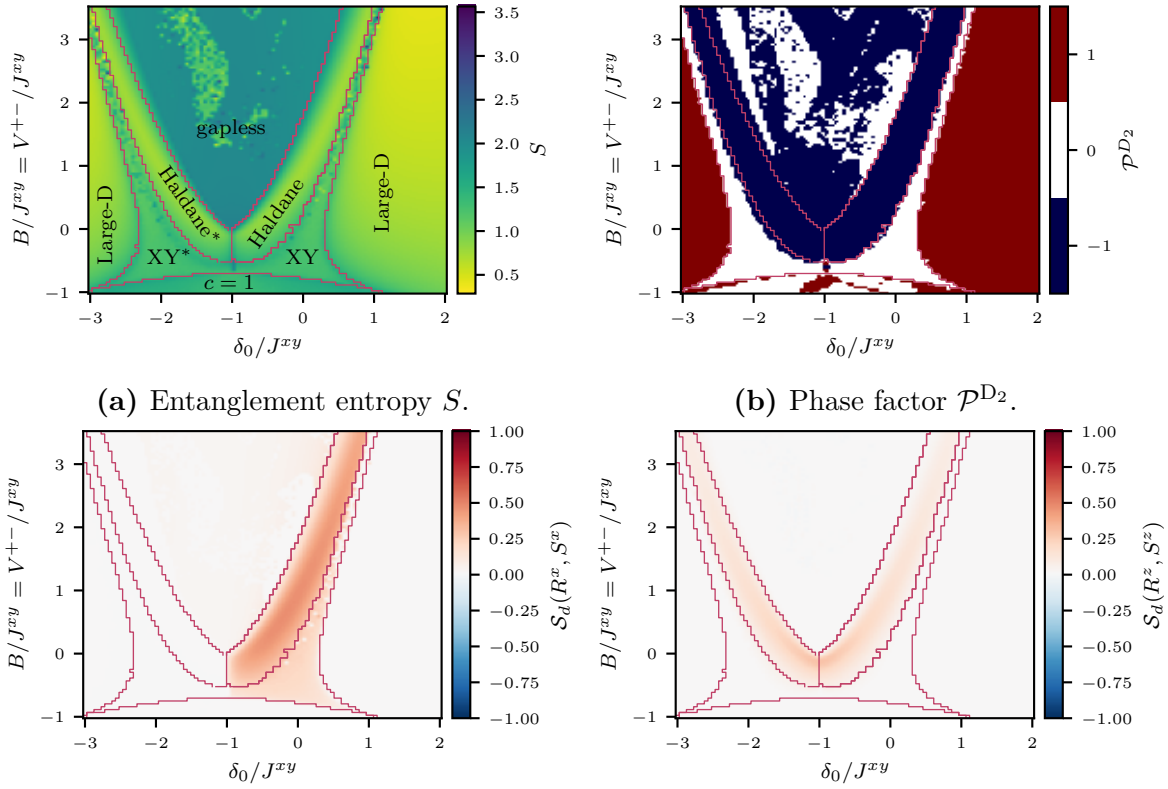

(a) Entanglement entropy S. **(b)** Phase factor $\mathcal{P}^{\mathrm{D}_2}$.

(c) Odd x string order parameter $\mathcal{S}_d(R^x, S^x)$. **(d)** Odd z string order parameter $\mathcal{S}_d(R^z, S^z)$.

Figure 3.24: Phase diagram for varying the parameters δ_0 and $B = V^{+-}$. Additional to XY there are two more gapless phases, one with central charge $c = 1$ and one (just called gapless), where we could not determine the central charge unambiguously.

Haldane phase in this parameter space is quite small and also the z string order parameter is small in the whole Haldane phase.

$D - B = V^{+-}$

Finally, we look at the $D - B = V^{+-}$ phase diagram in figure 3.25. We again find the familiar phases: FM, Haldane, XY and Large-D phase. As well as two gapless phases (one with central charge $c = 1$ and another gapless phase, which central charge again was not unambiguously).

In particular, we find a large Haldane phase with strong signatures (e.g. large string order parameters, see figures 3.25c and 3.25d).

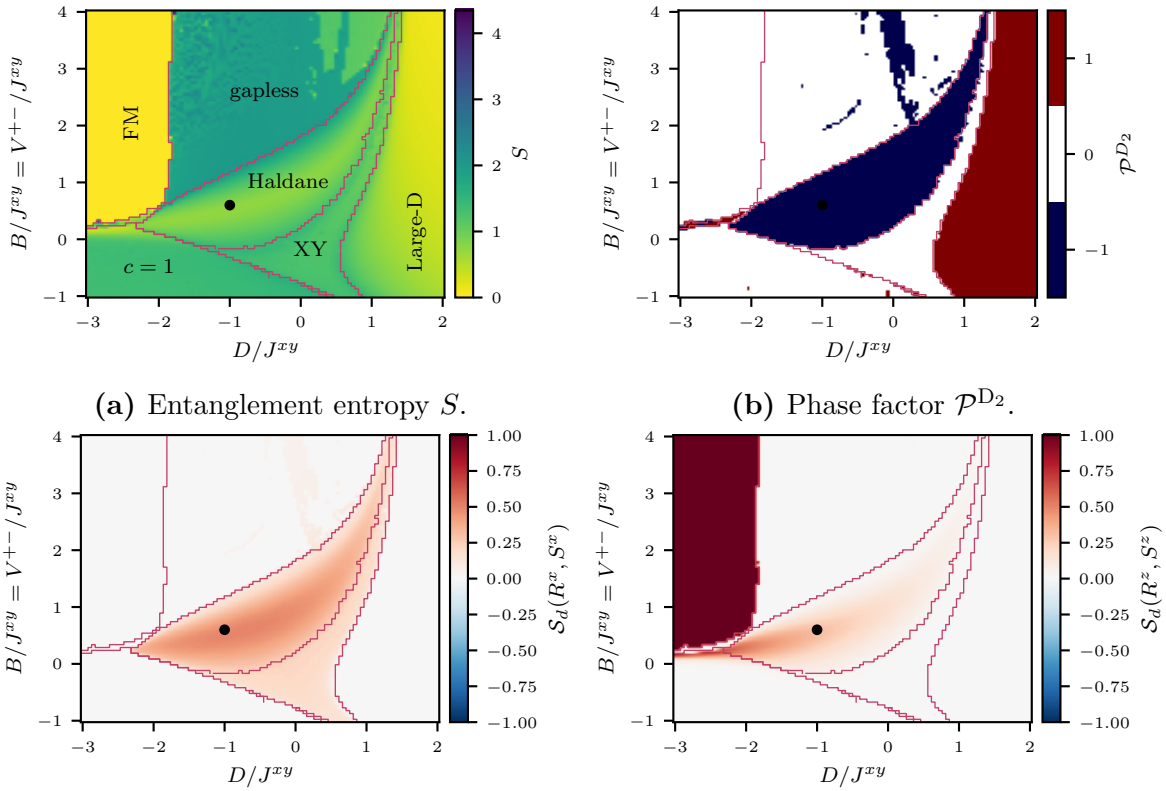

(a) Entanglement entropy S.

(b) Phase factor $\mathcal{P}^{\mathrm{D}_2}$.

(c) Odd x string order parameter $\mathcal{S}_d(R^x, S^x)$.

(d) Odd z string order parameter $\mathcal{S}_d(R^z, S^z)$.

Figure 3.25: Phase diagram for varying the parameters D and $B = V^{+-}$. The black dot denotes the proposed parameters (see equation (3.11)) for realizing the Haldane phase.

Let us end this chapter by proposing the following parameter set to realize the Haldane phase, which we choose by optimizing the x and z string order parameters, while still keeping some distance to the phase boundaries.

$$\begin{aligned} J^z = 0\,, \quad \delta_0 = 0\,, \quad \delta = 0\,, \quad \alpha = 3\,, \\ D/J^{xy} = -1\,, \quad B/J^{xy} = V^{+-}/J^{xy} = 0.6\,, \quad \alpha_{\mathrm{vdw}} = 6\,. \end{aligned} \tag{3.11}$$

These parameters correspond to the black dot in figure 3.25.

This parameter set is by no means the only possible way to realize the Haldane phase, as we discussed in the last part. Note that we so far also only explored some small subspaces of the full three-dimensional parameter regime of tuning D, δ_0 and $B = V^{+-}$. However, by looking at the $D - B = V^{+-}$ phase diagrams for different values of δ_0, at first glance we did not find any strongly more prominent points, that featured the Haldane phase with stronger string order parameters or other features, that would make it more interesting, than the proposed parameter set.

Furthermore, the scheme we are going to present in the next chapter to find an experimental Rydberg setup with that exact interaction strengths can be applied also to many of these possible parameter sets. The main reason we choose these parameters is, that a non-vanishing $B = V^{+-}$ parameter, which in terms of Rydberg interactions is a van der Waals interaction, allows us to choose small interatomic distances (at small interatomic distances we might not be able to tune these van der Waals interactions to zero). The small interatomic distances on the other hand allow us to also get strong dipole-dipole interaction, which means that J^{xy} will be large (on the order of 10MHz for interatomic distances of $3\,\mu$m), which also sets our energy scale for the excitation gaps. A detailed discussion of this follows in the next chapter.

4 Experimental proposal

4.1 Tuning the parameters

In chapter 2 we already started discussing the general concept of three level system near to a Förster resonance and introduced possible interaction terms for that system. Here we are going to specify this for a particular Förster resonance and will discuss the possibilities of tuning the different parameters in detail, which will make it possible to realize the proposed parameter set of the last section (see equation (3.11)). Note that all calculations of Rydberg energies and interaction strengths between Rydberg atoms are done using the *pairinteraction* software [31].

First, let us introduce the Förster resonance of interest for this section. We will use Rubidium (Rb) atoms and states of the near resonant Förster coupling

$$\left|37P_{3/2}\right\rangle \left|37P_{3/2}\right\rangle \rightarrow \left|37S_{1/2}\right\rangle \left|38S_{1/2}\right\rangle \,, \tag{4.1}$$

where the energy offset for no applied fields is

$$\left[2E(37P_{3/2}) - E(37S_{1/2}) - E(38S_{1/2})\right]/h \approx 104\,\mathrm{MHz}\,. \tag{4.2}$$

This Förster resonance has also already been studied experimentally, e.g. [43].

To be able to tune δ_0 and $B \approx V^{+-}$, we are considering a three level system of the configuration IV (see figure 2.2). In particular, we are using the following three states and again label these Rydberg states with spin 1 names

$$\begin{aligned} |+\rangle &= \left|38S_{1/2}, m_j = \frac{1}{2}\right\rangle \\ |0\rangle &= \left|37P_{3/2}, m_j = \frac{3}{2}\right\rangle \\ |-\rangle &= \left|37S_{1/2}, m_j = \frac{1}{2}\right\rangle \,. \end{aligned} \tag{4.3}$$

Note that $|+\rangle$ and $|-\rangle$ do have the same magnetic moments m_j.

A general energy spectrum of the single atom Rydberg states for varying electric fields $\boldsymbol{E} = E_z \boldsymbol{e}_z$ and magnetic fields $\boldsymbol{B} = B_z \boldsymbol{e}_z$ can be seen in figure 4.1. We marked the interesting states $|+\rangle$, $|0\rangle$ and $|-\rangle$ by colored dots. To be precise the states $|+\rangle$, $|0\rangle$ and $|-\rangle$ (as well as all the other Rydberg eigenstates $|n, l, j, m_j\rangle$) are no longer eigenstates of the system for applied electric fields or two atom interactions. Nevertheless, we marked the states, which had the largest overlap with these original eigenstates, and we will also refer to these states by these names.

The single atom excitation gap $\omega = (E_{|+\rangle} - E_{|-\rangle})/2$ is on the order of $\omega/h \approx 81\,\mathrm{GHz}$. The offset $D = (E_{|+\rangle} + E_{|-\rangle})/2 - E_{|0\rangle}$ for no applied fields is $D/h \approx 52\,\mathrm{MHz}$, which can easily be tuned by applying fields. This can already be seen by the different shifts in figures 4.1b and 4.1d and is also more clearly shown in figure 4.2. One can clearly see a (negative) linear dependence on the magnetic field and a quadratic dependence on the electric field (corresponding to a linear Zeeman effect and a quadratic Stark effect, see section 1.5).

For calculating interactions of two Rydberg atoms let us have a look at the two particle energy spectrum. Due to the single atom excitation energy ω the two atom energy levels split up in 5 different subspaces with the corresponding two atom states as shown in table 4.1. We define the state $|00\rangle$ to be at energy $E_{|00\rangle} = 0$.

Table 4.1: Two atom energy subspaces.

Approximate energy offset with respect to the $\lvert 00\rangle$ energy	States of interest in the corresponding subspaces
2ω	$\lvert ++\rangle$
ω	$\lvert +0\rangle$, $\lvert 0+\rangle$
0	$\lvert +-\rangle$, $\lvert 00\rangle$, $\lvert -+\rangle$
$-\omega$	$\lvert -0\rangle$, $\lvert 0-\rangle$
-2ω	$\lvert --\rangle$

For the sake of an example we will already state the proposed experimental parameters here

$$R = 3\,\mu\mathrm{m}\,, \quad \theta = 0.615\,\mathrm{rad}\,, \quad E_z = 3.19\,\mathrm{V/cm}\,, \quad B_z = 63.7\,\mathrm{G}\,. \tag{4.4}$$

We will use them to illustrate the dependencies of the two atom energies and interaction strengths from these setup parameters. After that we will then argue how we selected these specific parameters.

Remember that we defined the parameters of the spin 1 Hamiltonians (3.1) – (3.7) in terms of the interaction strengths of the Rydberg system by the following relations (see

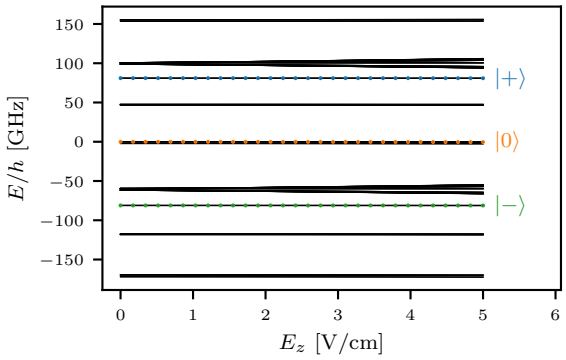

(a) Single atom spectrum for varying the electric field E_z ($B_z = 0$).

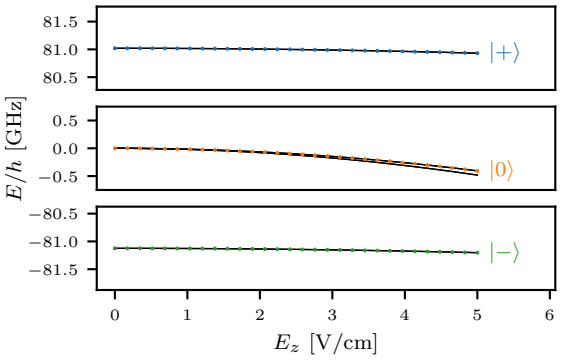

(b) Single atom spectrum over E_z ($B_z = 0$), zoomed in at the states of interest.

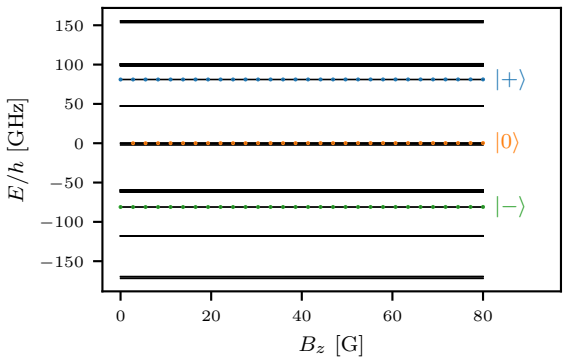

(c) Single atom spectrum for varying the magnetic field B_z ($E_z = 0$).

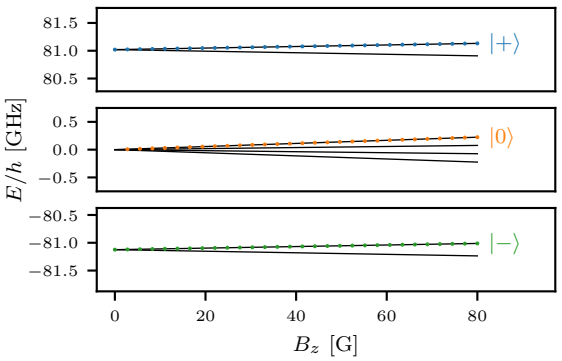

(d) Single atom spectrum over B_z ($E_z = 0$), zoomed in at the states of interest.

Figure 4.1: Single atom spectrum for varying the electric (E_z) and magnetic (B_z) fields in the energy range of the three states of interest $|+\rangle$, $|0\rangle$ and $|-\rangle$ (see equation (4.3)). The highlight of certain levels correspond to the largest overlap of these levels with the initial states $|+\rangle$, $|0\rangle$ and $|-\rangle$. We plotted all energies with respect to the energy of the state $|0\rangle$ at no applied fields.

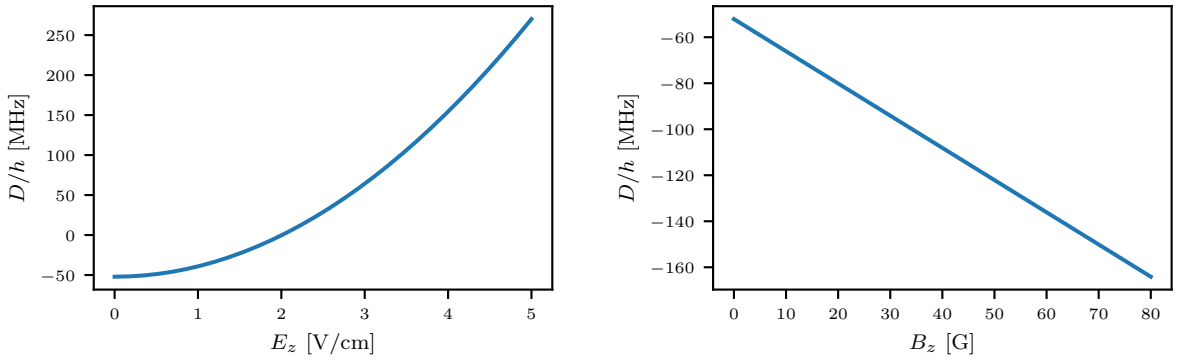

Figure 4.2: Energy offset $D = (E_{|+\rangle} + E_{|-\rangle})/2 - E_{|0\rangle}$ for varying the electric and magnetic field.

also chapter 2 for more details)

$$\begin{aligned} J^{xy} &= \frac{J^{+0} + J^{-0}}{2}\,, \quad \delta = \frac{J^{+0} - J^{-0}}{2}\,, \\ \delta_0 &= J^{00} - \frac{J^{+0} + J^{-0}}{2}\,, \quad B = B\,, \quad V^{+-} = V^{+-}\,. \end{aligned} \tag{4.5}$$

From the analytical expressions derived in chapter 2 (for configuration IV) we expect the following distance R and angle θ dependencies

$$\begin{aligned} J^{xy} &\propto \frac{3\cos^2\theta - 1}{R^3} \\ \delta_0 &\propto \frac{1}{R^3}\left[\sin^2\theta - \left(3\cos^2\theta - 1\right)\right] \\ B \approx V^{+-} &\propto \frac{1}{R^6} f(\theta)\,. \end{aligned} \tag{4.6}$$

Here $f(\theta)$ is a general function, that exact form depends on which second order process has the dominant contribution to the van der Waals interactions. We will come back to this second order processes at equation (4.8). The detuning δ of the J^{+0} and J^{-0} couplings will scale similar as J^{xy}, in fact we find for all considered setup parameters $\delta \approx -0.02 J^{xy}$.

Let us start by looking at distance dependence of the numerically calculated interactions. As expected we find in figure 4.3 a $1/R^3$ dependence for the dipole-dipole J^{xy} interaction. And the van der Waals interaction B (and V^{+-} which would look exactly the same as B) shows a $1/R^6$ distance dependence.

Furthermore, J^{xy} and δ_0 will also depend on the angle θ, which can be seen in figure 4.4a. Since we want to have an antiferromagnetic interaction $J^{xy} > 0$, we should choose an

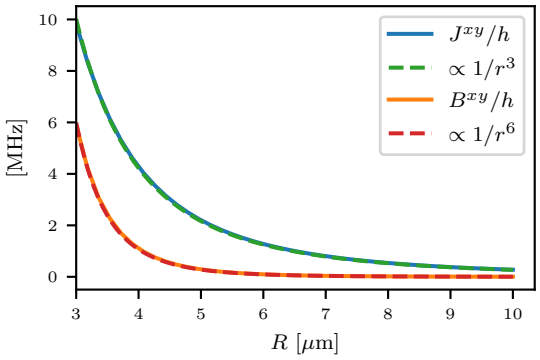

Figure 4.3: Distance R dependence of the dipole-dipole interaction J^{xy} and the van der Waals interaction B. As dashed lines the expected $1/R^3$ and $1/R^6$ behaviors and as solid lines the numerically calculated interactions for a setup defined by the parameters in equation (4.4).

angle $\theta < 0.955\,\text{rad}$. Because we use J^{xy} as energy scale we are also interested in δ_0/J^{xy}, which can be seen in figure 4.4b.

The parameters B and J^{xy} do have a different distance dependence, which we can use to vary the ratio of B/J^{xy}. Furthermore, B also strongly depends on the electric and magnetic fields, which we will see in the following. For that let us first look at the 0 energy subspace with the states $|{+}{-}\rangle$, $|00\rangle$ and $|{-}{+}\rangle$. The two atom energy spectrum for this subspace dependent on the fields can be seen in figure 4.5. We can clearly see multiply energy level crossings. First, near to the dashed lines for a magnetic field $B_z \approx 64\,\text{G}$ and an electric field of $E_z \approx 3.2\,\text{V/cm}$ we find the Förster resonance, were the detuning D of the $|00\rangle$ and the $|{+}{-}\rangle$ (as well as the $|{-}{+}\rangle$) state vanishes. This is the parameter point, which we are interested in.

Furthermore, we see for a varying electric field multiple energy crossings of the $|{+}{-}\rangle$ state with other auxiliary states. These will help us to understand the van der Waals interactions (which were also already introduced at the end of chapter 2). The auxiliary states of interest are

$$\begin{aligned} |v_1\rangle &= \left|37P_{3/2}, m_j = \frac{1}{2}\right\rangle \\ |v_2\rangle &= \left|37P_{3/2}, m_j = -\frac{1}{2}\right\rangle . \end{aligned} \tag{4.7}$$

These are exactly the states, which allow for the second order processes

$$\begin{aligned} |{+}{-}\rangle &\xrightarrow{\hat{H}^{\text{dd}}} |v_i v_j\rangle \xrightarrow{\hat{H}^{\text{dd}}} |{+}{-}\rangle \\ |{+}{-}\rangle &\xrightarrow{\hat{H}^{\text{dd}}} |v_i v_j\rangle \xrightarrow{\hat{H}^{\text{dd}}} |{-}{+}\rangle , \end{aligned} \tag{4.8}$$

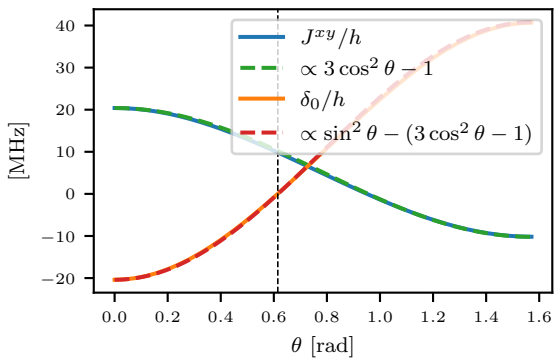

(a) Angle θ dependence of the dipole-dipole interactions J^{xy} and δ_0.

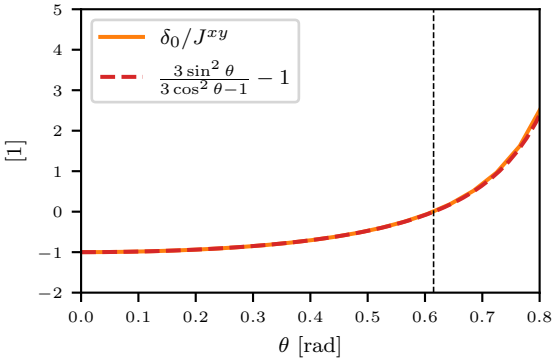

(b) Angle θ dependence of the δ_0 parameter in units of J^{xy}.

Figure 4.4: Angle θ dependence of the J^{xy} and δ_0 interactions. As dashed lines the analytical expected behaviors and as solid lines the numerically calculated interactions for a setup defined by the parameters in equation (4.4). The black vertical dashed line corresponds to the proposed parameter $\theta = 0.615\,\text{rad}$.

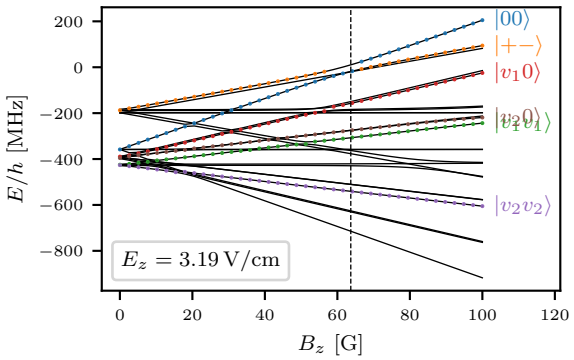

(a) Spectrum for varying the magnetic field B_z.

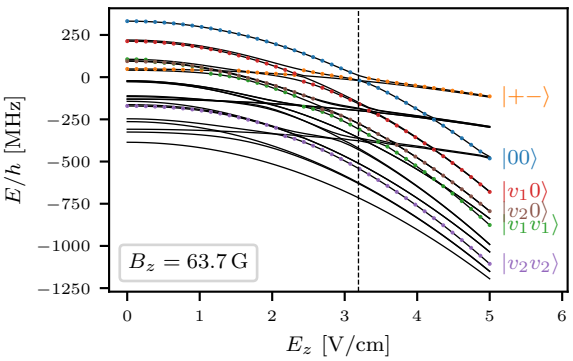

(b) Spectrum for varying the electric field E_z.

Figure 4.5: The two atom energy spectrum for states near to the $|+-\rangle$, $|00\rangle$ and $|-+\rangle$ states for a setup defined by equation (4.4). The dashed vertical lines corresponds to the proposed parameters (see equation (4.4)). The colored dots highlight the states with the largest overlaps to the relevant states (inverted states like $|+-\rangle$ and $|-+\rangle$ are only marked once, since they have the same overlaps).

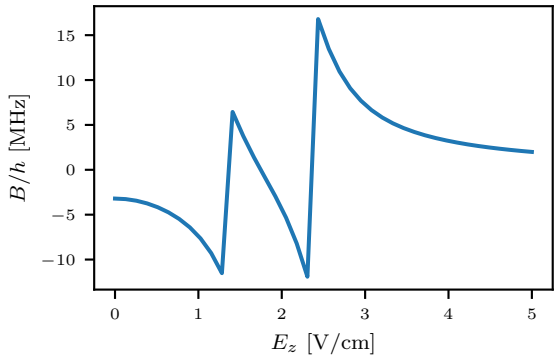

Figure 4.6: The van der Waals interaction B plotted over the electric field E_z. Each jump in B corresponds to a level crossing of the $|+-\rangle$ state in figure 4.5.

which are resulting in the interaction strengths B and V^{+-}.

If we now look at B (V^{+-} looks exactly the same) plotted over the electric field E_z in figure 4.6 we find jumps of the interaction strength exactly at the electric fields of additional level crossing with the auxiliary states ($E_z \approx 1.2\,\mathrm{V/cm}$ and $E_z \approx 2.2\,\mathrm{V/cm}$). This can be explained since the van der Waals interactions can be treated in second order perturbation theory, thus their interaction strength is proportional to $1/\Delta E$. At energy crossings the second order perturbation theory (which is not valid anymore at these energy crossings!) would diverge and flip its sign. Since also the *pairinteraction* software calculates the interactions perturbatively we can see this jumps in the calculated interactions in figure 4.6.

We end this discussion of second order processes by noting that for having an effective three level system with only small overlaps with other states, this additional auxiliary states must be well separated from the $|00\rangle$ - $|+-\rangle$ Förster resonance. This is the case for the parameters chosen here, since at the Förster resonance (marked by the vertical lines in figure 4.5) the smallest energy gap to another state is on the order of 200 MHz. However, this nearby auxiliary states are also, what gives rise to the big van der Waals interaction terms B and V^{+-}, which we are using to build our effective model featuring the Haldane phase.

We now got a first impression on how the parameters depend on the experimental setup, like the interatomic distance R, the angle θ between the interatomic axis and the quantization axis parallel to the fields, as well as the strength of the applied fields E_z and B_z.

Let us now discuss how to realize the proposed model parameters, which are again listed

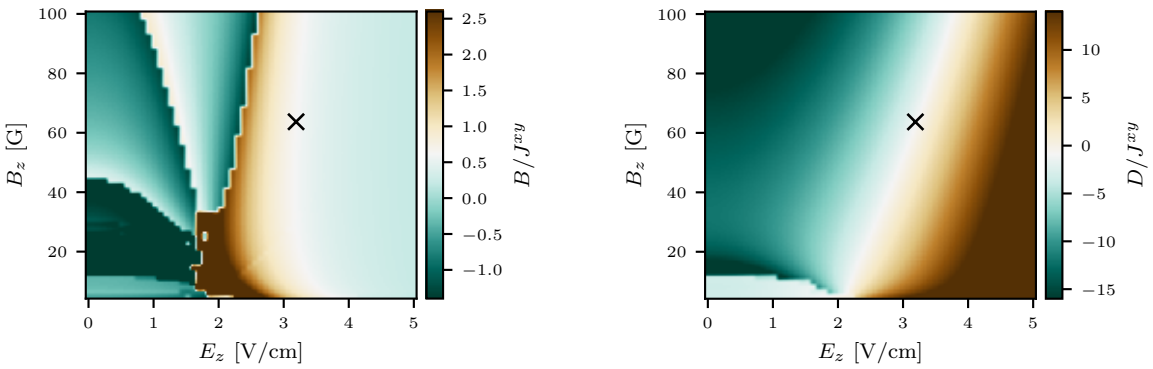

(a) Van der Waals interaction B. Each jump of the B values correspond to a level crossing of the $|+-\rangle$ state as explained before.

(b) Energy offset D.

Figure 4.7: The parameters B and D dependent on the electric field E_z and the magnetic field B_z. The value $B/J^{xy} = 0.6$ and $D/J^{xy} = -1$ are colored white, while values above and below are colored in brown and green. The black cross indicates the proposed fields $E_z = 3.19\,\mathrm{V/cm}$ and $B_z = 63.7\,\mathrm{G}$

here

$$D/J^{xy} = -1\,, \quad \delta_0 = 0\,, \quad B/J^{xy} = V^{+-}/J^{xy} = 0.6\,. \tag{4.9}$$

Note that the symmetry breaking parameter δ is barely tunable and for all parameters roughly is about $\delta/J^{xy} \approx -0.02$.

First, we can set $\delta_0 = 0$ by fixing the angle θ according to figure 4.4b. We find $\delta_0 = 0$ for $\theta \approx 0.615\,\mathrm{rad}$.

Next we want an as large as possible energy scale (to make the excitation gap as large as possible) and therefore choose a small interatomic distance $r = 3\,\mu\mathrm{m}$.

The last step is to adjust the electric and magnetic field, such that the final two parameters D and $B = V^{+-}$ are as close as possible to the wanted values in equation (4.9). We plot D as well as B over the electric and magnetic field to see if this is possible, see figure 4.7. In both plots we colored the desired values $D/J^{xy} = -1$ and $B/J^{xy} = +0.6$ white and values above/below are shown in brown/green. Indeed, it seems to be possible to find fields, for which the Rydberg system yields the desired parameters. We find for $B_z = 63.7\,\mathrm{G}$ and $E_z = 3.19\,\mathrm{V/cm}$ (marked by a black cross in figure 4.7) the desired parameters $B/J^{xy} = 0.60$ and $D/J^{xy} = -1.00$.

Note that this nice feature, that we can tune D and B with the electric and magnetic field differently would also allow us to realize other model parameter sets. For example in figure 4.8 we plotted the parameter B as function of the electric field E_z for a constant

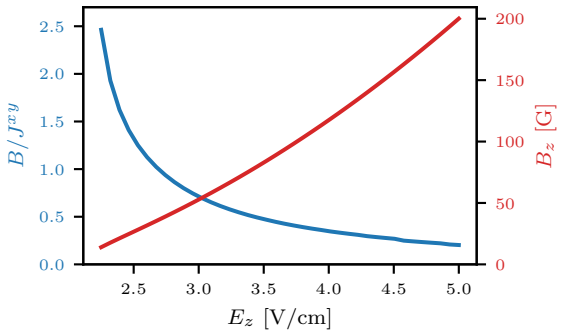

Figure 4.8: The van der Waals interaction B (blue line) plotted over the electric field E_z. For each value of the electric field E_z we tuned the magnetic field B_z (plotted in red), such that the parameter $D/J^{xy} = -1$ stayed constant. The calculations where done for a distance $R = 3\,\mu$m and an angle $\theta = 0.615\,$rad.

value $D/J^{xy} = -1$, which we achieved by adjusting the magnetic field B_z for each value of the electric field. We can clearly see that one could tune a wide range of B values.

We can picture tuning B while keeping D constant by looking again at figure 4.5. Staying at a constant D means we always go near to the Förster resonance where the $|{+}{-}\rangle$ and $|00\rangle$ states cross. Now by changing the electric field (and tuning the magnetic field to the resonance) we can shift the auxiliary states $|v_i v_j\rangle$. Thus, the energy offset ΔE for the second order process changes and the van der Waals interaction B changes according to $1/\Delta E$. We only have to keep in mind that for very small ΔE our effective three level approximation will fail. Since we are only interested in intermediate B this is however no problem for our parameter regime.

If we want even smaller values for B without the usage of very strong fields, one can in addition change the distance R. By increasing the distance R the ratio B/J^{xy} will decrease with $1/R^3$ (since B is a van der Waals term and J^{xy} a dipole-dipole interaction).

4.2 Experimental proposal

In the last section we discussed how to find experimental parameters, such that the interaction strengths are close to the theoretical proposed model parameters in equation (3.11).

Using these experimental parameters (see equation (4.10)) we can calculate the interactions also for next-nearest-neighbors (and more). Additionally, we will also consider all diagonal van der Waals terms (and not only V^{+-}).

In this section we are then going to show that this realistic model still features the Haldane phase We will do so by looking at finite size properties of this model. Furthermore, we will also discuss the stability of the Haldane phase in this model.

4.2.1 System

Let us start by describing our realistic model. We proposed the following experimental setup parameters

$$E = 3.19\,\mathrm{V/cm}\,, \quad B = 63.7\,\mathrm{G}\,, \quad R = 3\,\mu\mathrm{m}\,, \quad \theta = 0.615\,\mathrm{rad}\,, \tag{4.10}$$

and are using the three states

$$\begin{aligned} |+\rangle &= \left|38S_{1/2}, m_j = \frac{1}{2}\right\rangle \\ |0\rangle &= \left|37P_{3/2}, m_j = \frac{3}{2}\right\rangle \\ |-\rangle &= \left|37S_{1/2}, m_j = \frac{1}{2}\right\rangle . \end{aligned} \tag{4.11}$$

Calculating the onsite energies and interaction terms with the *pairinteraction* software [31] yields the following Hamiltonian

$$\begin{aligned} H = \sum_{i\neq j} \Big[& J_{ij}^{+0} \left|+_i 0_j\right\rangle \left\langle 0_i +_j\right| + J_{ij}^{-0} \left|-_i 0_j\right\rangle \left\langle 0_i -_j\right| + J_{ij}^{00} \Big(\left|+_i -_j\right\rangle \left\langle 0_i 0_j\right| + \left|-_i +_j\right\rangle \left\langle 0_i 0_j\right| \Big) \\ & + B_{ij} \left|+_i -_j\right\rangle \left\langle -_i +_j\right| + \frac{1}{2} \sum_{s_i, s_j \in \{+,0,-\}} V_{ij}^{s_i s_j} \left|s_i s_j\right\rangle \left\langle s_i s_j\right| \Big] \\ & + \sum_i D \Big(\left|+_i\right\rangle \left\langle +_i\right| + \left|-_i\right\rangle \left\langle -_i\right| \Big) . \end{aligned} \tag{4.12}$$

The parameters of this Hamiltonian are listed in table 4.2. Furthermore, if not stated otherwise we will consider a system of $N = 20$ atoms.

4.2.2 Ground state properties

Let us now discuss the ground state properties of this realistic model.

First, we can look at the string order parameters. In figure 4.9 we see the odd x and z string order parameter $\mathcal{S}_{1,1+d}(R^x, S^x)$ and $\mathcal{S}_{1,1+d}(R^z, S^z)$ dependent on the site distance

Table 4.2: Parameters of the Rydberg Hamiltonian (4.12) in MHz. We consider interactions up to the fifth-nearest neighbor.

$\lvert i-j\rvert$	1	2	3	4	5
J_{ij}^{+0}/h	9.59	1.24	0.37	0.16	0.08
J_{ij}^{-0}/h	10.09	1.31	0.39	0.16	0.08
J_{ij}^{00}/h	9.87	1.27	0.38	0.16	0.08
B_{ij}/h	5.91	0.10	0.01	0.00	0.00
$V_{ij}^{+-}/h = V_{ij}^{-+}/h$	5.88	0.09	0.01	0.00	0.00
$V_{ij}^{+0}/h = V_{ij}^{0+}/h$	1.96	0.02	0.00	-0.00	-0.00
$V_{ij}^{-0}/h = V_{ij}^{0-}/h$	2.22	0.03	0.00	-0.00	-0.00
V_{ij}^{++}/h	0.02	0.00	0.00	0.00	0.00
V_{ij}^{00}/h	-0.26	-0.03	-0.01	-0.00	-0.00
V_{ij}^{--}/h	-0.00	-0.00	-0.00	-0.00	-0.00

$D/h = -9.84$

d used to measure the string order parameter. Note that we always used the first site as leftmost site of the string order parameter ($i = 1$), and the $(1 + d)$ site as rightmost site of the string order parameter. Both saturate immediately after the first site to a large finite value ($\mathcal{S}_{1,1+d}(R^x, S^x) \approx \mathcal{S}_{1,1+d}(R^y, S^y) \approx 0.43$, $\mathcal{S}_{1,1+d}(R^z, S^z) \approx 0.36$).
On the other hand, as we expect from the Haldane phase, the even string order parameters $\mathcal{S}_{1,1+d}(R^\alpha, \mathbb{1})$ drop to zero after just a few sites (see figure 4.10). The increase of the even z string order parameter at large site distances is due to the edge states, which we will discuss below.

But first let us also notice that the local ferromagnetic order parameters $\mathcal{O}_{1,1+d}^{\mathrm{FM},\alpha}$ drop to zero after just a few sites (see figure 4.11). And again in z direction for site distances d of the order of the system size $N = 20$ the ferromagnetic order increases again indicating edge magnetization.

One advantage of doing finite DMRG simulations is that we are now able to also calculate low excited states. In figure 4.12 one can see an energy spectrum plotted over the total z magnetization S^z_{total} of the corresponding states. We can clearly see a fourfold ground state manifold, with a small energy splitting of $\sim 0.1\,\mathrm{MHz}$, and above that a large excitation gap ($\sim 1\,\mathrm{MHz}$). Furthermore, we find two of these ground states in the total magnetization $S^z_{\mathrm{total}} = 0$ sector and one respectively in the ± 1 sector. This is in perfect agreement with the fourfold ground state degeneracy we expect from the Haldane phase. The small energy splitting comes from the symmetry breaking terms in the Hamiltonian $\delta = (J^{+0} - J^{-0})/2$, as we will see when discussing the stability of this Haldane phase

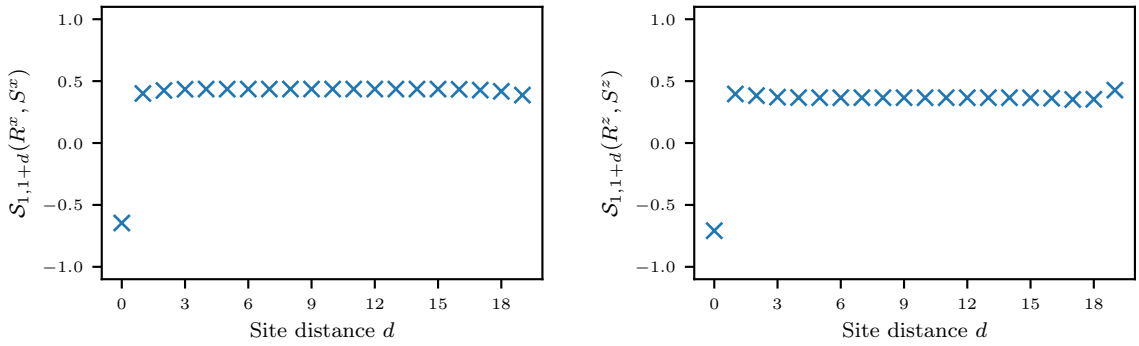

Figure 4.9: Odd x and z string order parameter for the finite realistic model as function of the site distance d.

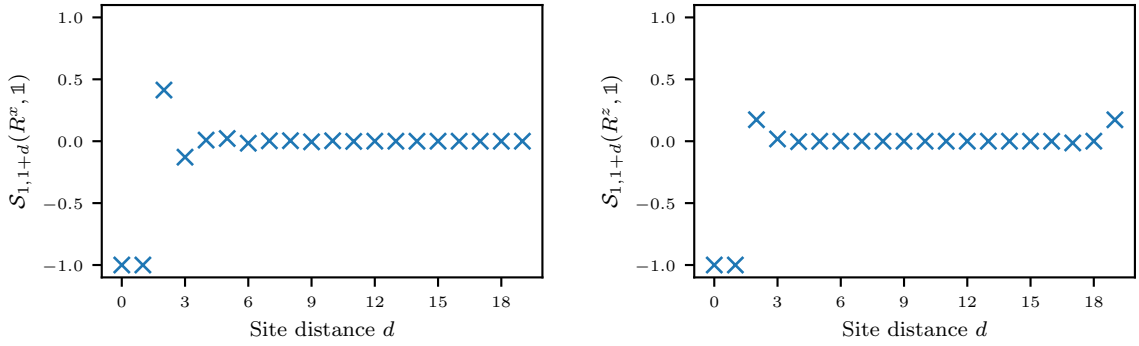

Figure 4.10: Even x and z string order parameter for the finite realistic model as function of the site distance d.

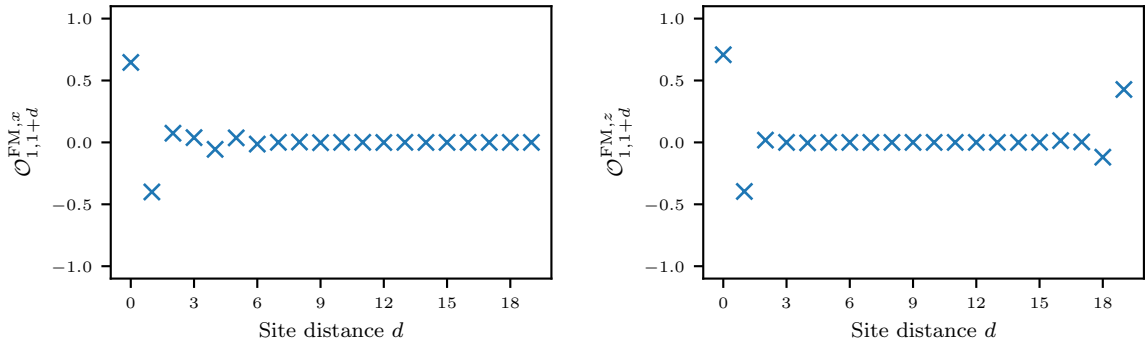

Figure 4.11: Ferromagnetic order parameter (x and z) for the finite realistic model as function of the site distance d.

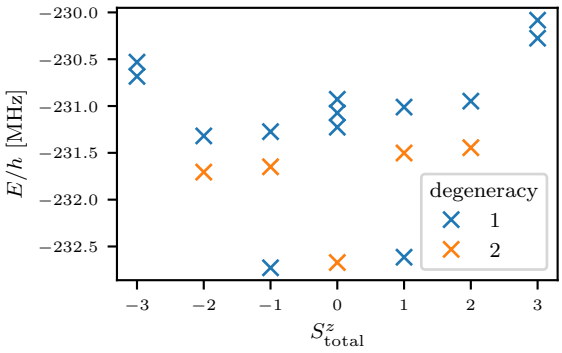

Figure 4.12: Energy spectrum of the realistic model for a system size of $N = 20$. The lowest energies for the charge sectors $S^z_{\text{total}} \in \{0, \pm 1, \pm 2, \pm 3\}$ have been calculated using consecutive DMRG runs. The energies are plotted over the total magnetization S^z_{total} of the states. Degeneracies of multiple states with the same energy E and magnetization S^z_{total} are color coded.

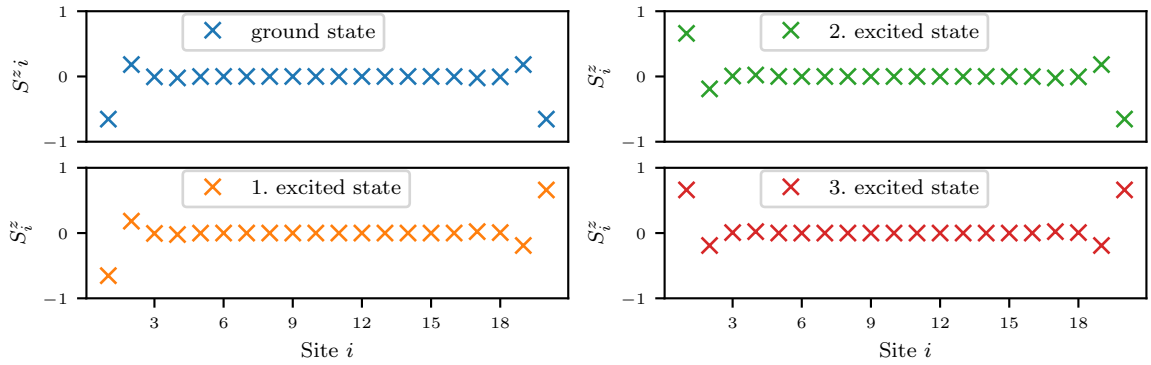

Figure 4.13: Local magnetization S^z_i of the four lowest eigenstates of the realistic model. We can clearly see fractional edge excitations.

(see figure 4.17).

To see the edge states of these ground states we plot in figure 4.13 the local magnetization of the four ground states. We can clearly see localized fractional excitations at the edges, where at each edge there is a ± 0.5 magnetization (if we sum over the 3 nearest edge sites). This fractionalized excitations at the edges effectively form two spin 1/2 degree of freedoms which explains the fourfold ground state degeneracy. The local magnetization in x and y direction of all four ground states is 0 at each site.

Furthermore, note the that the entanglement entropy for cutting the system into two halves of 10 sites is $S = 0.701$, and the two largest degenerate Schmidt values are $\Lambda_1^2 = \Lambda_2^2 = 0.4995$, thus the two corresponding Schmidt states have about 99.9 % of the

total weight. This is quite impressive, we achieved with realistic experimental parameters a Hamiltonian which features the Haldane phase and which ground state mainly consists of two Schmidt states, quite similar to the AKLT state, which can exactly be written with only two Schmidt states. Note that even in the XXZ model, where we tuned J^z, the smallest entanglement entropy in the Haldane phase was about $S = 0.855$ and the two largest Schmidt values had about 96.9 % of the total weight of all Schmidt states.

To conclude, our proposed model with experimental realistic parameters indeed features a Haldane phase with large string order parameters and a nearly fourfold degenerate ground state manifold with a large excitation gap of about 1 MHz.

4.2.3 Stability

We will now discuss the stability of the Haldane phase in this realistic model by adding additional terms to the Hamiltonian. We start by adding an additional onsite energy D. In figure 4.14 we can clearly see, that the near fourfold ground state degeneracy is stable for a range of offsets, and only for large offsets $|D| \gtrsim 5\,\text{MHz}$ a gap closing, indicating a phase transition, occurs. Furthermore, we see that our parameter choice was near optimal in the sense of maximizing the excitation gap and minimizing the entanglement entropy.

Similar also for changing the interactions by adding again a δ_0 term (with $\alpha = 3$, defined as in equation (3.5)) or a $B = V^{+-}$ term (with $\alpha_{\text{vdw}} = 6$, defined as in equation (3.6)) we find a stable Haldane phase for changes of the interactions up to a few MHz. The corresponding plots are in figures 4.15 and 4.16.

Thus, also in an imperfect experimental setup we expect to be able to find the Haldane phase.

Let us also have a look at adding the symmetry breaking detuning δ (with $\alpha = 3$, defined as in equation (3.4)). In figure 4.17 we can see that for changing δ the small splitting of the near fourfold ground state degeneracy gets larger. Note that for a small additional δ the splitting first gets even smaller, because this term counteracts the small symmetry breaking of the parameters of the realistic model. Furthermore, notice, that the entropy as well as the string order parameters do not change at all as long as there is no level crossing with the actual ground state, even if the original nearly degenerate first three excited states already have a large excitation gap to the ground state. It seems like the symmetry breaking term δ primarily shifts the energy of the subspaces for different total magnetization S^z_{total} against each other without changing the states itself. In figure 4.12 we could already see, that the lowest $S^z_{\text{total}} = \pm 1$ are shifted against each other, while

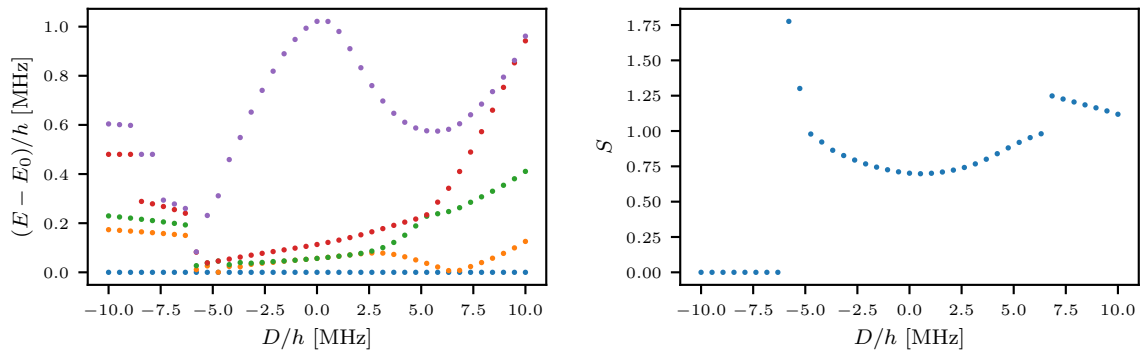

Figure 4.14: Energy spectrum $E-E_0$ for the five smallest eigenenergies and entanglement entropy S of the ground state as function of an additional onsite energy D.

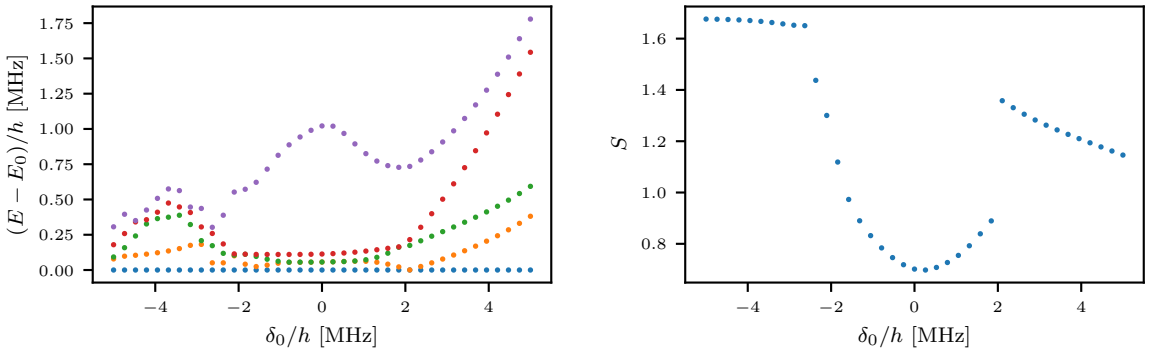

Figure 4.15: Energy spectrum $E-E_0$ for the five smallest eigenenergies and entanglement entropy S of the ground state as function of an additional dipole-dipole interaction δ_0.

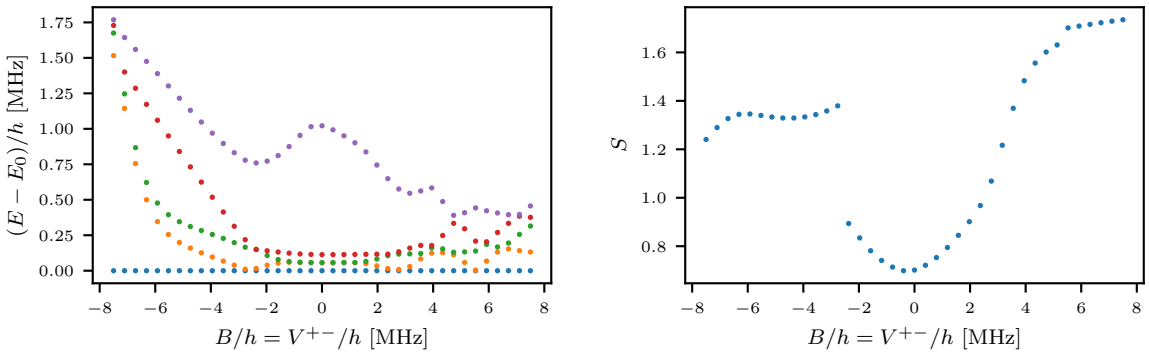

Figure 4.16: Energy spectrum $E-E_0$ for the five smallest eigenenergies and entanglement entropy S of the ground state as function of additional van der Waals interactions $B = V^{+-}$.

both ground states with $S^z_{\text{total}} = 0$ still were perfectly degenerate. This as we can see in figure 4.17 is also true if we vary δ.

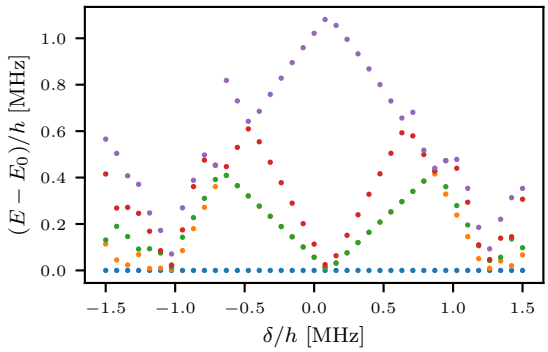

(a) Energy spectrum $E - E_0$ for the five smallest eigenenergies. For small δ the first (orange) and second (green) excited states are degenerate and one can only see the green dots.

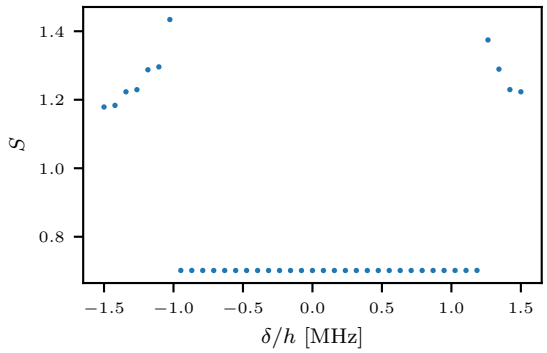

(b) Entanglement entropy S stays constant for a wide range of δ and only changes at the gap closing points.

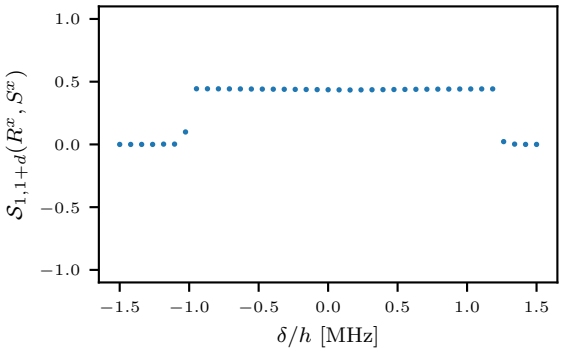

(c) The odd x string order parameter $\mathcal{S}_{1,1+d}(R^x, S^x)$ (we choose $d = N/2 = 10$) also stays constant in the Haldane phase up to the gap closing points.

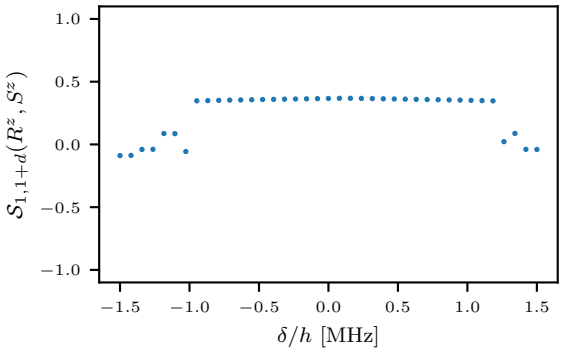

(d) The odd z string order parameter $\mathcal{S}_{1,1+d}(R^z, S^z)$ (we choose $d = N/2 = 10$) also stays constant in the Haldane phase up to the gap closing points.

Figure 4.17: Stability of the Haldane phase for a varying the symmetry breaking term δ.

Last but not least, we can also do a finite size scaling and look at how the properties depend on the system size N. It appears that we can find the properties of the Haldane phase already for very small system sizes (see figure 4.18). And we only have for very small systems finite size effects. This can be explained because the point in the Haldane phase we found has almost only two degenerate Schmidt states, quite similar to the AKLT state, and for the AKLT state there are also no finite size effects (in the sense

that the string order parameters and the ground state degeneracy stays the same for system sizes as small as $N = 3$ sites).

We finish this chapter by emphasizing again, that indeed we were able to find a parameter set, that can be realized using Rydberg atoms and that strongly features the Haldane phase.

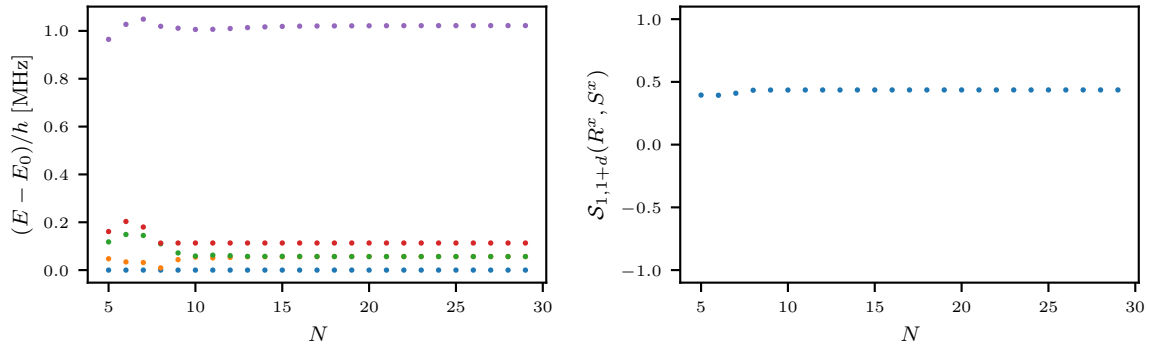

Figure 4.18: Finite size scaling. The energy spectrum $E - E_0$ for the five smallest eigenenergies and the x string order parameter $\mathcal{S}_{1,1+d}(R^x, S^x)$ (with $d = \lfloor N/2 \rfloor$) are plotted for varying system sizes N.

5 Conclusion

In this work we studied the Haldane phase with respect to a possible experimental realization using Rydberg atoms.

We started by introducing an effective three level system consisting of Rydberg levels near to a Förster resonance. This three level system can then be mapped to a spin 1 particle, which allows us to build a many particle spin 1 model with Rydberg atoms. We also determined the relevant spin coupling terms that are possible to realize using the Rydberg states.

Next we discussed the effect of these different interaction terms on the Haldane phase. For that we used the (infinite) density matrix renormalization group to find the ground state of the many particle Hamiltonians consisting of these different interaction terms. This allowed us to study the ground state properties as well as the phase diagrams for different parameters.

Finally, we used our knowledge about the phase diagrams to find an experimentally realizable model with strong signatures of the Haldane phase. Furthermore, we then discussed how we can tune the interactions of a Rydberg system to get as close as possible to this model. By doing so we propose an experimental setup that features the Haldane phase. We verified that the properties of this realistic model indeed agree with the Haldane state. Last but not least, we discussed the stability of the Haldane phase in this model.

Future work might involve the discussion of a preparation scheme for the ground state of the proposed model. In addition, further discussion of detecting the ground state properties in an experiment is needed. Especially the question of how to demonstrate the spin fractionalization, which should result in a spin 1/2 statistics of the edge excitations, is still not finally resolved.

A AKLT transformation

When discussing the phase diagram for the spin 1 XXZ model for an additional term δ_0 we found a certain symmetry for a reflection at the $\delta_0/J^{xy} = -1$ line of the phase diagram (see e.g. figure 3.18). In this appendix we want to discuss the reason for this symmetry. Let us start by writing down the Hamiltonian of interest (for simplicity we only consider nearest neighbor interactions)

$$\begin{aligned} H^{\mathrm{XXZ}+\delta_0} &= \sum_i \frac{J^{xy}}{2}(S_i^+ S_{i+1}^- + S_i^- S_{i+1}^+) + J^z S_i^z S_{i+1}^z + \frac{\delta_0}{2} P_{i,j}^0 \left(S_i^+ S_{i+1}^- + S_i^- S_{i+1}^+\right) P_{i,j}^0 \\ &= \sum_i H_{i,i+1}^{\mathrm{XXZ}+\delta_0} \,. \end{aligned} \tag{A.1}$$

Where we can write the nearest neighbor interactions as

$$H_{i,i+1}^{\mathrm{XXZ}+\delta_0} = \begin{pmatrix} J^z & 0 & 0 & 0 & 0 & 0 & 0 & 0 & 0 \\ 0 & 0 & 0 & J^{xy} & 0 & 0 & 0 & 0 & 0 \\ 0 & 0 & -J^z & 0 & J^{xy}+\delta_0 & 0 & 0 & 0 & 0 \\ 0 & J^{xy} & 0 & 0 & 0 & 0 & 0 & 0 & 0 \\ 0 & 0 & J^{xy}+\delta_0 & 0 & 0 & 0 & J^{xy}+\delta_0 & 0 & 0 \\ 0 & 0 & 0 & 0 & 0 & 0 & 0 & J^{xy} & 0 \\ 0 & 0 & 0 & 0 & J^{xy}+\delta_0 & 0 & -J^z & 0 & 0 \\ 0 & 0 & 0 & 0 & 0 & J^{xy} & 0 & 0 & 0 \\ 0 & 0 & 0 & 0 & 0 & 0 & 0 & 0 & J^z \end{pmatrix} \begin{matrix} |{+}{+}\rangle \\ |{+}0\rangle \\ |{+}{-}\rangle \\ |0{+}\rangle \\ |00\rangle \\ |0{-}\rangle \\ |{-}{+}\rangle \\ |{-}0\rangle \\ |{-}{-}\rangle \end{matrix} . \tag{A.2}$$

Note that a reflection at the $\delta_0/J^{xy} = -1$ line thus corresponds to flipping the sign of the four entries with $J^{xy} + \delta_0$ ($\{|{+}{-}\rangle\langle 00|, |00\rangle\langle {+}{-}|, |{-}{+}\rangle\langle 00|, |00\rangle\langle {-}{+}|\}$).

More general instead of thinking of a reflection we can achieve the same transformation by applying the following local unitary transformation at each site

$$U_i^\varphi = \begin{pmatrix} \mathrm{e}^{\mathrm{i}\varphi/2} & & \\ & 1 & \\ & & \mathrm{e}^{\mathrm{i}\varphi/2} \end{pmatrix} = \mathrm{e}^{\mathrm{i}\varphi/2} |{+}\rangle\langle {+}| + |0\rangle\langle 0| + \mathrm{e}^{\mathrm{i}\varphi/2} |{+}\rangle\langle {+}| \,. \tag{A.3}$$

Choosing $\varphi = \pi$ would correspond to the reflection of above. We also define the global unitary transformation

$$U^{\varphi}_{\text{global}} = \bigotimes_i U^{\varphi}_i \,. \tag{A.4}$$

To discuss the effect of this transformation in more detail let us switch to the analytical solvable AKLT model, see equation (1.66). For simplicity, we rescale the AKLT Hamiltonian and apply a constant energy shift, ending up with

$$\begin{aligned} H^{\text{AKLT}} &= \sum_i \boldsymbol{S}_i \boldsymbol{S}_{i+1} + \frac{1}{3} \left(\boldsymbol{S}_i \boldsymbol{S}_{i+1}\right)^2 \\ &= \sum_i H^{\text{AKLT}}_{i,i+1} \,, \end{aligned} \tag{A.5}$$

with $J = 1$ and $\beta = 1/3$. We can again write the nearest neighbor interactions as

$$H^{\text{AKLT}}_{i,i+1} = \begin{pmatrix} \beta + J & 0 & 0 & 0 & 0 & 0 & 0 & 0 & 0 \\ 0 & \beta & 0 & J & 0 & 0 & 0 & 0 & 0 \\ 0 & 0 & 2\beta - J & 0 & J - \beta & 0 & \beta & 0 & 0 \\ 0 & J & 0 & \beta & 0 & 0 & 0 & 0 & 0 \\ 0 & 0 & J - \beta & 0 & 2\beta & 0 & J - \beta & 0 & 0 \\ 0 & 0 & 0 & 0 & 0 & \beta & 0 & J & 0 \\ 0 & 0 & \beta & 0 & J - \beta & 0 & 2\beta - J & 0 & 0 \\ 0 & 0 & 0 & 0 & 0 & J & 0 & \beta & 0 \\ 0 & 0 & 0 & 0 & 0 & 0 & 0 & 0 & \beta + J \end{pmatrix} \begin{matrix} |{+}{+}\rangle \\ |{+}0\rangle \\ |{+}{-}\rangle \\ |0{+}\rangle \\ |00\rangle \\ |0{-}\rangle \\ |{-}{+}\rangle \\ |{-}0\rangle \\ |{-}{-}\rangle \end{matrix} \,. \tag{A.6}$$

Note we numerically checked, that for $J = 1$ and $\beta = 1/3$ if we would add again the δ_0 term the reflection center now would be at $\delta_0 = -2/3$, in perfect agreement with the new values $J - \beta$ (instead of just J^{xy}) for the matrix entries $|{+}{-}\rangle \langle 00|$ and similar.

However, let us focus on the more general transformation U^{φ}. We define a new Hamiltonian H^{φ} with the free parameter φ, that is the transformed AKLT Hamiltonian

$$H^{\varphi} = U^{\varphi}_{\text{global}} H^{\text{AKLT}} (U^{\varphi}_{\text{global}})^{\dagger} \,. \tag{A.7}$$

Since we know the ground state of the AKLT model $|\psi_{\text{AKLT}}\rangle$ (see equation (1.72)), the ground state of H^{φ} is simply given by transforming the AKLT ground state

$$|\psi_{\varphi}\rangle = U^{\varphi}_{\text{global}} |\psi_{\text{AKLT}}\rangle \,. \tag{A.8}$$

Thus, we can write the new ground state as MPS with transformed tensors

$$|\psi_{\varphi}\rangle = \sum_{\boldsymbol{s}} \text{tr}\left[\ldots \tilde{M}^{s_i} \ldots\right] |\boldsymbol{s}\rangle \,, \tag{A.9}$$

with

$$\tilde{M}^+ = \mathrm{e}^{\mathrm{i}\varphi/2} M^+ = \sqrt{\frac{2}{3}} \mathrm{e}^{\mathrm{i}\varphi/2} \sigma^+ , \quad \tilde{M}^0 = M^0 = \sqrt{\frac{1}{3}} \sigma^z$$
$$\text{and} \quad \tilde{M}^- = \mathrm{e}^{\mathrm{i}\varphi/2} M^- = -\sqrt{\frac{2}{3}} \mathrm{e}^{\mathrm{i}\varphi/2} \sigma^- . \tag{A.10}$$

Since H^φ is just the unitary transformed AKLT Hamiltonian the new Hamiltonian is in a gapped phase, with fourfold ground state degeneracy and two degenerate Schmidt values $\Lambda_1 = \Lambda_2$ for all φ .

Furthermore, one can check that the following properties are independent of φ (the calculations are exactly the same as in section 1.4).
The transfer matrix T stays the same and thus also the eigenvalues and eigenvectors.
All the ferromagnetic order parameters are still vanishing $\mathcal{O}_\infty^{\mathrm{FM},\alpha} = 0$.
And also the generalized transfer matrix (gTM) T^Σ stays the same for simple rotation symmetries R^α and inversion symmetry. Thus, these symmetry factors $\mathcal{R}^{R^x} = \mathcal{R}^{R^y} = \mathcal{R}^{R^z} = \mathcal{R}^{\mathcal{I}} = 1$ and phase factors $\mathcal{P}^{\mathrm{D}_2} = \mathcal{P}^{\mathcal{I}} = -1$ are also still the same.

However, let us consider the more interesting case of the time reversal (TR) symmetry. The representation of TR symmetry for spin 1 particles can be written as $T = R^y K$, where R^y is a rotation around the y axis and K is the complex conjugation operator (see section 1.3.2).

Thus, we can calculate the gTM T^T

$$T^T_{(\alpha_0,\alpha_0'),(\alpha_1,\alpha_1')} = \sum_{s,s'} \tilde{M}^s_{\alpha_0,\alpha_1} R^y_{s,s'} K \tilde{M}^{s*}_{\alpha_0',\alpha_1'}$$
$$T^T = \sum_s R^y_{s,s'} \tilde{M}^s \otimes \tilde{M}^s = \frac{1}{3} \begin{pmatrix} 1 & & & \\ & -1 & -2\mathrm{e}^{\mathrm{i}\varphi} & \\ & -2\mathrm{e}^{\mathrm{i}\varphi} & -1 & \\ & & & 1 \end{pmatrix} . \tag{A.11}$$

The eigenvalues of this matrix are

$$\eta_1 = \frac{1}{3}\left(1 + 2\mathrm{e}^{\mathrm{i}\varphi}\right) , \quad \eta_2 = \frac{1}{3}\left(1 - 2\mathrm{e}^{\mathrm{i}\varphi}\right) , \quad \eta_3 = -\frac{1}{3} , \quad \eta_3 = -\frac{1}{3} , \tag{A.12}$$

with the corresponding eigenvectors (already reshaped into matrices)

$$\boldsymbol{\eta}_1 = \begin{pmatrix} 0 & 1 \\ -1 & 0 \end{pmatrix} , \quad \boldsymbol{\eta}_2 = \begin{pmatrix} 0 & 1 \\ 1 & 0 \end{pmatrix} , \quad \boldsymbol{\eta}_3 = \begin{pmatrix} 1 & 0 \\ 0 & 0 \end{pmatrix} , \quad \boldsymbol{\eta}_4 = \begin{pmatrix} 0 & 0 \\ 0 & 1 \end{pmatrix} . \tag{A.13}$$

This means that the TR symmetry is broken for $\varphi \notin \{0, \pi\}$ (meaning $\left|\mathcal{R}^{\mathrm{TR}}\right| < 1$) and it is symmetric for $\varphi = 0$ or $\varphi = \pi$ ($\left|\mathcal{R}^{\mathrm{TR}}\right| = 1$). However, the corresponding eigenvector of

the largest eigenvalue (which corresponds to the projective symmetry representation of the TR) differs for $\varphi = 0$ or $\varphi = \pi$

$$U_{\mathrm{TR}} = \begin{cases} \mathrm{i}\sigma^y & \text{for } \varphi = 0 \\ \sigma^x & \text{for } \varphi = \pi \end{cases} \tag{A.14}$$

From that we can also calculate the phase factor

$$\begin{aligned} \mathcal{P}^{\mathrm{TR}} &= \begin{cases} \frac{1}{\chi} \operatorname{tr}\left(U_{\mathrm{TR}} U_{\mathrm{TR}}^*\right) & \text{if } \left|\mathcal{R}^{\mathrm{TR}}\right| = 1 \\ 0 & \text{else} \end{cases} \\ &= \begin{cases} -1 & \text{for } \varphi = 0 \\ +1 & \text{for } \varphi = \pi \\ 0 & \text{else} \end{cases} . \end{aligned} \tag{A.15}$$

This is perfect agreement with our observation for the XXZ model and the additional δ_0 term. The Haldane phase for $\delta_0/J^{xy} > -1$ (corresponding to $\varphi = 0$) in figure 3.18 is also a topological phase with respect to TR symmetry, while for $\delta_0/J^{xy} < -1$ (corresponding to $\varphi = \pi$) the mirrored Haldane phase is again symmetric under TR, but is now a trivial phase (with $\mathcal{P}^{\mathrm{TR}} = +1$).

Finally, we also want to discuss the string order parameters in this model. First, note that all even string order parameters $\mathcal{S}_d(R^\alpha, \mathbb{1})$ are vanishing independently of φ. Furthermore, the odd z string order parameter $\mathcal{S}_d(R^z, S^z)$ is independent of φ (the calculation is the same as in equation (1.82)). More interestingly is the odd x string order parameter $\mathcal{S}_d(R^x, S^x)$. For each φ one can construct an x string order parameter, that yields the same result as $\mathcal{S}_d(R^x, S^x)$ in the simple AKLT model

$$\begin{aligned} \tilde{\mathcal{S}}_\infty(U^\varphi R^x (U^\varphi)^\dagger, U^\varphi S^x (U_i^\varphi)^\dagger) &= -\lim_{|i-j|\to\infty} \langle\psi_\varphi| U_i^\varphi S_i^x (U_i^\varphi)^\dagger \left(\prod_{k=i+1}^{j-1} U_k^\varphi R_k^x (U_k^\varphi)^\dagger\right) U_j^\varphi S_j^x (U_j^\varphi)^\dagger |\psi_\varphi\rangle \\ &= -\lim_{|i-j|\to\infty} \left(\langle\psi_{\mathrm{AKLT}}| \left(U_{\mathrm{global}}^\varphi\right)^\dagger\right) U_i^\varphi S_i^x (U_i^\varphi)^\dagger \left(\prod_{k=i+1}^{j-1} U_k^\varphi R_k^x (U_k^\varphi)^\dagger\right) U_j^\varphi S_j^x (U_j^\varphi)^\dagger \left(U_{\mathrm{global}}^\varphi |\psi_{\mathrm{AKLT}}\rangle\right) \\ &= -\lim_{|i-j|\to\infty} \langle\psi_{\mathrm{AKLT}}| S_i^x \left(\prod_{k=i+1}^{j-1} R_k^x\right) S_j^x |\psi_{\mathrm{AKLT}}\rangle \\ &= \mathcal{S}_d^{\mathrm{AKLT}}(R^x, S^x) = \frac{4}{9} \end{aligned} \tag{A.16}$$

Note that in fact $U^\varphi R^x (U^\varphi)^\dagger = R^x$, however $U^\varphi S^x (U^\varphi)^\dagger \neq S^x$.

However, one might think it is enough to look at only one x string order parameter for all parameters φ. Using the normal odd x string order parameter $\mathcal{S}_d(R^x, S^x)$ yields

$$\begin{aligned}\mathcal{S}_\infty(R^x, S^x) &= -\lim_{|i-j|\to\infty} \langle\psi_\varphi| S_i^x \left(\prod_{k=i+1}^{j-1} R_k^x\right) S_j^x |\psi_\varphi\rangle \\ &= \frac{4}{9}\cos^2\frac{\varphi}{2}\,. \end{aligned} \tag{A.17}$$

Especially note that for $\varphi = \pi$ this is zero $\mathcal{S}_d(R^x, S^x) = 0$. This agrees with the numerical results for the mirrored Haldane phase with $\delta_0/J^{xy} < -1$ (see figure 3.18).

In fact, we strongly suspect, that there are no hermitian endpoint operators O^A and O^B (that are independent of φ), such that $\mathcal{S}_\infty(R^x, O^A, O^B)$ is nonzero for all φ. This is a somewhat surprising result. Although the ground state is always in the Haldane phase and protected by the D_2 symmetry there is only a unique string order parameter in z direction, but none in x direction that identifies the Haldane phase for all φ.

However, keep in mind that for every φ on its own there is a string order parameter also in x direction, as discussed in equation (A.16).

B Details on the DMRG code

We described the basic idea of the DMRG algorithm in section 1.2. In this appendix we are giving some additional information on the (i)DMRG simulations performed in this work. The code for all simulations used the TeNPy library (version 0.9.0) [19] to perform the DMRG sweeps.

We used a implementation for the DMRG sweeps, that started with small bond dimensions χ and then (slowly) increased the bond dimension up to some maximal bond dimension. For each χ we performed a minimum number of DMRG sweeps until the energy and entropy reached a certain convergence criteria or a maximal number of sweeps was performed. Before increasing the allowed bond dimension we performed a measurement of all properties we were interested in. This allowed us to also use results of smaller bond dimensions, check the convergence process of specific properties and also do some bond dimension extrapolation to higher bond dimensions.

XXZ model

The iDMRG simulations in section 3.2.1 were performed using a unit cell of 2 sites. Thus, we were also able to find the ground state of the AFM phase, which needs a unit cell of 2. Furthermore, we did not apply any charge conservation. We started all simulations with a bond dimension of $\chi = 4$ and increased it in steps of 4 up to a maximal bond dimension of $\chi = 200$.

The convergence process of the simulation for a gapped phase (Haldane phase of the XXZ model with $J^z/J^{xy} = 0.5$) can be seen in figure B.1. Clearly the energy and entropy are converging fast. In comparison, for a gapless phase (XY phase of the XXZ model with $J^z/J^{xy} = -0.3$) the convergence process can be seen in figure B.2. While the energy still also converges for the gapless phase, the entropy clearly does not converge for increasing bond dimensions.

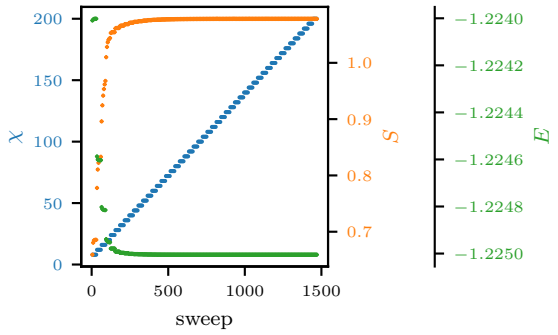

(a) Allowed bond dimension χ, entropy S and energy E of the updated ground states plotted over the iDMRG sweep.

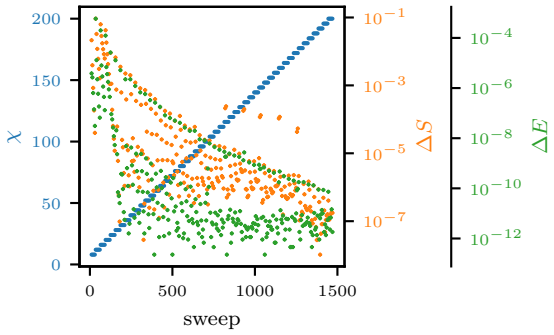

(b) Allowed bond dimension χ, entropy change to the last sweep ΔS and energy change to the last sweep ΔE of the updated ground states plotted over the DMRG sweep.

Figure B.1: Convergence of the iDMRG algorithm in a gapped phase (XXZ model with $J^z/J^{xy} = 0.5$).

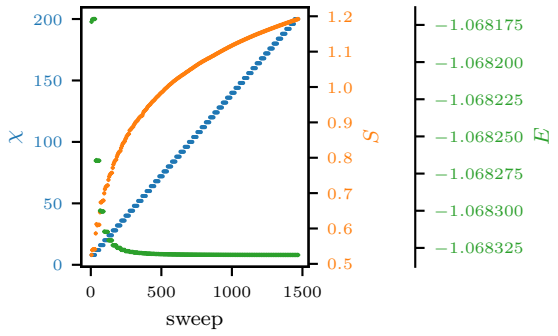

(a) Allowed bond dimension χ, entropy S and energy E of the updated ground states plotted over the DMRG sweep.

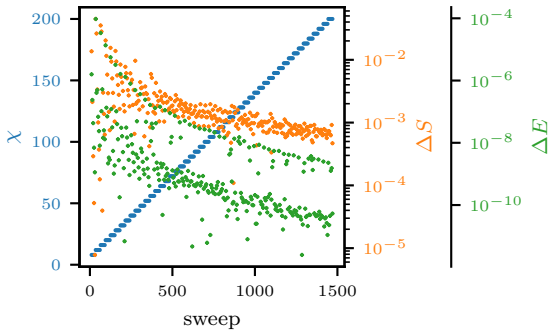

(b) Allowed bond dimension χ, entropy change to the last sweep ΔS and energy change to the last sweep ΔE of the updated ground states plotted over the DMRG sweep.

Figure B.2: Convergence of the DMRG algorithm in a gapless phase (XXZ model with $J^z/J^{xy} = -0.3$).

2d phase diagrams

The iDMRG simulations in section 3.2.2 were performed with similar settings as in section 3.2.1 (see before). However since we were not interested anymore in the bond dimension scaling we increased χ not in steps of 4 but according to the following list $\chi \in [8, 16, 32, 50, 64, 80, 100, 125, 150, 175, 200]$. Similar to figure B.1 and figure B.2 the entropy and energy for the ground state for gapped phases converged fast, while the entropy of gapless phases did not converge for increasing bond dimensions (which we also used to identify the central charges of these gapless phases, similar to figure 3.6).

Experimental proposal

In section 4.2 we used a finite DMRG algorithm to calculate the ground state of system sizes up to $N = 30$. In principle the DMRG algorithm is able to also calculate much larger system sizes (for one-dimensional systems a few hundred sites are easily accessible). However, since our proposed model had only weak finite size effects, system sizes of up to 30 where enough to demonstrate the relevant properties.

Similar to before we used bond dimensions up to $\chi = 200$ and increased them accordingly to $\chi \in [8, 16, 32, 50, 64, 80, 100, 125, 150, 175, 200]$. For calculating the ground state properties we again did not use any charge conservation.
But for calculating the excitation spectrum in figure 4.12 we used total spin conservation and started the different DMRG runs with an initial guess quantum state in the different sectors $S^z_{\text{total}} \in \{0, \pm 1, \pm 2, \pm 3\}$. For calculating multiple states in the same sector, the new state gets orthogonalized against all old states in the same charge sector. We also checked, that the spectrum for the lowest states looks the same, if we do not apply any charge conservation. However, to also get the lowest states of the charge sectors $S^z_{\text{total}} = \pm 3$ the simulations are more robust if we use charge conservation.

Bibliography

[1] K. v. Klitzing, G. Dorda, and M. Pepper. "New Method for High-Accuracy Determination of the Fine-Structure Constant Based on Quantized Hall Resistance". In: *Phys. Rev. Lett.* 45.6 (Aug. 1980), pp. 494–497. DOI: 10.1103/physrevlett.45.494.

[2] F.D.M. Haldane. "Continuum dynamics of the 1-D Heisenberg antiferromagnet: Identification with the O(3) nonlinear sigma model". In: *Physics Letters A* 93.9 (Feb. 1983), pp. 464–468. DOI: 10.1016/0375-9601(83)90631-x.

[3] G. Semeghini, H. Levine, A. Keesling, S. Ebadi, T. T. Wang, D. Bluvstein, R. Verresen, H. Pichler, M. Kalinowski, R. Samajdar, A. Omran, S. Sachdev, A. Vishwanath, M. Greiner, V. Vuletić, and M. D. Lukin. "Probing topological spin liquids on a programmable quantum simulator". In: *Science* 374.6572 (Dec. 2021), pp. 1242–1247. DOI: 10.1126/science.abi8794.

[4] Sylvain de Léséleuc, Vincent Lienhard, Pascal Scholl, Daniel Barredo, Sebastian Weber, Nicolai Lang, Hans Peter Büchler, Thierry Lahaye, and Antoine Browaeys. "Observation of a symmetry-protected topological phase of interacting bosons with Rydberg atoms". In: *Science* 365.6455 (Aug. 2019), pp. 775–780. DOI: 10.1126/science.aav9105.

[5] Pimonpan Sompet, Sarah Hirthe, Dominik Bourgund, Thomas Chalopin, Julian Bibo, Joannis Koepsell, Petar Bojović, Ruben Verresen, Frank Pollmann, Guillaume Salomon, Christian Gross, Timon A. Hilker, and Immanuel Bloch. *Realising the Symmetry-Protected Haldane Phase in Fermi-Hubbard Ladders*. 2021. URL: https://arxiv.org/abs/2103.10421.

[6] Xiao-Gang Wen. "Colloquium : Zoo of quantum-topological phases of matter". In: *Rev. Mod. Phys.* 89.4 (Dec. 2017). DOI: 10.1103/revmodphys.89.041004.

[7] Hal Tasaki. *Physics and Mathematics of Quantum Many-Body Systems*. Springer International Publishing, 2020. DOI: 10.1007/978-3-030-41265-4.

[8] Nicolai Lang. "Topological Phases of Matter". In: (2021). URL: https://serv.nl5.de/documents/TPM_SS21.pdf.

[9] Nicolai Lang. "One-Dimensional Topological States of Synthetic Quantum Matter". In: (2019). URL: https://serv.nl5.de/theses/PhD_Nicolai_Lang_2019-DIGITAL-A4-08-08-19-V11.pdf.

[10] L. D. Landau. "On the theory of phase transitions". In: *Zh. Eksp. Teor. Fiz.* 7 (1937), pp. 19–32.

[11] H. L. Stormer, A. Chang, D. C. Tsui, J. C. M. Hwang, A. C. Gossard, and W. Wiegmann. "Fractional Quantization of the Hall Effect". In: *Phys. Rev. Lett.* 50.24 (June 1983), pp. 1953–1956. DOI: 10.1103/physrevlett.50.1953.

[12] A.Yu. Kitaev. "Fault-tolerant quantum computation by anyons". In: *Annals of Physics* 303.1 (Jan. 2003), pp. 2–30. DOI: 10.1016/s0003-4916(02)00018-0.

[13] Xie Chen, Zheng-Cheng Gu, and Xiao-Gang Wen. "Local unitary transformation, long-range quantum entanglement, wave function renormalization, and topological order". In: *Phys. Rev. B* 82.15 (Oct. 2010). DOI: 10.1103/physrevb.82.155138.

[14] Xie Chen, Zheng-Cheng Gu, and Xiao-Gang Wen. "Classification of gapped symmetric phases in one-dimensional spin systems". In: *Phys. Rev. B* 83.3 (Jan. 2011). DOI: 10.1103/physrevb.83.035107.

[15] F. D. M. Haldane. "Nonlinear Field Theory of Large-Spin Heisenberg Antiferromagnets: Semiclassically Quantized Solitons of the One-Dimensional Easy-Axis Néel State". In: *Phys. Rev. Lett.* 50.15 (Apr. 1983), pp. 1153–1156. DOI: 10.1103/physrevlett.50.1153.

[16] Ian Affleck, Tom Kennedy, Elliott H. Lieb, and Hal Tasaki. "Rigorous results on valence-bond ground states in antiferromagnets". In: *Phys. Rev. Lett.* 59.7 (Aug. 1987), pp. 799–802. DOI: 10.1103/physrevlett.59.799.

[17] Ulrich Schollwöck. "The density-matrix renormalization group: a short introduction". In: *Phil. Trans. R. Soc. A.* 369.1946 (July 2011), pp. 2643–2661. DOI: 10.1098/rsta.2010.0382.

[18] Ulrich Schollwöck. "The density-matrix renormalization group in the age of matrix product states". In: *Annals of Physics* 326.1 (Jan. 2011), pp. 96–192. DOI: 10.1016/j.aop.2010.09.012.

[19] Johannes Hauschild and Frank Pollmann. "Efficient numerical simulations with Tensor Networks: Tensor Network Python (TeNPy)". In: *SciPost Phys. Lect. Notes Physics Lecture Notes* (Oct. 2018). DOI: 10.21468/scipostphyslectnotes.5.

[20] M B Hastings. "An area law for one-dimensional quantum systems". In: *J. Stat. Mech.* 2007.08 (Aug. 2007), P08024–P08024. DOI: 10.1088/1742-5468/2007/08/p08024.

[21] J. Eisert, M. Cramer, and M. B. Plenio. "Colloquium: Area laws for the entanglement entropy". In: *Rev. Mod. Phys.* 82.1 (Feb. 2010), pp. 277–306. DOI: 10.1103/revmodphys.82.277.

[22] Frank Pollmann and Ari M. Turner. "Detection of symmetry-protected topological phases in one dimension". In: *Phys. Rev. B* 86.12 (Sept. 2012). DOI: 10.1103/physrevb.86.125441.

[23] D. Pérez-García, M. M. Wolf, M. Sanz, F. Verstraete, and J. I. Cirac. "String Order and Symmetries in Quantum Spin Lattices". In: *Phys. Rev. Lett.* 100.16 (Apr. 2008). DOI: 10.1103/physrevlett.100.167202.

[24] Steven R. White. "Density matrix formulation for quantum renormalization groups". In: *Phys. Rev. Lett.* 69.19 (Nov. 1992), pp. 2863–2866. DOI: 10.1103/physrevlett.69.2863.

[25] Steven R. White. "Density-matrix algorithms for quantum renormalization groups". In: *Phys. Rev. B* 48.14 (Oct. 1993), pp. 10345–10356. DOI: 10.1103/physrevb.48.10345.

[26] Marcel den Nijs and Koos Rommelse. "Preroughening transitions in crystal surfaces and valence-bond phases in quantum spin chains". In: *Phys. Rev. B* 40.7 (Sept. 1989), pp. 4709–4734. DOI: 10.1103/physrevb.40.4709.

[27] Frank Pollmann, Ari M. Turner, Erez Berg, and Masaki Oshikawa. "Entanglement spectrum of a topological phase in one dimension". In: *Phys. Rev. B* 81.6 (Feb. 2010). DOI: 10.1103/physrevb.81.064439.

[28] Tom Kennedy and Hal Tasaki. "HiddenZ2×Z2symmetry breaking in Haldane-gap antiferromagnets". In: *Phys. Rev. B* 45.1 (Jan. 1992), pp. 304–307. DOI: 10.1103/physrevb.45.304.

[29] Thomas F. Gallagher. *Rydberg Atoms*. Cambridge University Press, Sept. 1994. DOI: 10.1017/cbo9780511524530.

[30] David Peter. "Quantum states with topological properties via dipolar interactions". PhD thesis. 2015. URL: http://dx.doi.org/10.18419/opus-5169.

[31] Sebastian Weber, Christoph Tresp, Henri Menke, Alban Urvoy, Ofer Firstenberg, Hans Peter Büchler, and Sebastian Hofferberth. "Calculation of Rydberg interaction potentials". In: *J. Phys. B: At. Mol. Opt. Phys.* 50.13 (June 2017), p. 133001. DOI: 10.1088/1361-6455/aa743a.

[32] Z.-X. Gong, M. F. Maghrebi, A. Hu, M. Foss-Feig, P. Richerme, C. Monroe, and A. V. Gorshkov. "Kaleidoscope of quantum phases in a long-range interacting spin-1 chain". In: *Phys. Rev. B* 93.20 (May 2016). DOI: 10.1103/physrevb.93.205115.

[33] Frank Pollmann, Erez Berg, Ari M. Turner, and Masaki Oshikawa. "Symmetry protection of topological phases in one-dimensional quantum spin systems". In: *Phys. Rev. B* 85.7 (Feb. 2012). DOI: 10.1103/physrevb.85.075125.

[34] Matthew Fishman, Steven R. White, and E. Miles Stoudenmire. *The ITensor Software Library for Tensor Network Calculations*. 2021. URL: https://arxiv.org/abs/2007.14822.

[35] Wei Chen, Kazuo Hida, and B. C. Sanctuary. "Ground-state phase diagram ofS=1XXZchains with uniaxial single-ion-type anisotropy". In: *Phys. Rev. B* 67.10 (Mar. 2003). DOI: 10.1103/physrevb.67.104401.

[36] Yao Heng Su, Sam Young Cho, Bo Li, Hong-Lei Wang, and Huan-Qiang Zhou. "Non-local Correlations in the Haldane Phase for an XXZ Spin-1 Chain: A Perspective from Infinite Matrix Product State Representation". In: *J. Phys. Soc. Jpn.* 81.7 (July 2012), p. 074003. DOI: 10.1143/jpsj.81.074003.

[37] Guang-Hua Liu, Wei Li, Wen-Long You, Gang Su, and Guang-Shan Tian. "Entanglement spectrum and quantum phase transitions in one-dimensional XXZ model with uniaxial single-ion anisotropy". In: *Physica B: Condensed Matter* 443 (June 2014), pp. 63–69. DOI: 10.1016/j.physb.2014.03.007.

[38] J M Kosterlitz and D J Thouless. "Ordering, metastability and phase transitions in two-dimensional systems". In: *J. Phys. C: Solid State Phys.* 6.7 (Apr. 1973), pp. 1181–1203. DOI: 10.1088/0022-3719/6/7/010.

[39] Pasquale Calabrese and John Cardy. "Entanglement entropy and quantum field theory". In: *J. Stat. Mech.: Theor. Exp.* 2004.06 (June 2004), P06002. DOI: 10.1088/1742-5468/2004/06/p06002.

[40] Frank Pollmann, Subroto Mukerjee, Ari M. Turner, and Joel E. Moore. "Theory of Finite-Entanglement Scaling at One-Dimensional Quantum Critical Points". In: *Phys. Rev. Lett.* 102.25 (June 2009). DOI: 10.1103/physrevlett.102.255701.

[41] H. J. Schulz. "Phase diagrams and correlation exponents for quantum spin chains of arbitrary spin quantum number". In: *Phys. Rev. B* 34.9 (Nov. 1986), pp. 6372–6385. DOI: 10.1103/physrevb.34.6372.

[42] Atsuhiro Kitazawa, Kiyohide Nomura, and Kiyomi Okamoto. "Phase Diagram of S=1 Bond-Alternating XXZ Chains". In: *Phys. Rev. Lett.* 76.21 (May 1996), pp. 4038–4041. DOI: 10.1103/physrevlett.76.4038.

[43] I. I. Ryabtsev, D. B. Tretyakov, I. I. Beterov, and V. M. Entin. "Observation of the Stark-Tuned Förster Resonance between Two Rydberg Atoms". In: *Phys. Rev. Lett.* 104.7 (Feb. 2010). DOI: 10.1103/physrevlett.104.073003.

Acknowledgement

I would like to use this opportunity to thank all the people who made this thesis possible and supported me during this time.

First, I would like to express my gratitude to Prof. Hans Peter Büchler for giving me the opportunity to do this work at the ITP3. He guided me through this masters project and encouraged my curiosity in physics. Furthermore, I want to thank him for giving me the possibility to attend a summer school in Les Houches.

I also want to thank my secondary corrector Prof. Jörg Main for the useful discussions.

Further I would like to thank all the members of the ITP3 for the great time and the many interesting discussions. In particular, I want to mention Sebastian Weber, who always had time whenever I needed some help. And also Nicolai Lang, who is an outstanding physicist and teacher (as tutor as well as lecturer). It is not self-evident that someone as talented as he also cares about helping younger students and sharing his knowledge.

I am also grateful to all my friends, who kept me company during these five years of study. Especially I want to thank Jonas Zatsch and Julius Fischer for five awesome years. Also, I would like to thank Johannes Reiff, who always had some advice regarding LaTeX or python.

In addition, I would like to acknowledge the financial as well as the non-material support by the German Economy Foundation (Stiftung der Deutschen Wirtschaft).

Finally, I want to thank my family for their support. Your unconditional support made me to the person I am today, and I am extremely grateful for that, thank you.